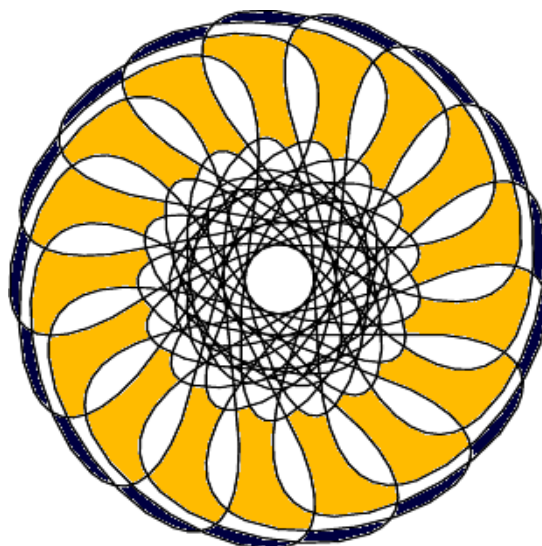


Zeolites as catalysts for the oligomerisation of glycerol

By Taha Ahmed



Bachelor's Diploma thesis

Author: Taha Ahmed

E-mail: taah1384@student.su.se

Supervisor: Dr. Mats Johnsson, Stockholm University

External supervisor: Dr. Neil Cruise, Perstorp AB

Project period: March 26, 2007 – October 26, 2007

Zeolites as catalysts for the oligomerisation of glycerol

Department of physical, inorganic and structural chemistry

Stockholm University, 2008

Abstract

Ten commercially available zeolites were tested as monofunctional and bifunctional catalysts for the selective oligomerisation of glycerol to di- and triglycerol without additional solvents in a laboratory-scale batch mode process. Catalyst performance was analysed with respect to zeolite acidity, surface area, porosity and crystallinity, using common analysis techniques as gas chromatography, atomic absorption spectroscopy, powder X-ray diffraction, and gas sorption analysis. The results suggest that activity and selectivity increase with zeolite acidity, and that the addition of a metal does not itself improve catalyst performance. Rather, the specific combination of zeolite and metal plays the most important role. The best monofunctional and bifunctional catalysts gave approximately 15 mass percent diglycerol. The catalysts ability to withstand the process conditions without losing surface area or crystallinity varied, although more acidic materials showed greater resilience.

The author introduces the subject from an environmental point of view, with a focus on the current glycerol challenge facing the chemical industry.

Contents

1	Introduction	1
1.1	Report outline	1
2	Background	2
2.1	General aspects of catalysis	6
2.1.1	Heterogeneous catalysis	7
2.1.2	Surface chemistry and analysis	8
2.2	Zeolites	11
2.2.1	Catalysis and zeolites	18
2.3	Properties and uses of glycerol	20
2.4	Properties and uses of glycerol's oligomers	20
2.5	Oligomerisation of glycerol	22
2.5.1	By homogeneous catalysis	23
2.5.2	By heterogeneous catalysis	23
3	Experimental	25
3.1	Zeolites	25
3.2	Glycerol and polyglycerol	25
3.3	Impregnation	26
3.3.1	Metal salts	27
3.4	Heating programs	29
3.4.1	G1 heating program	31
3.4.2	G6 heating program	32
3.4.3	G6IM heating program	32
3.5	Surface area measurements	33
3.6	Powder XRD analysis	33
3.7	GC analysis	35
3.8	AAS analysis	35
4	Results	36
4.1	Zeolite BEA	43
4.2	Zeolite FAU-13X	46
4.3	Zeolite FAU-600	49
4.4	Zeolite FAU-720	52
4.5	Zeolite FAU-760	55
4.6	Zeolite FAU-780	57
4.7	Zeolite FAU-900	59
4.8	Zeolite MOR	61
4.9	Zeolite USY	64
4.10	Zeolite ZSM-5P	66

5 Discussion & conclusions	69
5.1 Concluding remarks	72
6 References	75
A Appendix	79

List of Figures

1	Structure of glycerol.	2
2	Making synthetic glycerol from petroleum products	3
3	Production of biodiesel from renewable resources.	4
4	Transesterification.	4
5	Epicerol™ process	5
6	Adsorption hysteresis.	10
7	Basic adsorption isotherms.	11
8	FAU framework.	13
9	MFI framework.	15
10	BEA framework.	16
11	MOR framework.	17
12	Di- and triglycerol formulas.	21
13	Dehydration of glycerol.	22
14	Catalytic test setup.	30
15	G1 procedure overview.	31
16	Firing program.	32
17	G6 procedure overview.	33
18	G6IM procedure overview.	34
19	Adsorption isotherms for start materials.	36
20	Impregnated BEA PXRD diffractograms.	44
21	Impregnated FAU-13X PXRD diffractograms.	48
22	Impregnated FAU-600 PXRD diffractograms.	51
23	Impregnated FAU-720 PXRD diffractograms.	54
24	Impregnated FAU-900 PXRD diffractograms.	59
25	Impregnated MOR PXRD diffractograms.	63
26	Impregnated USY PXRD diffractograms.	64
27	Impregnated ZSM-5P PXRD diffractograms.	68
28	Preserved relative surface area.	70
29	Acidity versus diglycerol ratio.	71
30	Acidity versus diglycerol ratio for bifunctional materials.	72
A.1	Isotherms zeolite initial state.	81
A.2	Catalytic test setup.	82
A.3	G1 heating programs	83
A.4	G6 heating programs	84
A.5	G6IM heating programs	85
A.6	Pore size distributions.	86
A.7	Pore size distributions.	87
A.8	Pore size distributions.	88
A.9	BEA powder X-ray diffractograms	93
A.10	FAU-13X powder X-ray diffractograms	94
A.11	FAU-600 powder X-ray diffractograms	95
A.12	FAU-720 powder X-ray diffractograms	96

A.13 FAU-760 powder X-ray diffractograms	97
A.14 FAU-780 powder X-ray diffractograms	98
A.15 FAU-900 powder X-ray diffractograms	99
A.16 MOR powder X-ray diffractograms	100
A.17 USY powder X-ray diffractograms	101
A.18 ZSM-5P powder X-ray diffractograms	102

List of Tables

1 Zeolite materials presented.	25
2 Glycerol and polyglycerol chemicals.	26
3 Impregnated metals experimental amounts.	28
4 Metal salts data.	29
5 BET surface areas of zeolites.	37
6 BET surface areas of impregnated zeolites.	38
7 Leaching of metal, experimental (absolute) values.	38
8 Leaching of metal, relative values.	39
9 G6 glycerol composition.	40
10 Cs- G6IM glycerol composition.	42
11 Mg- G6IM glycerol composition.	42
12 Mn- G6IM glycerol composition.	42
13 BEA BET.	43
14 BEA atomic absorption results.	43
15 BEA 10 min glycerol composition.	45
16 BEA 1 h glycerol composition.	45
17 BEA 6 h glycerol composition.	45
18 FAU-13X BET.	47
19 FAU-13X 6 h glycerol composition.	47
20 FAU-13X atomic absorption results.	47
21 FAU-600 BET.	49
22 FAU-600 atomic absorption results.	49
23 FAU-600 1 h glycerol composition.	50
24 FAU-600 6 h glycerol composition.	50
25 FAU-720 BET.	53
26 FAU-720 6 h glycerol composition.	53
27 FAU-720 atomic absorption results.	53
28 FAU-760 BET.	56
29 FAU-760 6 h glycerol composition.	56
30 FAU-780 BET.	58
31 FAU-780 6 h glycerol composition.	58
32 FAU-900 BET.	60
33 FAU-900 6 h glycerol composition.	60
34 FAU-900 atomic absorption results.	60

35	MOR atomic absorption results.	61
36	MOR BET.	61
37	MOR 10 min glycerol composition.	62
38	MOR 1 h glycerol composition.	62
39	MOR 6 h glycerol composition.	62
40	USY BET.	65
41	USY 6 h glycerol composition.	65
42	USY atomic absorption results.	65
43	ZSM-5P 10 min glycerol composition.	67
44	ZSM-5P 1 h glycerol composition.	67
45	ZSM-5P 6 h glycerol composition.	67
46	ZSM-5P BET.	68
47	ZSM-5P atomic absorption results.	68
48	Relative surface area of monofunctional catalysts.	69
A.1	G1 heating cycles details.	79
A.2	G6 heating cycles details.	79
A.3	G6IM heating cycles details.	80
A.4	M-file <code>xyreader.m</code>	89
A.5	M-file <code>ghplot.m</code>	90
A.6	M-file <code>huberplot.m</code>	91
A.7	M-file <code>plotpxrd.m</code>	92

1 Introduction

Thanks to the growing environmental concern within the chemical industry, new ways to reduce the environmental impact of production processes are pursued. Since the chemical industry traditionally relies heavily on organic catalytic processes, large amounts of organic waste is accrued. To reduce this waste, new catalytic processes, i.e., new catalysts, have to be employed. Ever since the sixties, when zeolites were first used in petroleum cracking, they have found new and exciting applications in chemical industry, over time shifting from the heavy chemical industry towards more fine chemical and biochemical processes.

With the recent surge for biofuel (especially biodiesel) production in Europe and America, biofuel producers find themselves facing a new problem. Glycerol, a by-product of biodiesel, used to be an economic incentive for biodiesel production. With the large increase in biodiesel capacity, glycerol has become a liability.

One of the possible solutions to the glycerol problem is to refine (oligomerise) the glycerol, preferentially to di- and triglycerol. Certainly, di- and triglycerol are valuable commodities on the market, used as ingredients or precursors in an extensive array of products.

The aim of this project is to characterise ten commercially available zeolites with regard to their performance as catalysts for the oligomerisation of glycerol at elevated temperature.

1.1 Report outline

This report is divided into five main parts.

The “Background” section report starts with describing the process of biodiesel production, which is the main source of glycerol. Some other common synthesis routes are also described. After elaborating on heterogeneous catalysis and surface chemistry, the basic properties of the four framework types used in this project are described. Finally, the properties and common uses of glycerol and glycerol’s oligomers are overviewed, as well as traditional routes of oligomerising glycerol.

The “Experimental” section describes the experimental methods employed throughout the project.

The “Results” section presents direct observational data as well as calculated quantities derived from observational data. The results are summarised for all ten materials, but also presented material-by-material in greater detail.

In the “Conclusions” section, my conclusions are presented.

Additional data, some tables and figures, as well as a few MATLAB scripts, is included in the appendix for completeness.

2 Background

With increasing petroleum prices world-wide, and fuel-demand expected to keep rising, the market for alternative fuels is expanding and will likely keep doing so for the foreseeable future.

Liquid bio-fuels, primarily bio-diesel and bio-alcohol, are transportation fuels, processed from agricultural crops and other renewable feedstock that can be used instead of fossil fuels in common internal combustion engines (Enguđanos et al., 2002).

Common renewable fuels include:

- Bio-alcohols (gasoline additives)
 - Bio-ethanol (as ETBE, ethyl tert-butyl ether)
 - Bio-methanol (as MTBE, methyl tert-butyl ether)¹
- Bio-diesel (additive to petrodiesel).

Biodiesel is a renewable fuel produced from vegetable oil extracted from a variety of crops, such as soybean, sunflower seed, rapeseed, peanut, cottonseed, oil palm, etc., (Wikipedia, 2007b). World production of biodiesel is approximately 3.5 million metric tonnes per annum (Foglia et al., 2006), and growing rapidly. This growth in biodiesel production, however, is accompanied by increased glycerol supplies, a major by-product of biodiesel production. This increase in availability of glycerol lowers its value and adversely impacts biodiesel economics. Accordingly, it is desirable to find new outlets for glycerol (Foglia et al., 2006).

The global annual production of biodiesel equals roughly 350,000 tonnes of crude glycerol; which has an expected annual growth of between 10 and 25 percent until 2010 (Henard, 2007). Biodiesel production is the primary source of glycerol world-wide, and expected to account for 65% of glycerol production by 2010 (Henard, 2007).

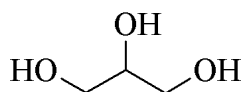


Figure 1. Chemical structure of glycerol, also commonly called glycerine.

Glycerol was discovered by the Swedish chemist C. W. Scheele in 1779 when he heated olive oil and lead oxide (David, 1996). Today we know that glycerol is a main component of all vegetable and animal fats. Ever since its discovery, the applications of glycerol has increased—today it is an indispensable chemical found in various products.

¹The renewability of methanol from natural gas is debated.

Glycerol has historically been obtained as a by-product of soap production or from the hydrolysis of fats and oils. This was also the main commercial supply of glycerol up until the second World War. With the rise of the petroleum industry, glycerol supply shifted to synthesis from propene ($\text{H}_3\text{C}-\text{HC}=\text{CH}_2$), a major by-product of petroleum cracking.

First the propene is chlorinated, producing hydrochloric acid and allyl chlo-

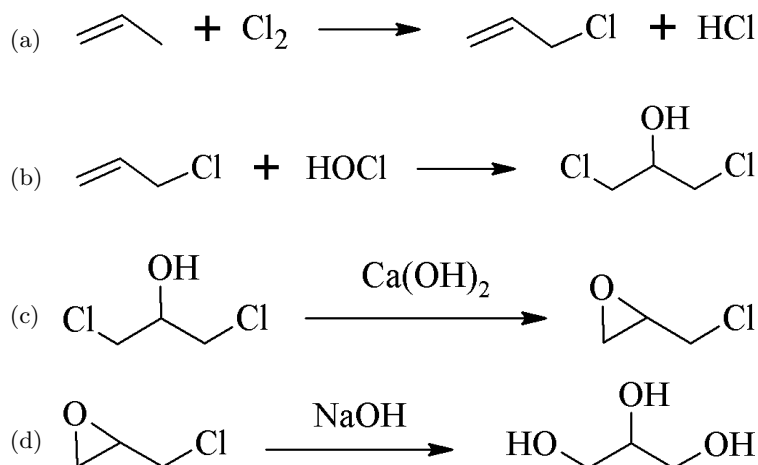


Figure 2. Reactive pathway for industrial production of glycerol from propene, a by-product of petro-cracking. European Oleochemicals and Allied Products Group (2007).

ride (Fig. 2a). The allyl chloride is then hypochlorinated, making one mole of dichlorohydrin for each mole of allyl chloride (Fig. 2b). The dichlorohydrin is treated with $\text{Ca}(\text{OH})_2$, making an equimolar amount of epichlorohydrin, as well as calcium chloride and water (Fig. 2c). In the last step, the epichlorohydrin is hydrolysed in the presence of a strong base, producing glycerol and sodium chloride (Fig. 2d).

Currently the main supply of glycerol is as a by-product of biodiesel production, i.e, with a renewable resource as feedstock. Fig. 3 shows the predominant method of producing biodiesel industrially: transesterification of rapeseed oil at roughly atmospheric pressure and low temperature (65°C) in a batch process. Yields are normally above 98% (Enguádanos et al., 2002). The main product is rapeseed methyl ester, or RME, which can be mixed into petrodiesel in concentrations up to 20% with little or no modification of the diesel engine.

Fig. 4 shows the chemical reaction of transesterification, in this case of a triglyceride (vegetable or animal fat). The alcohol (methanol) reacts with the triglyceride splitting each COOC bond, creating three alkyl esters (in this case methyl esters). The reaction between the alcohol and the glyceride is reversible, therefore the alcohol is added in excess to drive the reaction

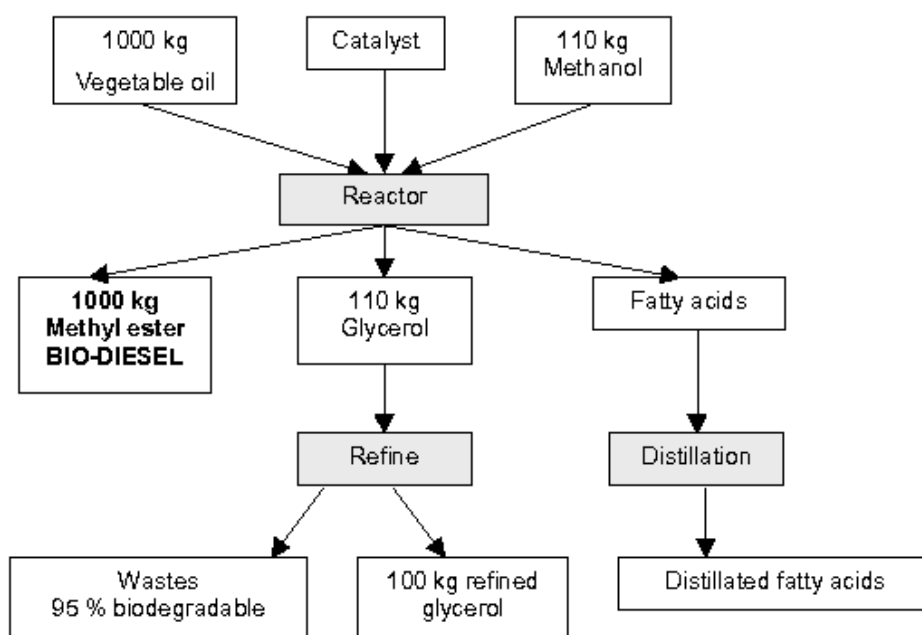


Figure 3. Production of biodiesel from renewable resources: each 1000 kg of biodiesel produced gives 100 kg of glycerol as by-product. Image from Enguídanos et al. (2002, p. 2).

teabag paper reinforcement (Solvay S. A., 2007). Fig. 5 shows the principal

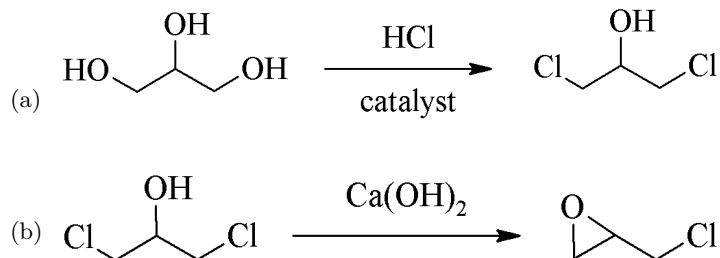


Figure 5. Making epichlorohydrin from renewable glycerol, as in Solvay’s commercial Epicerol™ process. Solvay Chemicals, Inc. (2007).

reactions of the Epicerol™ process. Since a few years back, most industrial production of glycerol from petroleum by-products has ceased, due to the rapid increase in glycerol from biodiesel production. The development of new industrial synthetic processes *from* glycerol is a natural step considering the current market conditions.

No details on the catalyst which is used in the first step of the Epicerol™ process (Fig. 5a) are available, other than it being a solid material. The catalysis is thus heterogeneous. The organic reactions involved (from glycerol to epichlorohydrin or the reverse) are well-known to organic chemists. The secret lies in the catalyst, which makes this process economically and industrially feasible.

So far we have seen how glycerol is predominantly produced world-wide, and some of the alternative ways. We have shown that the glycerol glut from biodiesel production is of low economic value, and that refining this glycerol to higher purity leads to big earnings. Additionally, as we have seen, a few companies are currently in a pre-production phase for converting glycerol into C3-epoxides.

Now we turn back to our application of refining glycerol. We start by a basic review of catalysis.

2.1 General aspects of catalysis

Catalysts are employed in virtually all chemical reactions of industrial importance. Examples of such are petroleum cracking, fertilizer production, and methanol synthesis from CO and H₂. Perhaps the most well-known utility is as catalytic converters in automobiles all over the world. In short, catalysts make it possible to produce materials, or sustain reactions, that would otherwise have been unobtainable or prohibitively expensive.

In the following, starting from a common definition of a catalyst, the general properties of a catalyst will be described.

A catalyst is a *substance* that *increases the rate* at which a chemical reaction approaches *equilibrium* without itself becoming *permanently* involved in the reaction. (Richardson, 1989)

Thermodynamic equilibrium is unchanged, together with thermodynamic properties as ΔG_r , ΔH_r , and K_r . The catalyst affects the kinetics of the reaction by lowering the activation energy; which in turn is achieved by the catalysts ability to provide low-energetic pathways for the reaction, e.g., by providing a solid surface for the reaction to take place on. It is now necessary to introduce the term *catalytic activity*. Catalytic activity is intimately related to the fact that a catalyst only affects the kinetics. Catalytic activity is measured in moles per second (in the SI system). A catalyst will make a reaction reach equilibrium faster, just how fast is given by its activity.

A catalyst, in principle, promotes only one reaction, even if several reactions take place. A catalyst is thus able of improving not only activity but also selectivity. Since the catalyst is a chemical, reacting with reactants and products through chemisorption or complexing, its reactivity depends upon its own chemical structure (Richardson, 1989). Thus, and this is very important in all fields of catalysis, a catalyst is *selective*.

An ideal catalyst does not get permanently involved in the reaction it catalyses (again drawing from the definition). An ideal catalyst should in principle be able to continuously catalyse a reaction without ever needing replacement or regeneration. But in all real-life reactions, the catalyst loses its activity over time. It *does* get permanently involved in the reaction, sooner or later, and thus loses its catalytic activity. This is known as *deactivation*.

The main properties of a catalyst in an industrial application are, in no specific order:

- Activity.
- Selectivity.
- Deactivation.

The relative order of importance between these properties is not obvious. But given that today's industry emphasize efficient utilization of feedstocks and energy, the relative order of importance is, according to Richardson (1989), selectivity > deactivation > activity.

An industrial catalyst is subject to mechanical, thermal and chemical stresses, which will eventually cause its deactivation (Richardson, 1989). Mechanical stresses are caused by friction, which are in turn caused by mixing, stirring, or convection in the reactor. There can also be *fouling* of the catalyst, whereby reactor debris is deposited on the catalyst particles. This is especially relevant at industrial scale, but even in the laboratory setup fouling may have occurred caused by glass, rubber or packing materials in and around the reactor.

Thermal stress, on the other hand, weakens the catalyst so that it may undergo phase changes, surface changes or even particle sintering. At high enough temperatures catalyst components may vaporise, essentially destroying the catalyst. A catalyst is also subject to chemical stresses, chiefly poisoning and coking. Poisoning is slightly temperature dependent, and may be reversible or irreversible, depending on poison and catalyst. There are three types of general poisoning reactions: (i) independent compounds present in the feed deactivate a catalyst site with a mechanism different from the main reaction, (ii) parallel reaction generates poison, or (iii) series reactions generate poison. A poison is any compound resulting in strong adsorption to the catalytic site, thereby blocking the access of the feed. Coking is described in section 2.2.1.

Usually, the field of catalysis as a whole is divided into three divisions: homogeneous, enzyme and heterogeneous catalysis (Thomas and Williams, 2005). In homogeneous catalysis the reactants and catalyst are in the same phase, most commonly as liquids. Advantages with homogeneous catalysis is high yields and high selectivity. Also, the techniques of organometallic chemistry is easily adopted for studying such reactions. Enzyme catalysis, or biocatalysis, is the field of studying the catalytic function of enzymes. Enzymes are tremendously active, as well as displaying a selectivity which surpasses anything man-made. The field of heterogeneous catalysis is where the current work belongs. A more detailed description of heterogeneous catalysis will be made in the next section.

2.1.1 Heterogeneous catalysis

In heterogeneous catalysis, the reactants and catalyst exist in different phases. Most commonly, solid catalysts are used with gaseous or liquid reactants. The main advantage of heterogeneous catalysis is its simplicity of use in industry. Theoretically it may be harder to grasp what is going on compared to homogeneous catalysis, but that is usually no problem as long as it works. First of all, a solid catalyst can be shaped into pellets, or rings, or spheres etc., and it can be used in slurries as well as fluid beds and so on. This versatility in application simplifies construction of new processes and leads to dependable operation (Richardson, 1989). Compared to homogeneous catalysis, another important difference crystallises: the products need no special separation step to remove residual catalyst. This is a major drawback of homogeneous catalysis. This is reflected in the fact that whereas homogeneous catalysis only finds limited industrial use, heterogeneous catalysis has numerous applications in industry.

It is important to note that heterogeneous catalytic processes occur not only in industrial processes, as mentioned above, but also in nature. For example, the process whereby the ozone hole is formed is a heterogeneous catalytic process (McCash, 2002, p. 151). Heterogeneous catalysis as such

is an interesting process to study, but for now we will restrict ourselves to industrial applications.

Heterogeneous catalysis introduces phenomena that we did not need account for in homogeneous catalysis, such as diffusion and adsorption. These are, with a common name, interfacial phenomena, normally studied within the realm of surface chemistry. So, to grasp heterogeneous catalysis, we need to study surface chemistry.

2.1.2 Surface chemistry and surface analysis

Surface chemistry deals with the chemical interactions at phase boundaries. We will treat solid/gas and solid/liquid surfaces in this section (the latter only briefly). These interfaces represent two main applications in this thesis. Solid/gas interface interactions are central for the surface area and porosity measurements done with the ASAP 2020™. Solid/liquid interface interaction plays a part in the oligomerisation of glycerol on the zeolites.

Heterogeneous catalysis is intimately connected to phenomena at surfaces (phase boundaries). The phenomena occurring at solid/gas boundaries have been studied extensively since the emergence of high-vacuum chambers in the 1960's (The Royal Swedish Academy of Sciences, 2007). Reactions on surfaces are much harder to study than in solutions, because (i) measurements must be done under high-vacuum, (ii) the reactions take place on an atomic mono-layer, and (iii) any impurities in the solid phase will not dilute as in solutions. Additionally, reaction mechanisms are usually more complicated than in the liquid state.

Where solid surfaces and gas molecules coexist, a huge number of gas molecules hit the surface every split second (Micromeritics, 2008). When a gas molecule hits the surface, the collision is either *elastic* (like a billiard ball hitting the cushion of a billiard table) with no energy exchange between the surface and the incident molecule, or *inelastic* (the gas molecule sticks to the surface for some time, then rebounds at an angle unrelated to the incident angle). The latter case represents the phenomena of *adsorption*. The term adsorption was coined in 1881 by Kayser to describe the increased concentration of gas molecules at a solid surface, a phenomenon observed as early as 1777 by Fontana and Scheele (Roque-Malherbe, 2007).

Adsorption on a solid surface is a dynamic equilibrium. As more gas molecules hit the surface, and each linger for a while, the concentration of gas on the surface increases until the adsorption rate equals the desorption rate. In fact, the concentration of gas on the surface will always exceed the concentration in the bulk of the gas. To use an analogy by Micromeritics (2008): “this is somewhat analogous to the fact that you will find a higher concentration of automobiles at an intersection with a stop sign compared to the concentration of autos along comparable section of street leading to the intersection.” In other words, the adsorbed state represents a lower energy

state of the system than the state with free gas molecules.

The actual bonding that takes place between the surface and the adsorbate (the particle that is adsorbed by the adsorbent) is always exothermic, and usually described as either one of two kinds.

Physisorption is the attraction of the adsorbate by weak forces, usually van der Waals forces, that overcome the repulsive forces associated with close contact. Physisorption represents a weakly bound state, usually with enthalpies (heat of adsorption) of a few kilojoules per mole. No change in the chemical nature of the adsorbate is associated with physisorption.

Chemisorption is a stronger attraction between the adsorbate and the surface, involving electron exchange between the surface and the adsorbate, thus forming a chemical bond between them. The bond may be covalent or ionic or anything in between (McCash, 2002). The heat of adsorption is usually between 50-1000 kJ/mol. Chemisorption is only possible for the first adsorbate layer, any additionally adsorbed layers are by definition physisorbed. Chemisorption can be either dissociative or non-dissociative (McCash, 2002). The former occurs when, e.g., H_2 is adsorbed on a metal surface. As the hydrogen molecule is chemisorbed, the H–H bond is broken. Non-dissociative chemisorption occurs when a molecule is chemisorbed without intramolecular configuration changes, i.e., without breaking any bonds.

In short, an unpolluted solid surface will always adsorb neighboring gas molecules due to the existence of unsaturated surface bonds (Roque-Malherbe, 2007). The adsorbates may only chemisorb if some kind of chemical interaction with the surface is possible. If not, they will always physisorb.

In my surface analysis experiments, using the ASAP2020 (Accelerated Surface Area and Porosimetry analyser) from Micromeritics, the gas sorption technique was used to characterise the surface and area properties of the investigated materials.

An adsorption isotherm is a plot of the gas volume against the relative pressure. From the shape of an adsorption isotherm, information on much about the structure of the adsorbing material can be deduced (Webb and Orr, 1997).

The isotherm of a porous material may display hysteresis, which shape will depend on the pore size distribution. Fig. 6 is typical for meso- and macroporous materials. At low relative pressures, adsorption will occur in the pores, where the gas molecules will be more attracted than at the external surface. As the gas pressure rises, multilayers and eventually condensation will form in the pores, from the rim inward. The wide hysteresis loop indicates that the evaporation process is significantly different from the condensation process. As pressure drops, gas will have to evaporate from an essentially liquid surface (condensed phase), which inhibits the evaporation. The decreasing portion of the loop will lag behind until all pores have emptied (Webb and Orr, 1997).

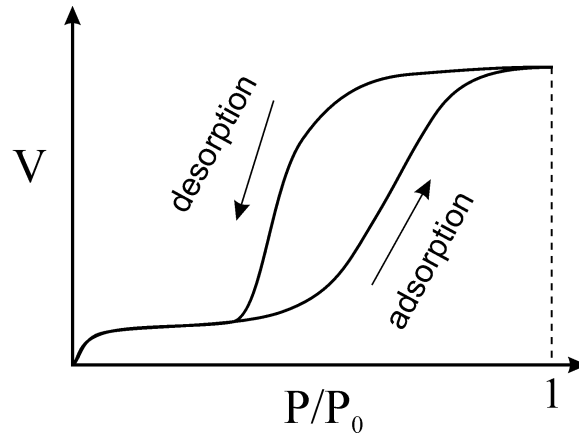


Figure 6. General adsorption isotherm showing (exaggerated) hysteresis loop. As the gas pressure is increased, the volume follows the adsorption curve. When decreasing the pressure, the volume follows the desorption curve. Such excessive hysteresis is typical for meso- and macroporous materials.

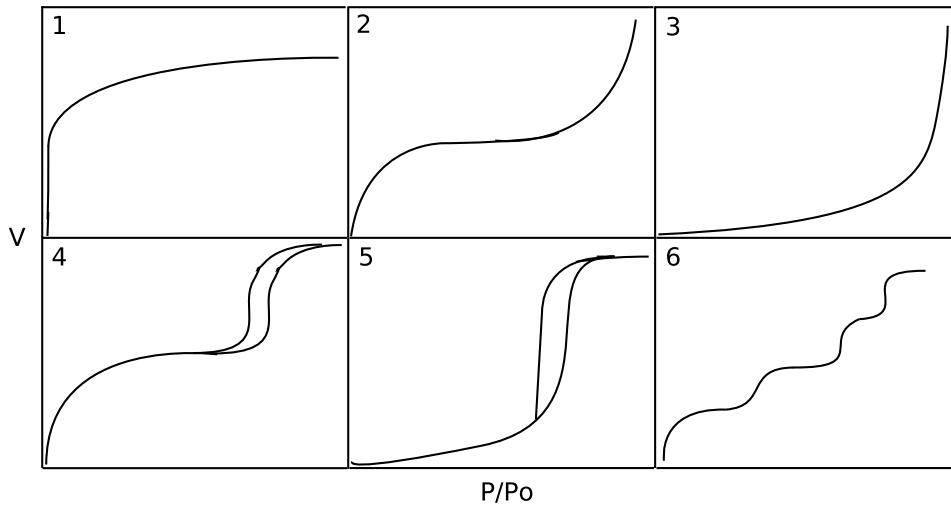


Figure 7. The six basic adsorption isotherm types, sketched by freehand.

In most basic treatises on gas adsorption techniques, six basic isotherm shapes are presented. To comply with tradition, we will do the same (Fig. 7). The deductions in the following assumes that the isotherms were collected at the boiling point of liquid N₂, 77.35 K at atmospheric pressure.

Type 1 is characteristic of adsorbents with extremely small pores: microporous or even slightly smaller. Type 2 is typical for a non-porous material. The shape of the curve can be explained as follows: the initial rise is due to gas molecules adsorbing to the most energetic sites on the adsorbent, and then to less energetic sites. As these less energetic sites are occupied, the rise of the curve diminishes, until it flattens. When we reach the midpoint of the curve, additional layers of gas molecules are forming on the surface (multi-layer formation). The final rise is due to condensation of the gas into a bulk liquid. Desorption will create no hysteresis. Curves of type 3 and type 5 are typical of systems where the gas-gas interactions are more favourable than the gas-surface interactions. Such systems are useless for surface and pore analysis. Type 4 shows the isotherm shape of a material with very large pores (macroporous or larger). Type 6 is a rare occurrence, and would be the isotherm shape of a non-porous solid with almost uniform surface.

Type 1 is most important for microporous surface analysis. Of course, a real material may have pores, cracks, and imperfections making for an isotherm composed of different parts from different isotherm types.

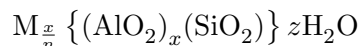
The ASAP2020 instrument is capable of determining many more material parameters than just surface structure. Using the BET (Brunauer-Emmett-Teller) theory (Brunauer et al., 1938), we can calculate for example, the surface area. Using more modern (and mathematically complicated) theories, such as Density Functional Theory, the instrument software can determine other parameters, such as pore size distribution and total pore volume. The former will be used to characterise the starting materials.

For surface area determinations using the BET theory, the whole isotherm is not necessary. We need only collect data to a pressure of about $0.4P/P_0$; the instrument has default pressure tables for the most common gases built-in to its software (Webb and Orr, 1997). This makes it possible to determine surface area by collecting just a few datapoints in this range. This is called a multipoint BET analysis.

2.2 Zeolites

Zeolites are microporous crystalline aluminosilicates having a uniform pore structure and exhibiting ion-exchange behavior (Weitkamp & Puppe, 1999). Zeolites are naturally occurring minerals, but the vast majority are synthetic. The framework (structure) of zeolites consists of SiO₄ and AlO₄ tetrahedra, connected to each other at their apices, sharing all oxygens. The tetrahedrally coordinated Si or Al atoms are named “T-atoms”. A framework consisting of only SiO₄ tetrahedra would be electrically neutral, but for each

AlO_4 tetrahedra introduced, one negative charge is created. To maintain overall electrical neutrality, the framework has to coordinate a cation for each framework alumina unit. The general framework formula for a zeolite is $(\text{AlO}_2)_x(\text{SiO}_2)_{(n-x)}$, where n is the number of tetrahedra per unit-cell, and $x \geq n/2$. The chemical composition of an aluminosilicate zeolite (framework as well as coordinated cations, M, and water) can be expressed as



where n is charge of the extraframework cation, and x the number of aluminium tetrahedra per unit-cell. z is the amount of water contained in the zeolite's voids.

A zeolite framework is a very special structure. Due to the way the alumina and silica tetrahedra are connected, all metal-oxygen tetrahedra are exposed to the surface, in a crystallographic way of speaking. Additionally, all surfaces exposed in the intracrystalline voids and channels are crystallographically perfect surfaces (local coordination of the atoms is unchanged), contrary to the usual crystal surface which is made up of broken bonds. The terminated outer surface has broken bonds, of course, but is usually small compared to the internal micropore surface in a zeolite. The exact ratio depends on the crystallite size and the porosity.

Zeolites are natural ion-exchangers, due to their capability to coordinate cations around their framework. The specific ion-exchange capacity varies with the structure of the zeolite and the exchange cation. Generally, a zeolite's ion-exchange capability increases with decreasing Si/Al ratio. The extraframework cations are always coordinated by the framework oxygens. Extraframework cations are not only useful for ion-exchange reactions. They also introduce electrical fields over the framework, effectively polarizing the framework. This may affect reactions inside the zeolite.

The pores of a specific zeolite are uniform in size and shape, since the material is crystalline. The pore dimensions are determined by the number of SiO_4 or AlO_4 tetrahedra in the ring which circumscribes the pore. Common pore sizes comprise 8-, 10- and 12-membered rings. The pore diameter depends on the spatial arrangement of the constituting tetrahedra. If the tetrahedra are arranged in an ideally circular and planar manner, the maximum possible free diameter results. This is the case in the faujasite structure (Weitkamp & Puppe, 1999). In most cases though, the pores are not circular, or planar, but rather puckered and sometimes elliptic.

The pore mouths of zeolites can be either "windows" to larger cavities or cages, or simply openings to cylindrical channels, which may be interconnected 1-, 2- or 3-dimensionally. Bear in mind that the zeolite framework is not rigid at normal temperatures. The framework is subject to constant molecular vibration, which increases with temperature, giving the pores some flexibility in both size and shape.

An important feature of zeolites is their inherent acidity. This is attributed to the exchangeable protons attached to the zeolite framework. In principle, all acid organic chemistry could be performed with zeolites (Weitkamp & Puppe, 1999).

The basic reasons for using zeolites as catalysts or catalyst support materials, is (i) they are cation exchangers (acidity), (ii) they have pore dimensions in the same order as the dimensions of our reactants and products (molecular sieve effect), and (iii) they have very large surface areas.

The catalytic function of zeolites is a result of the acidic sites (Al^{3+} tetrahedra) in the structure. An aluminium ion carries an effective negative charge (an extra electron), which results in an increased negative charge on the coordinating oxygen ions. It is the oxygen ions that constitute the acidic site (they may bond to a hydrogen ion, which can be used to protonate something, e.g. a double bond in a hydrocarbon).

If we combine the molecular sieve effect with the catalytic effect of a zeolite, we get shape-selective catalysis. Before going into some more detail, I would like to point out that zeolites can be either monofunctional or bifunctional (as catalysts). Monofunctional zeolites have only the acidic function, and bifunctional zeolites are additionally modified by the presence of (usually) a transition or noble metal. (Jens Weitkamp and Lothar Puppe (eds.), 1999, p. 356)

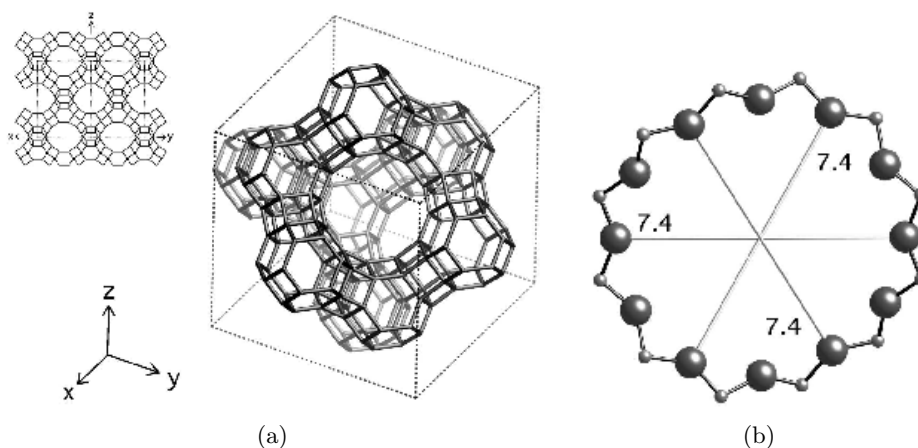


Figure 8. Faujasite framework (a) in 3D and 2D (small drawing upper left corner). Box signifies the unit cell. (b) shows 12-ring along [111]. Distances given in Ångström.

The free diameter values (effective pore width) and crystallographic data stated below are based upon an oxygen radius of 1.35 Å. The chemical formulas below are taken from Structure Commission of the International Zeolite Association (2001), Atlas of Zeolite Framework Types.

The faujasite family of zeolites comprises zeolite X, zeolite Y, hexagonal

faujasite and several mixed faujasites (Chen et al., 1994). Faujasite is a naturally occurring mineral, although for most applications it is synthesized.

Faujasite has the typical unit-cell formula $|\text{H}_{58}(\text{H}_2\text{O})_{240}|[\text{Al}_{58}\text{Si}_{134}\text{O}_{384}]$, and the cubic space-group $F d\bar{3}m$ (227), $a = 24.74 \text{ \AA}$ (Fig. 8). The framework density is $12.7 \text{ T}/1000 \text{ \AA}^3$. Faujasite has a 3-dimensional, interconnected channel system, with 12-member ring pores, and large supercages where the channels intersect.

Faujasites can be synthesized with a variety of Si/Al values.

The dealuminated form of zeolite Y, “ultrastable zeolite Y” (USY), is widely used as active component of cracking catalysts (Weitkamp & Puppe, 1999). The framework of USY has a low Si/Al ratio and is usually stabilized by aluminium cations. Due to the low framework aluminium concentration, USY has significantly lower ion-exchange capability than zeolite Y.

The MFI-type structure (Fig. 9) features a 2-dimensional interconnected channel system, where one set of channels are straight, and the other bent in a zig-zag fashion. MFI has medium-sized pores (10-member rings).

The most important zeolite of the MFI framework type is ZSM-5. First reported in 1973 by Argauer and Landolt, and used successfully as catalyst in methanol-to-gasoline conversion in 1976 by Mobil, this zeolite has received continuous attention since. ZSM-5 has proven itself very useful in industrial catalytic applications, especially for hydrocarbon conversion.

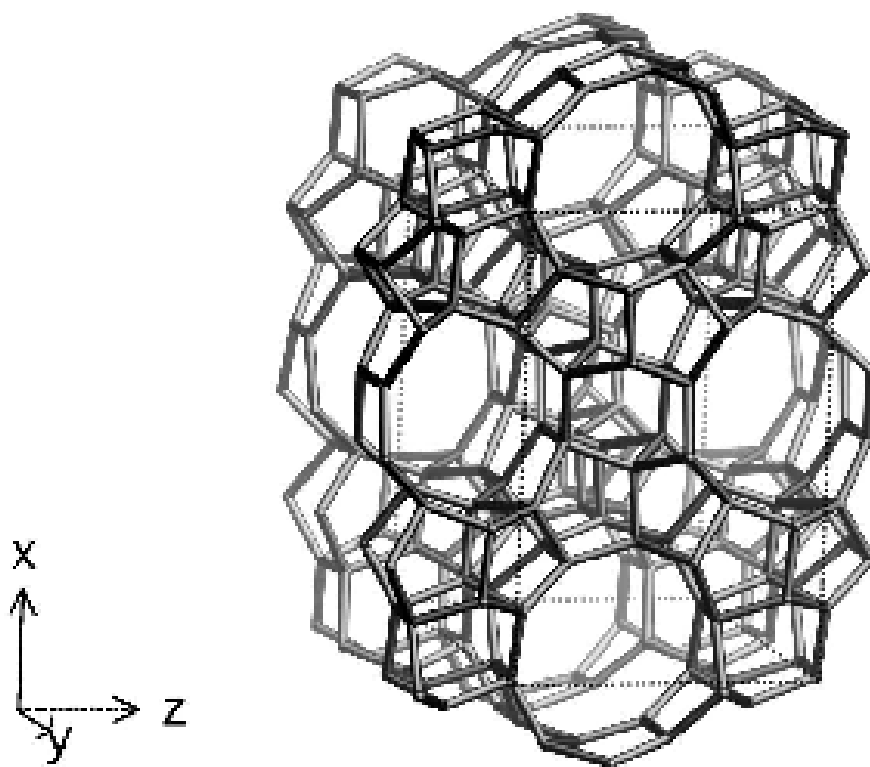
ZSM-5 has a typical unit-cell formula $|\text{H}_n(\text{H}_2\text{O})_{16}|[\text{Al}_n\text{Si}_{96-n}\text{O}_{192}]$, where $n < 27$. It crystallizes in the orthorhombic crystal system, with space-group $Pnma$ (62), $a = 20.07 \text{ \AA}$, $b = 19.92 \text{ \AA}$, $c = 13.42 \text{ \AA}$. The framework density of MFI is $17.9 \text{ T}/1000 \text{ \AA}^3$.

ZSM-5 has, unlike the other zeolites, channels of uniform size without large supercages and small apertures. The absence of “bottlenecks” in its channel system is believed to be a significant factor for its low coke forming propensity as acidic catalyst (Chen et al., 1994).

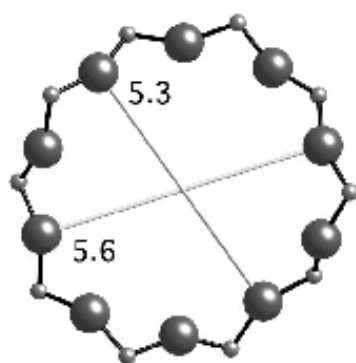
Zeolite beta (Fig. 10) was the first high-silica zeolite to be developed synthetically (Chen et al., 1994); it was synthesized from alkaline aluminosilicate gels in the presence of sodium and tetraethylammonium cations in 1967 (Weitkamp & Puppe, 1999). Its typical unit-cell formula is $|\text{H}_7|[\text{Al}_7\text{Si}_{57}\text{O}_{128}]$. Zeolite beta is a large pore (12-membered ring apertures) zeolite, with an intricate 3-dimensional channel network. In two directions the channels are straight with cages at their interconnections. In the third direction, the channels are tortuous but not blocked.

Zeolite beta crystallizes in the tetragonal system, with space-group $P4_122$ (91), $a = 12.661 \text{ \AA}$, $c = 26.406 \text{ \AA}$. Its framework density is $15.1 \text{ T}/1000 \text{ \AA}^3$.

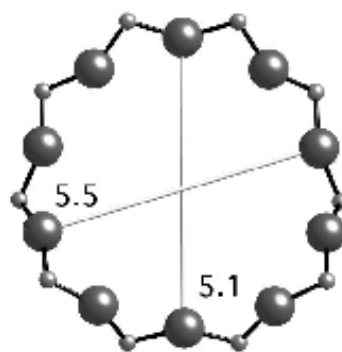
Mordenite (Fig. 11) is a natural high-silica zeolite whose typical unit-cell formula is $|\text{H}_8(\text{H}_2\text{O})_{24}|[\text{Al}_8\text{Si}_{40}\text{O}_{96}]$. Mordenite has a 12-membered oxygen ring system, which makes it a member of the large-pore zeolites. It also has a smaller, limiting 8-ring pore channel along the larger channels, intersecting with the 12-ring channels. Mordenite crystallizes in the orthorhombic crystal



(a)

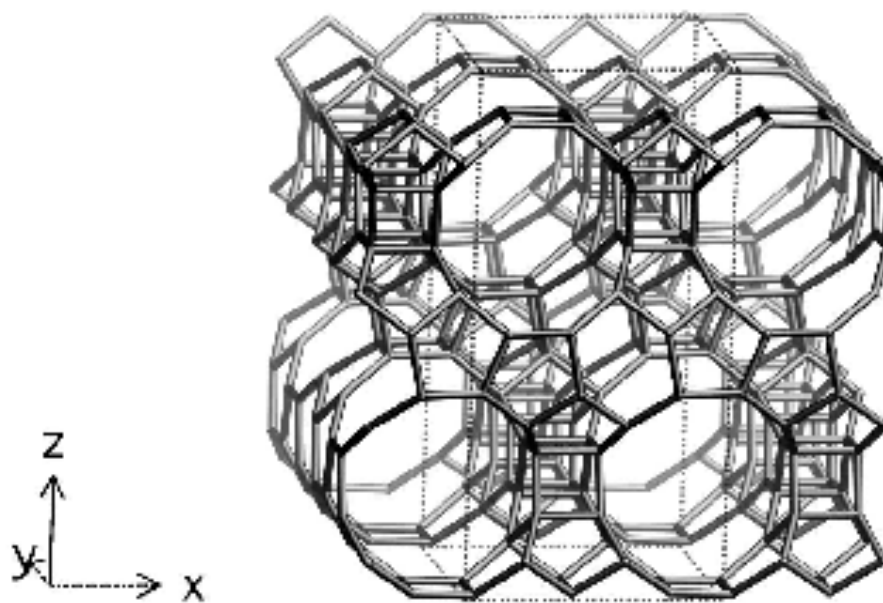


(b)

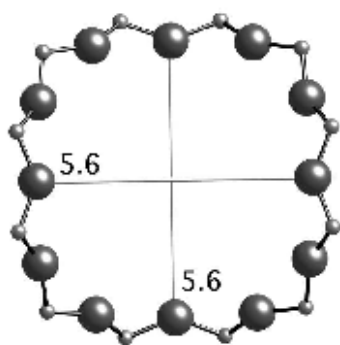


(c)

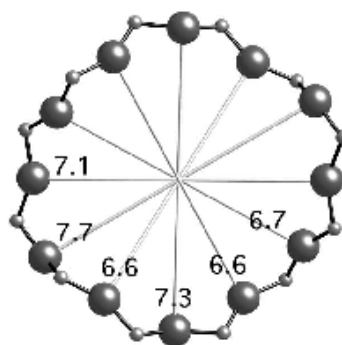
Figure 9. (a) MFI framework. Dotted box signifies the unit cell. (c) shows 10-ring viewed along [100], and (b) shows 10-ring viewed along [010]. Distances given in Ångström.



(a)



(b) 001



(c) 100

Figure 10. (a) BEA framework. Dotted box signifies the unit cell. (b) shows 12-ring viewed along [001], and (c) shows 12-ring viewed along [100]. Distances given in Ångström.

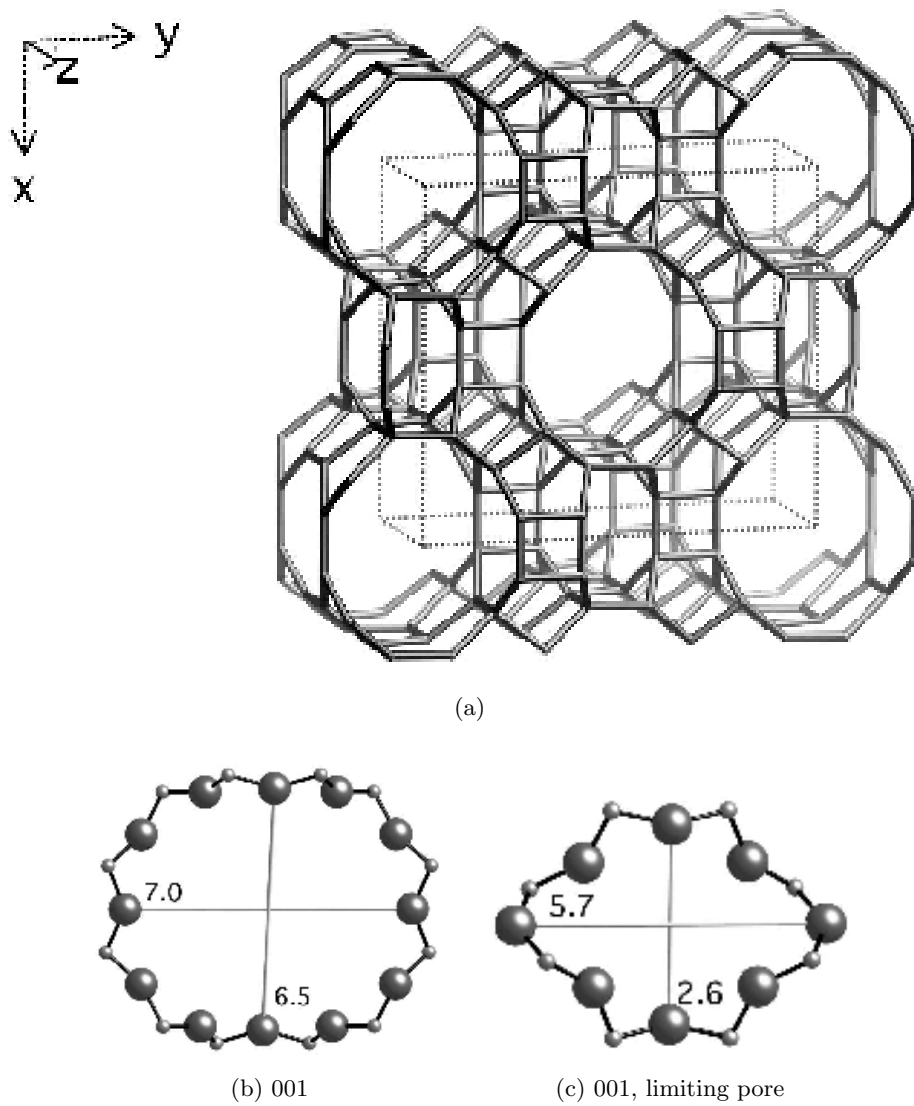


Figure 11. (a) MOR framework. Dotted box signifies the unit cell. (b) shows 12-ring viewed along [001], and (c) shows limiting 8-ring pore viewed along [001]. Distances given in Ångström.

system, with space-group $Cmcm$ (63), $a = 18.1 \text{ \AA}$, $b = 20.5 \text{ \AA}$, $c = 7.5 \text{ \AA}$. The framework density is $17.2 \text{ T}/1000 \text{ \AA}^3$.

Mordenite has, as described above, a dual pore system, consisting of interconnecting channels of 12-ring and 8-ring openings. The channels are parallel in the z direction (both 12- and 8-membered rings), with intersecting 8-ring channels in the y direction. The intersections between the 12- and 8-membered channels create cages that are larger than the pore dimensions. In total, mordenite has a 2-dimensional channel network. But the 12-membered ring channels are one-dimensional. (Weitkamp & Puppe, 1999)

2.2.1 Catalysis and zeolites

In addition to what has already been said in the previous section, I think the most interesting aspect of zeolite catalysis is the special diffusion, or adsorbate movement along the zeolite surface, that takes place in zeolites.

When dealing with diffusion in zeolites, three regimes must be considered: bulk, Knudsen, and configurational diffusion (Chen et al., 1994, p. 74). In the following discussion, gaseous reactants are assumed. I assume liquid reactants would behave similarly.

Bulk diffusion occurs when the volume in which diffusion occurs is much larger than the mean free path of the molecules. For a zeolite catalyst made into pellets, bulk diffusion would occur *between the pellets*. On a smaller scale, say, between the zeolite and the support particles (e.g., alumina) Knudsen diffusion would predominate. Or to put it differently, the diffusion would be best described by the Knudsen diffusivity formula (which we will not present here). On this level, the mean free path of the molecules is larger than the pore diameter. When the molecule hits the pore wall, it adsorbs, and is subsequently released in a random direction. Since the pore diameter is smaller than the mean free path, the molecule is more likely to hit a pore wall than a neighboring molecule. Knudsen diffusion is concentration independent. Finally, as the molecule enters the zeolite pores, it experiences attractive forces from two walls at the same time (metaphorically speaking), since the pore diameter is about the same size as the molecule itself. We have now moved into the regime of configurational diffusion. The molecule is now in constant close contact with the zeolite framework. The motion of the molecule will depend on the size and shape of the zeolite pore, as well as the chemical interaction between the surface and the diffusing molecule.

Configurational diffusion means that, in essence, the diffusing molecule can only transverse the surface of the zeolite pore by jumping from one active site to another. This is very different from what a chemist usually associates with diffusion. From a theoretical point of view, there is no easily derived general equation describing configurational diffusion (Chen et al., 1994, p. 81). Since a diffusing molecule in a zeolite pore is constantly experiencing the potential field of the solid, it becomes hard to define clearly

whether this molecule is in a gaseous or some sort of vibrational solid state. I think it suffices, for now, to envisage the diffusing molecules as riding the surface, jumping from one site to another constantly.

Although configurational diffusion (intracrystalline diffusion) severely limits the mass transfer in a zeolite, this is seldom the rate limiting step, except for bulky molecules. According to Chen et al. (1994), “the relative importance of intracrystalline diffusional effects to those of macropore diffusion [...] for a given reaction system should be proportional to the diffusional path length raised to the second power.”

Diffusional path length is, of course, another measure of crystallite size. So, as crystallite size increases, the relative importance of intracrystalline diffusion to macropore diffusion would increase. Since most zeolite catalysts have a small crystallite size (e.g., 20 Å), and catalyst particles in the order of 100 µm, intracrystalline diffusion would have to be more than a billion times slower than macropore diffusion to be rate limiting. This is not the case except for molecules that do not fit into the micropores. (Example taken from Chen et al. (1994)).

Finally, I would like to describe the phenomena of coking. Coking is the process whereby carbonaceous deposits accumulate on the zeolite surface. Coking occurs virtually anytime a zeolite catalyst is used with hydrocarbon reactants, e.g., glycerols. Coke is not a well defined substance, but everybody seems to agree that it is insoluble, solidlike deposits with low hydrogen content that attach strongly to the catalytic surface (Chen et al., 1994).

For a non-porous surface, a measure of the amount of coking (the amount of deactivated sites) would be proportional to the number of catalytic sites covered by coke. For a microporous zeolite, the pore size, shape and interconnectivity all plays a role. In unidimensional zeolites, like mordenite, a single coke “molecule” in a channel would deactivate (block) all sites the length of that channel. For a more interconnected zeolite, such as zeolite X (FAU), a coke blockage in one channel would only block that channel to the next intersection. But, as the space available increases, the coking rate will increase. Additionally, coke may also deposit on the external surface, effectively blocking pore apertures.

Coke affects zeolite catalysts depending on the pore structure, and according to experimental results discussed in Chen et al. (1994), coking impact activity on two levels. First, by direct site deactivation. Second, by blocking the path to acidic sites inside the zeolite pores. This renders acidic sites inaccessible, and also affects diffusion. In effect, the coke has changed the internal structure of the zeolite.

2.3 Properties and uses of glycerol

Glycerol's vast usage stems from its favourable properties. Glycerol is a transparent, viscous liquid. It is odour- and colourless. And it is sweet-tasting (60% as sweet as sucrose) and of low toxicity. It is also strongly hygroscopic (in an exothermic reaction). It is completely soluble in water and alcohol, and insoluble in hydrocarbons (Li, 1998).

In fact, the uses of glycerol are so numerous, that we can by no means enumerate all of them. But allow me to present a few in the next paragraph, with several of the examples taken from an excellent essay by David (1996).

One can roughly divide the usage of glycerol into the areas of food additives, cosmetics and personal care, pharmacy, and industrial applications. Because of its hygroscopic properties, glycerol is used as moistening agent for baked goods. It is also added to candies and icings to prevent crystallisation. Water/glycerol mixtures have been shown to prevent crystallisation (Dashnau et al., 2006). Glycerol is used as a solvent for food colors and carrier for extracts and flavouring agents; because of its low volatility, it keeps the flavours from evaporating.

In pharmaceutical products, glycerol's emollient² and demulcent³ properties makes it useful ingredient in salves, and its sweetness is used in tinctures to improve taste. In cosmetics glycerol is a major additive in lotions, creams and toothpaste, used mainly to impart smoothness.

Glycerol's use in chemical industry cover a whole range of products and applications. Glycerol is the main starting material for nitroglycerine, which is used in the manufacture of dynamites and munitions. When reacted with dibasic acids, such as phthalic acid, it makes alkyd resins, an important class of chemicals used in coatings and paints. Glycerol is also used as a levigating agent⁴ to reduce the particle size of a powder on grinding. Glycerol is sprayed on pre-processed tobacco to prevent crumbling, due to its excellent humectant⁵ properties.

That was just a few of glycerol's many uses. In the next section we will look into the oligomers of glycerol, di- and triglycerol, and their possible advantages over glycerol.

2.4 Properties and uses of glycerol's oligomers

This is an appropriate time to define what I mean with the expression "oligomers of glycerol". An oligomer is, in my opinion, a short polymer, generally shorter than ten units. In this report, the term oligomer is used to describe glycerols up to and including pentaglycerol. The term "polyg-

²Emollient: softening and soothing, especially to the skin.

³Demulcent: an oil or salve etc., that soothes inflamed or injured skin.

⁴Levigating agent: auxiliary agent, usually liquid, when grinding powders.

⁵Humectant: a substance that absorbs or helps another substance retain moisture.

lycerols” is a general descriptor encompassing oligomers as well as higher polymers of glycerol.

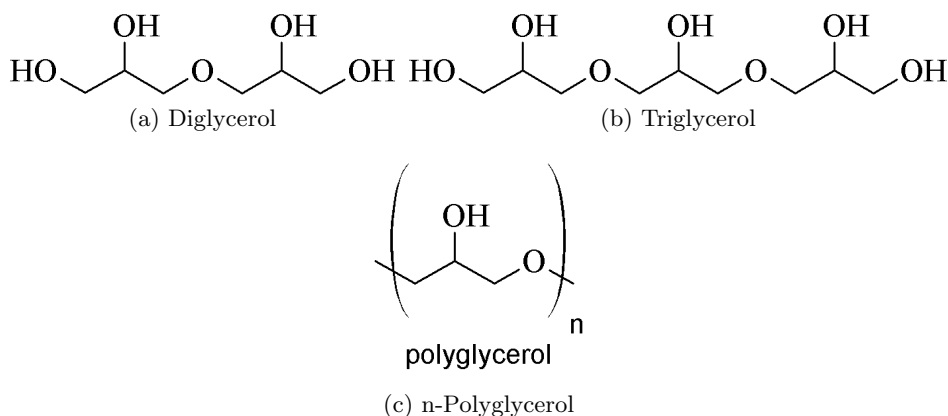


Figure 12. Structure formulas of diglycerol, triglycerol, and a general glycerol polymer. Note that the relative hydroxyl content, and thus hydrophilicity, decreases with chain length.

The viscosity of glycerol oligomers increases with chain length. The use of higher polyglycerols (higher or equal to heptaglycerol) is restricted in food applications (EU Commission, 1998), where the desired polyglycerols are usually di- and triglycerol. A positive effect of increased chain length is decreased volatility, which reduces the evaporation of an added fragrance, e.g., in deodorants and mouthwashes (Solvay Chemicals, Inc., 2004). Other properties that follow chain length is increasing thermal stability and increasing refractive index. Additionally, the humectant property of glycerol is reduced as the chain length increases (since the hydrophilicity decreases).

Polyglycerols as such have a number of applications. Most notably, they are used in essentially all personal care applications, such as skin, oral or hair care products, as either additives or excipients⁶. Also, polyglycerols can be used as reactants in the production of polyurethanes and polyesters (Solvay Chemicals, Inc., 2005).

Although the applications of polyglycerols as such are numerous, as evidenced in the preceding paragraphs, the *polyglycerol esters* find much more widespread application.

Polyglycerol esters (PGE) are non-ionic surfactants. The polyglycerol part, usually made up of a linear di- or triglycerol, is connected to the fatty acid part with an ester linkage. The length and shape of the fatty acid may vary. An important property of polyglycerol esters, and surfactants in general, is the hydrophilic-lipophilic balance (HLB). In the simplest method,

⁶An excipient is an inactive substance used as a carrier for the active ingredients in a formulation.

the ratio is simply calculated as the molar mass of the hydrophilic part divided by the molecule's molar mass. The general behavior of a surfactant in a two-phase system can be predicted from the HLB (Wikipedia, 2007a).

PGEs are used in a whole range of applications. As emulsifiers in food and personal care products, as dispersants, thickeners or solubilizers in products like paints and inks, and as antifogging or antistatic agents in plastic films. Because of their approved use in food (not all PGEs are approved), polyglycerol ester is used as a lubricant for food handling equipment. All in all, polyglycerol esters and other polyglycerol derivatives are used in a whole range of consumer and industrial applications.

2.5 Oligomerisation of glycerol

The obvious way of polymerising glycerol is to simply add several glycerol molecules after each other, building arbitrarily long chains of polyglycerol. This kind of reaction is a condensation, or etherification, where one mole of water is created for every ether linkage formed. Simple as it may seem, condensation of glycerol may lead to a number of different products. Apart from getting linear polymer chains of varying lengths, one will get branched chains and to some extent also cyclic polyglycerols. If the condensation is done in the presence of air, one will also likely get *acrolein*, the simplest aldehyde. Acrolein is toxic and highly volatile, and used extensively as an intermediate in the chemical industry. To prevent formation of acrolein CO_2

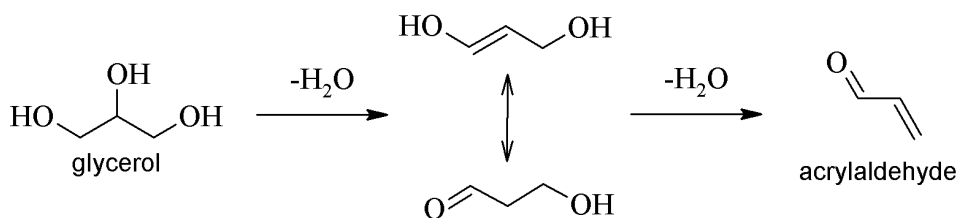


Figure 13. Dehydration of glycerol leading to formation of acrylaldehyde, or acrolein.

or N_2 can be bubbled through the reaction mixture (Márquez-Alvarez et al., 2004).

Polymerisation of glycerol is normally done with a specific linear polyglycerol as the intended product, most commonly, the linear di- and/or triglycerols. As the polyglycerol chain grows (by adding more glycerol units), the viscosity increases and the hydrophilicity decreases.

In the following section we will describe the process of polymerising glycerol by homogeneous catalysis and outline its advantages and drawbacks.

2.5.1 Polymerisation of glycerol by homogeneous catalysis

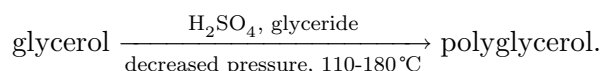
The obstacles encountered on polymerising glycerol using condensation reactions are normally dealt with by reacting glycerol with epichlorohydrin in appropriate ratios to get the intended linear polyglycerol with high yields. This process is employed by Solvay, a large producer of polyglycerols (Solvay S. A., 2005). So the common solution to polymerising glycerol is to abandon the condensation route altogether.



The polymerisation reaction is followed by hydrolysis, neutralisation, and finally purification of the product (Solvay S. A., 2005). This process is also described in detail in a patent by Jakobson and Siemanowski (1990).

A drawback of this method of producing polyglycerols is the introduction of chlorinated reactants which inevitably lead to hydrochloric acid and other chlorinated by-products. Unfortunately, it seems there is no good way to polymerise glycerol homogeneously by simple condensation (etherification) without losing control of the final product's polyglycerol composition.

There is also a pretty old method (Seiden and Martin, 1976), which implements the following reaction:



The polyglycerol composition is regulated by quenching the reaction at an appropriate time with a base that neutralises the catalyst (sulfuric acid). Then unreacted glycerol and cyclic diglycerol is removed by distillation.

An interesting fact noted by Seiden and Martin (1976) is that during the glycerol polymerisation process the initial rate of diglycerol formation is higher than that of the longer chain polymers. Further, the patent author claims, that “the diglycerol content reaches its maximum concentration when about 50 percent of the glycerol has been polymerised. From that point onwards, the rate of diglycerol formation is lower than the rate at which diglycerol is further polymerised. Accordingly, the concentration of diglycerol decreases.” As it is, we can only take this fact for true under the conditions employed by this author. And those conditions are unfortunately rarely used today. Besides, the polyglycerol composition control offered by this method is unsatisfactory given present industrial standards.

2.5.2 Polymerisation of glycerol by heterogeneous catalysis

This field is quite new, at least academically, and it has been hard to find publications describing this matter. Much of the research is probably kept secret for commercial reasons.

But, some work is public, and it has been done by one research group, as it seems. The articles of Clacens et al. (1998), Clacens et al. (2002) and Barrault et al. (2004) describe, in detail, the heterogeneous polymerisation of glycerol, mainly by mesoporous materials but also by some zeolites (mainly ZSM-5).

The experimental setup of the catalytic testing step in this project is largely based on that in the above-mentioned articles.

In these articles, several impregnation metals are used, such as Cs, Mn, Al, Mg, and La. Additionally, these metals were also incorporated in the porous framework (at synthesis). Activity was found to be higher in the impregnated materials, probably partly due to catalysis taking place on soluble metal oxides.

To conclude this section, an industrial heterogeneous catalyst for the selective polymerisation of glycerol is yet to be presented. Which makes this field so much more exciting.

3 Experimental

3.1 Zeolite materials

Ten commercially available zeolites (see Table 1) were chosen for catalytic testing by the project supervisors in cooperation. All Zeolyst and Sigma Aldrich materials had about the same physical properties. The zeolites were white powders, slightly hygroscopic, with particle sizes around a few micrometers (not measured). No binder was incorporated in those materials, i.e., the materials were pure zeolites.

The two zeolites from Tosoh Corporation were supplied by professor Osamu Terasaki at the department. The ultrastable Y differed from the other zeolites mainly by its flow properties. **USY** flowed very smoothly, almost like usual sand, indicating a large particle size. The **ZSM-5P** zeolite is the only one in this test with a binder material incorporated, in this case clay. The clay is used to form the material into cylindrical pellets, about half a centimeter long and a few millimeters in diameter. 20% of the material, by weight, consists of clay. So even though the zeolite itself is very siliceous, the large amount of clay (hydrophilic) reduces the material’s overall silicity significantly.

Table 1. The ten zeolites used as catalysts to oligomerise glycerol.

Framework type	Product name	Si/Al ratio	Producer	Designation
BEA*	CP811C-300	180	Zeolyst	BEA
FAU	CBV 720	15	Zeolyst	FAU-720
FAU	CBV 760	30	Zeolyst	FAU-760
FAU	CBV 600	2.6	Zeolyst	FAU-600
FAU	CBV 780	40	Zeolyst	FAU-780
FAU	Molecular Sieve 13X	2.5	Sigma Aldrich	FAU-13X
FAU	Molecular Sieve Y	2.4	Sigma Aldrich	FAU-900
FAU	USY	1020	Tosoh	USY
MFI	ZSM-5	4200 ^a	Tosoh	ZSM-5P
MOR	CBV 90A	45	Zeolyst	MOR

^aThis value represents the zeolite crystal itself. The material as a whole has an effective silicity that is significantly lower due to the large amount of clay incorporated into the pellets.

3.2 Glycerol and polyglycerols

The glycerol used as reactant during the course of these experiments was glycerol 99%, puriss. Producer: Riedel-de Haën. The chemical is an odour-

less, transparent, clear liquid. Gas chromatography of the chemical showed 99.8% glycerol content.

Table 2. Properties of glycerol, linear diglycerol and linear triglycerol.

	Glycerol	Diglycerol	Triglycerol
Formula	$C_3H_8O_3$	$C_6H_{14}O_5$	$C_9H_{20}O_7$
FW	92.0944 g/mol	166.172 g/mol	240.251 g/mol
Density	1.261 g/cm ³	1.276 g/cm ³ ^a	1.284 g/cm ³ ^a
CAS	56-81-5	59113-36-9	56090-54-1
Boiling point	290 °C	N/A	240 °C ^b
Melting point	17.8 °C	N/A	N/A
Flash point	160 °C	230 °C ^a	281 °C ^b

^aFor commercial grade polyglycerol by Solvay, Solvay S. A. (2005).

^bAt pressure 0.2 mbar, Solvay Chemicals, Inc. (2003).

Pure diglycerol and triglycerol are clear, transparent liquids, although triglycerol may be slightly yellowish (Solvay S. A., 2005).

3.3 Functionalisation of zeolite with metal: impregnation

The mass of zeolite powder (approximately 17 g) was immersed in 50 mL of solvent. The solvent is a solution of the appropriate metal salt, with a controlled concentration, i.e., controlled mass of metal ions, in de-ionised water.

A mass of 17 g (or as close as practically possible) was measured on an analytical balance and transferred into a 250-mL glass bottle (with plastic screw lid). Fifty milliliter of the appropriate metal salt solution was then transferred into the same container, and the contents subsequently shaken to wet all of the zeolite.

The zeolite was then kept immersed in this metal solution while mechanically agitated (with a table-top shaker) to continually keep the zeolite particles dispersed in the solution. The zeolite particles tended to settle unless agitated.

The shaking was halted after 24 hours at the earliest or after 48 hours at the most. The separation of the impregnated zeolite (solid phase) from the excess metal salt solution (liquid phase) was accomplished by centrifugating and decanting. Using conventional filtering was considered, tested, and due to gross practical problems discarded.

Centrifugation was done in an Heraeus Megafuge 1.0, with the dispersion still in the 250-mL glass bottles. After centrifugation for 8 minutes at no less than 2000 rpm the solid phase settles, leaving an almost transparent, colourless liquid phase (except for Fe, which was rust-red). The liquid

was decanted, and the solid impregnated material suffered a heat treatment detailed in the following.

In the normal case one would, subsequent to decanting, have transferred the wet sediment to a crucible for heat treatment. As it was, no programmable furnaces with the proper operational temperature range were available, so a small variation had to be invented.

The wet sediment was put in a stainless steel warming cabinet and the temperature was increased five degrees every five minutes (manually) until reaching 120°C. Now the (usually) completely dry solid “cake” of sedimented zeolite is easy to transfer to a crucible for heat treatment in a furnace (programmed ramping at 1°C/min to 450°C for one hour before self-cooling). Temperature program sketched in Fig. 16.

The impregnated zeolite is now ready to be used as catalyst for the oligomerisation of glycerol.

A couple of notes on the heating treatment: any excess liquid (which is always present in the wet sediment) will leave metal atoms behind on the zeolite outer surface as well as onto the surface of the container. As the intraporous water is evaporated, a mass transfer of water takes place: from the inner cavities and pores to the outer surface of the zeolite particle. As this occurs, any solvated metal ions will follow this “flow” of water molecules, at least to some degree. Therefore a slow heating rate (1 degree per minute) was used to decrease the effect of this mass transfer on the metal ions and keep them inside the pores.

3.3.1 Description of metal salts

The following metal salts were used to transfer the metal ions onto the zeolite framework. They were chosen with the application at hand in mind, thus they all are rather easy dissolved in water (nitrates and acetates) except the molybdenum compound, which needed some dilute ammonia to dissolve.

Magnesium nitrate hexahydrate Chemical by Sigma-Aldrich (237175-100G) at 99%, ACS reagent grade. White powder with large particles. Density 1.636 g/cm³.

Manganese nitrate hexahydrate Chemical by ALDRICH (288640-500G) at 98% purity. Stored at 2 – 8 °C. Large aggregated crystallites. Has a light pink colour. Strongly hygroscopic.

Caesium acetate Chemical by ALDRICH (450154-25G) at 99.99+% purity. Sticky, white powder with small crystallites.

Table 3. Data for the impregnation of the zeolites, as experimentally measured. Ideal values are 17 g of zeolite and 2500 μmol metal per gram zeolite. Each zeolite batch was immersed in 50 mL of metal salt solution.

Zeolite	Caesium		Magnesium		Manganese	
	Zeolite mass [g]	Metal content [mmol/g]	Zeolite mass [g]	Metal content [mmol/g]	Zeolite mass [g]	Metal content [mmol/g]
BEA	17.0008	2499.67	17.0012	2499.21	17.0060	2498.43
MOR	17.0030	2499.67	17.0032	2499.21	17.0018	2498.43
ZSM-5P	17.0066	2499.67	17.0062	2499.21	17.0059	2498.43
USY	17.0097	2499.67	17.0084	2499.21	17.0450	2498.43
FAU-720	17.0028	2499.67	17.0120	2499.21	17.0114	2498.43
FAU-13X	17.0100	2499.59	17.0065	2500.24	17.0095	2499.18
FAU-600	17.0095	2499.59	17.0155	2500.24	17.0064	2499.18
FAU-900	17.0021	2499.59	17.0050	2499.48	17.0030	2499.18

Table 4. Data of metal salts used in experiments.

Metal salt	Formula	CAS	Producer
Magnesium nitrate hexahydrate	$\text{Mg}(\text{NO}_3)_2 \cdot 6 \text{H}_2\text{O}$	13446-18-9	Sigma-Aldrich
Manganese nitrate hexahydrate	$\text{Mn}(\text{NO}_3)_2 \cdot 6 \text{H}_2\text{O}$	15710-66-4	Aldrich
Caesium acetate	CsCH_3COO	3396-11-0	Aldrich
Molybdic acid	MoO_3	7782-91-4	Sigma-Aldrich
Iron nitrate nonahydrate	$\text{Fe}(\text{NO}_3)_3 \cdot 9 \text{H}_2\text{O}$	7782-61-8	Sigma-Aldrich

Molybdic acid Chemical by Sigma-Aldrich (232084-100G). Purity given as “ $\leq 85.0\%$ as MoO_3 ”, ACS reagent grade. White, easily flowing, dense fine-grained powder. Density 3.1 g/cm^3 .

Iron nitrate nonahydrate Chemical by Sigma-Aldrich. Faint lilac colour, with medium-sized particles. Density 1.68 g/cm^3 .

3.4 Heating programs (catalytic tests)

After deciding that heating by electrical mantle would be most convenient, I discovered, upon testing the system, that mixing the reaction components was necessary. Because of the electrical mantle, mixing by magnetic stirrer would need exceptionally strong magnets—which was not available. Thus I had to resort to mechanical mixing, i.e., by propeller.

The experimental setup was as follows. The reaction vessel was a 500 mL three-neck round-bottom flask. The center neck was NS 29/32 and the tilting necks NS 14/23.

The propeller was inserted through the center neck, and the neck was sealed with special glassware. Through the tilted, smaller neck, a stainless steel fitted thermoelement type K and a gas inlet was inserted through a rubber insulation. In the other tilted neck a Dean-Stark piece with attached reflux cooler was fitted.

A steady flow of nitrogen gas was kept during the whole heating cycle and during the cooling period (gas flow was monitored directly in the reaction vessel). Mixing was upheld at slow rates during the heating cycle. Temperature was monitored constantly using a digital thermometer with LCD display. Temperature was logged manually at intervals.

The experiment comprised three kinds of heating programs, or catalytic tests, performed independently of each other in the sense that no material was transferred from one heat program into another (a fresh material sample was used for every test). In the first set of heating programs, from here on referred to as **G1**, the zeolites were immersed in a volume of glycerol held at a temperature of 260°C for one hour (masses of glycerol and catalyst in

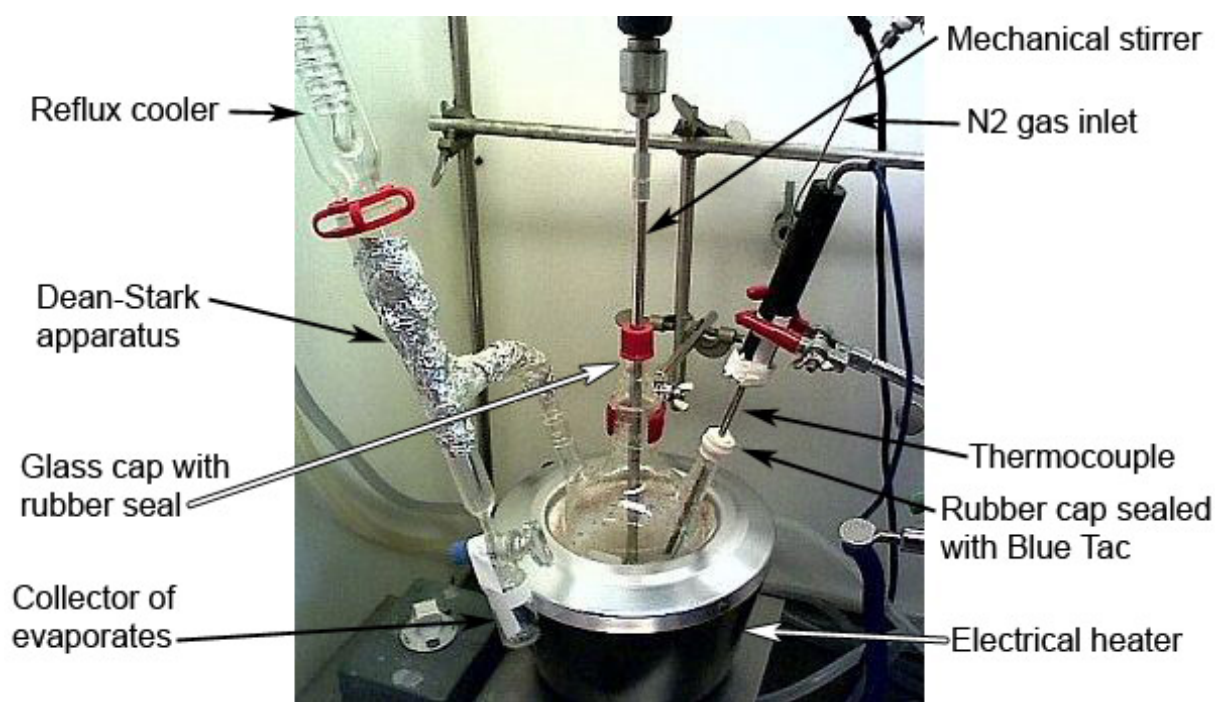


Figure 14. Photo depicting catalytic test setup, common to G1, G6 and G6IM heating programs.

the Appendix). In the second set of heating programs, referred to as **G6**, zeolites were subjected to six hours in glycerol at 260°C. In the third and final set of heating programs, referred to as **G6IM**, a selection of zeolites were impregnated with a metal and subjected to six hours in glycerol at 260°C. Detailed temperature data for all runs is included in the Appendix; in Fig. A.3, Fig. A.4 and Fig. A.5.

So, to conclude, **G1** and **G6** runs were clean zeolites in glycerol for one and six hours, while **G6IM** were impregnated zeolites for six hours.

In the following sections, experimental procedure for each program is detailed further.

3.4.1 G1 heating program

The zeolite was poured into the reaction vessel and the mass determined. A measured amount of glycerol was then added to the reaction vessel so as to give a zeolite to glycerol ratio of approximately 2 mass percent.

The reaction vessel was then mounted with the rest of the reaction setup, as depicted in Fig. 14. Most often, two such setups were running simultaneously, as in Fig. A.2 on page 82.

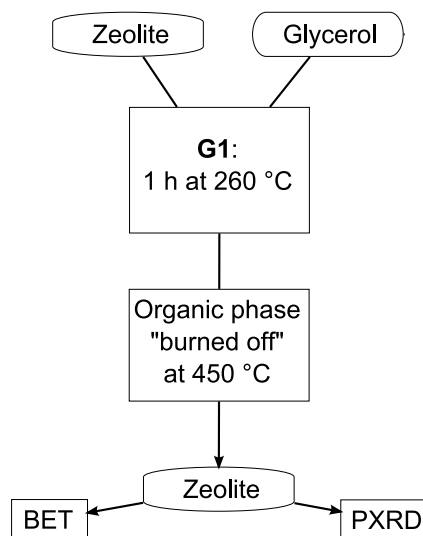


Figure 15. G1 procedure overview as flowchart.

Water cooling, mechanical mixing and gas flow were kept running for some time before heating was started. The heater was set at full effect until temperature reached around 250°C. Heater effect was then controlled manually during the rest of the run to maintain the temperature around 260°C.

When the hour had passed, power was shut off and the heater was physically removed from the reaction vessel. Mixing and gas flow were kept

constant during cooling.

The whole batch was transferred to small sample bottles (scintillation bottles with screw cap) and stored. The zeolite was usually dispersed in the thick organic solution. Within a couple of days, a zeolite phase settled (in most cases).

Most experiments produced at least two scintillation bottles worth of material (zeolite dispersed in thick organic phase), so one bottle was stored and the contents of the other poured into a porcelain crucible and fired in a furnace with closed ventilation. The remaining inorganic material was

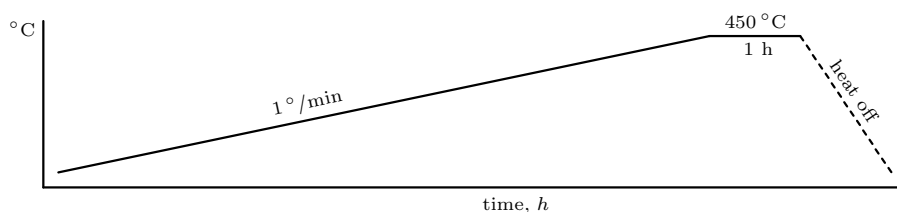


Figure 16. Firing program for calcination of glycerol-treated zeolite, as well as calcination of impregnated zeolite.

collected and subjected to BET (see Table 5) and PXRD (see Appendix) analyses.

3.4.2 G6 heating program

Same procedure initially as described in the previous section.

Temperature was maintained at around 260°C for six hours, then the power was shut off and the heater was physically removed from the reaction vessel. Mixing and gas flow were kept constant during cooling. During cooling a sample of the organic phase (~2 mL with small amounts of zeolite still dispersed) was extracted using a glass-pipette and collected in plastic sample vials (PP, $M_p \approx 160^\circ\text{C}$) for gas chromatography analysis.

The whole batch was then transferred to sample bottles and stored. Most experiments produced at least two scintillation bottles worth of material (zeolite dispersed in thick organic phase), so typically one bottle was stored and the contents of the other poured into a porcelain crucible and fired in a ventilated furnace.

After firing the inorganic material was collected and subjected to BET analysis (see Table 5) and PXRD analysis (see Appendix).

3.4.3 G6IM heating program

Same procedure as in Section 3.4.2. Additionally, samples were taken at 10 minutes, 1 hour and 6 hours. At least one such sample per catalytic test was analysed with gas chromatography and atomic absorption spectroscopy

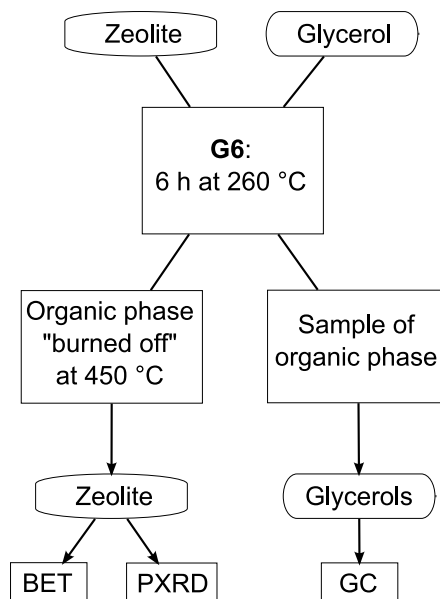


Figure 17. G6 procedure overview as flowchart.

(usually the one at 6 hours). The impregnation was done as described in section 3.3.

3.5 Surface area measurement procedure

Using a Micromeritics ASAP2020™. Following standard procedure for sample preparation. Mass weighed on analytical balance six consecutive times and an average is used in the calculation of sample mass. Degassing was done at vacuum, increasing temperature by 10°C/min to 400°C and holding at that temperature for six hours.

Complete isotherms were collected for the starting materials (Fig. 19). Full isotherm data was used to calculate pore width distributions, using the model: Tarazona NLDFT, Cylindrical Pores, Esf=30.0K. Except for the starting materials, all other samples were subjected to simpler, less time-consuming multipoint BET analysis.

3.6 Powder X-ray diffraction analysis

Most of the diffractograms were recorded with the department's Guinier-Hägg camera (using Cu K_α radiation), operated by Lars Göthe.

The photographic film obtained from the Guinier-Hägg camera was digitised by a LS-20 densitometer (digital transmission reader) connected to an old IBM PC with some even older controller-software.

The obtained transmission file is processed through SCANPI, a software

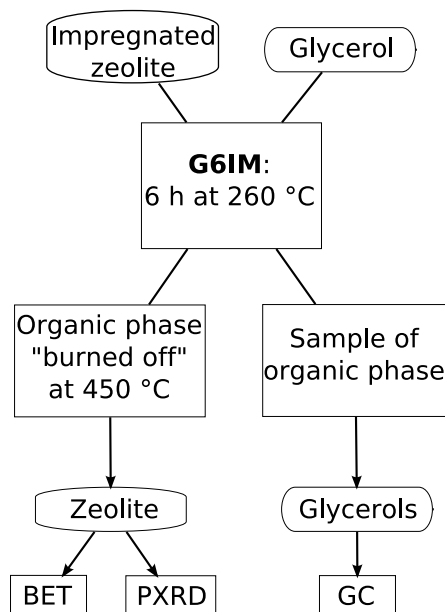


Figure 18. G6IM procedure overview as flowchart.

that analyses the transmission data and produces, among other things, a *.FIN file, which is the XRD profile given as a list of intensity values separated by a given step-length. This file is converted into xy-format by ConvX, a free converter software for XRD file formats (Bowden, 2007). The *.xy-file was plotted with EasyPlot version 4.00 (Spiral Software, 2006).

All other powder X-ray diffractograms were collected using a Huber G670 diffractometer (Huber, 2007), connected to a computer, which plots the diffractogram as a graph, on-screen, directly. Results have varied significantly between the two techniques. The Huber has proven to be more reliable in most cases.

Since zeolites consist of only light elements, rather large amounts were used in each analysis to keep the imaging time feasibly short (30 min) on the Huber. For the impregnated zeolites amounts were reduced, since the introduced metals absorbed strongly. The Mg- and Mn-zeolites proved to be easy to collect diffractograms for, but with Cs the results were awful, probably due to fluorescence. Decreasing the imaging time or decreasing sample amount did not help: the peaks were so broad they could hardly be called peaks. Only Mg- and Mn-zeolite diffractograms were therefore collected.

The Huber produces a digital diffractogram as a raw data file, which can be displayed graphically by the instrument's own software. To be able to reproduce the diffractogram on another computer system, the raw data file has to be converted into a more common format, e.g., as a list of x and y

values.

This conversion is done with a small program, called `gdf2xy`, written by a faculty member at the department. There is no documentation on this program, but it has worked flawlessly so far. The `*.xy`-file is plotted with EasyPlot version 4.00 (Spiral Software, 2006).

3.7 Gas chromatography analysis

The oligomer distribution after each catalytic test was analysed with GC by Perstorp AB at their analytical chemistry lab in Perstorp. The samples were analysed with respect for the following compounds: glycerol (G), linear diglycerol (PG-2), cyclic diglycerol (CPG-2), linear triglycerol (PG-3), cyclic triglycerol (CPG-3), tetraglycerol (PG-4), and pentaglycerol (PG-5). Higher unidentified oligomers and other organic compounds are labelled “rest”.

3.8 Atomic absorption spectroscopy analysis

Atomic absorption spectroscopy, a method used to quantify metal concentration in a solution, was performed for the following metals: Cs, Mg, Mn, Fe, and Mo. AAS was utilised to determine the amount of metal leached from the bifunctional catalyst into the organic solution.

AAS analysis was performed by the analytical chemistry lab in Perstorp. The detection levels for the different metals in solution is, Mg 0.0005 mg/L, Mn 0.01 mg/L, and Cs 0.002 mg/L.

4 Results

The results are presented in tabular or, when applicable, graphical format. Results are presented for each zeolite, one-by-one, in the subsequent sections. In this section (below) the same results are presented for all zeolites alongside each other, to simplify comparisons.

Originally, I intended to characterise the materials by SEM and EDS in addition to the other techniques used. Since good luck has been evading me lately, the electron microscope broke down after just a few analyses. I am glad to say, anyway, that the few EDS data I collected fit well with the other results.

The surface area measurements, mostly five-data-point collections, give the surface area of the material; compared to the area of the starting material, this makes a good measurement of the “fitness” of the catalyst material. The surface areas given below are always BET areas (Brunauer et al., 1938).

The powder X-ray diffractograms (PXRD) shows the degree of crystallinity of the material. It also contains other information, but for practical issues, all we will try to deduce from it is crystallinity, which in turn shows how well the material sustained the test conditions.

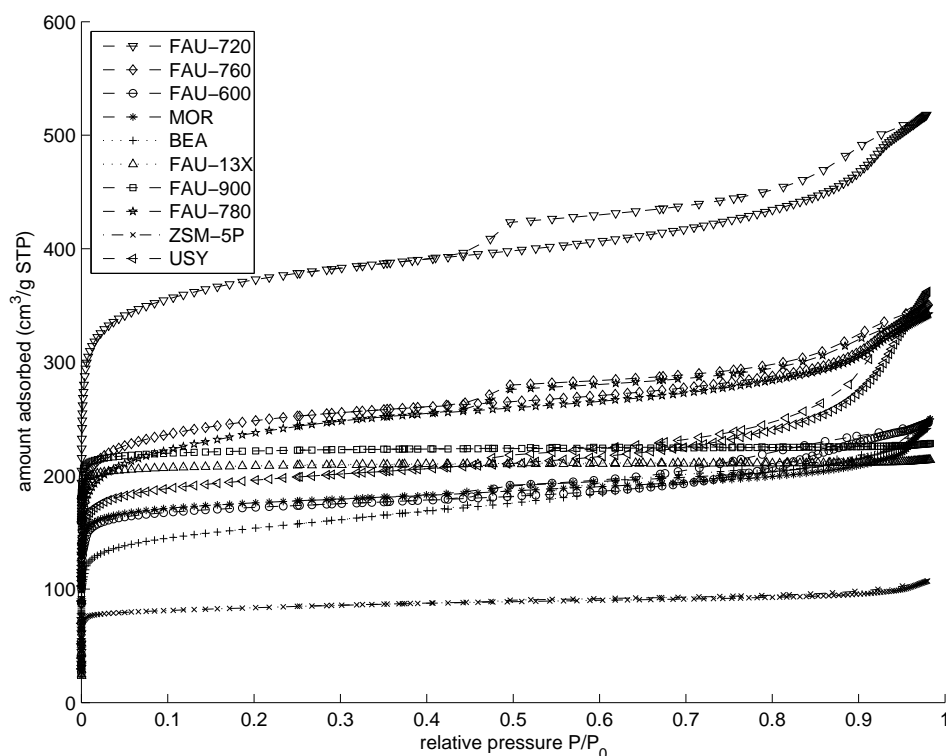


Figure 19. Nitrogen adsorption isotherms for starting materials. For larger image please see Fig. A.1 on page 81.

The complete adsorption isotherms of the ten starting zeolites is presented in Fig. 19 and in a larger version in Fig. A.1. All isotherms display the precipitous rise of the curve at low relative pressures, typical for microporous materials. A few materials, like **FAU-720**, have pronounced hysteresis, which indicates the presence of meso- or macropores as well.

Collecting complete isotherms gives us the possibility to apply DFT (density functional theory) to calculate the pore width distribution. Please see Figures A.6, A.7, and A.8. It is interesting to see, that the pore width distributions do vary quite a lot among these commercial zeolites, with some of them, like **FAU-13X**, **MOR** and **BEA**, having outstanding uniformity, while others, as **USY** and the rest of the faujasites, show very poor pore size uniformity. And as expected, the only bound zeolite among them, **ZSM-5P**, displays the widest pore size distribution.

Table 5. Measured BET surface areas (m^2/g) of zeolites, before and after glycerol heating cycles. Sorted by clean surface area, descending.

Zeolite	Clean	G1 -treated	G6 -treated
FAU-720	1382 ± 10	532 ± 7.5	508 ± 7.4
FAU-760	920 ± 6.5	525 ± 5.7	732 ± 6.3
FAU-780	874 ± 4.6	1024 ± 11	761 ± 7.0
FAU-900	835 ± 9.9	101 ± 0.32	205 ± 0.35
FAU-13X	785 ± 9.4	57.9 ± 0.25	262 ± 2.5
USY	729 ± 6.5	650 ± 8.8	761 ± 7.3
MOR	657 ± 6.5	496 ± 10	775 ± 5.3
FAU-600	643 ± 6.6	443 ± 6.2	476 ± 5.0
BEA	567 ± 3.5	859 ± 11	679 ± 7.6
ZSM-5P	311 ± 3.0	282 ± 2.2	322 ± 3.7

Table 5 shows surface areas of all zeolites as (i) untreated, clean materials, (ii) **G1**-treated (one hour monofunctional catalytic test), and as (iii) **G6**-treated (six hours monofunctional catalytic test). The six zeolites with the largest surface area are all of the faujasite framework type. **ZSM-5P** featured the smallest surface area, which is expected since it is the only material pressed into pellets, and belongs to the MFI framework type.

The overall trend in Table 5 is thus what we would expect. The three-dimensional, supercage framework of FAU has larger surface area than the two-dimensional, essentially cage-free frameworks of **ZSM-5P** (MFI) and mordenite (MOR). Zeolite beta (**BEA***), which also has a three-dimensional, large-pore framework, is oddly out of place. This could be due to experimental error, since the surface areas of the **G1**- and **G6**-treated **BEA** are substantially larger.

The surface area of the impregnated zeolites (see Table 6) was on av-

Table 6. Experimentally determined surface areas (m^2/g) of impregnated zeolites. Values acquired by 5-point BET analysis.

Zeolite	Measured surface area [m^2/g]		
	Mg	Mn	Cs
FAU-720	643 ± 14		
FAU-13X	422 ± 10		
USY	608 ± 13		
MOR	442 ± 9.8		
FAU-600	545 ± 13	561 ± 13	245 ± 5.5
BEA	795 ± 15		
ZSM-5P	260 ± 3.8		

erage about 70% of the clean zeolite. The only exception is **BEA**, which boosted its area by 40% after impregnation. The lack of values for most manganese and caesium zeolites is because surface area measurements were never done, because of high usage of the surface measurement instrument at the department. Compared to the surface areas of the clean zeolites (Table 5), all impregnated zeolites have slightly lower areas, except for **BEA**, which only strengthens my doubt in the “clean” value.

The fact that the surface area actually decreases, is probably due to intracrystalline metal deposits (in the best case) or extracrystalline aperture blocking (in the worst case). There is no definite way of telling which without performing electron microscopy.

Table 7. Concentration of metal ions (ppm) in organic phase after **G6IM**-treatment, except for Fe and Mo values, which would correspond to a **G1IM**-treatment. Data obtained by AAS analyses.

Material	Mg metal per kg of organic phase, or ppm (mass)				
	Cs	Mg	Mn	Fe	Mo
BEA	$1.96 \cdot 10^4$	738	400		
MOR	$4.2 \cdot 10^3$	470	457		
ZSM-5P	$2.0 \cdot 10^3$	225	333		
USY	$3.5 \cdot 10^3$	783	694		
FAU-720	$1.9 \cdot 10^3$	665	294		
FAU-900	$1.9 \cdot 10^3$	194	370		
FAU-600	$1.8 \cdot 10^3$	134	195	$1.7 \cdot 10^3$	$2.6 \cdot 10^3$
FAU-13X	$2.7 \cdot 10^3$	165	387		

Caesium oxide (assuming we have formed the oxide) is clearly most easily

dissolved in the glycerol/polyglycerol phase. The average over all zeolites was 4700 mg Cs per kg of organic phase (or 6.7 mass percent, cf. Table 8). The Fe and Mo impregnations were only done for zeolite **FAU-600**, so they are a little hard to draw any conclusions from, other than that they are of the same magnitude as Cs-leaching. The average magnesium leaching is two and a half times larger than that for manganese.

Table 8. Mass percent of metal leached, relative to original metal load (by impregnation), after **G6IM**-treatment. Fe and Mo values correspond to a **G1IM**-treatment.

Material	Mass percent leached				
	Cs	Mg	Mn	Fe	Mo
USY	5.2%	6.1%	2.3%		
ZSM-5P	2.9%	1.8%	1.1%		
BEA	28.2%	5.7%	1.3%		
MOR	5.9%	3.7%	1.6%		
FAU-720	2.6%	5.0%	1.0%		
FAU-600	2.6%	1.0%	0.7%	5.5%	5.5%
FAU-13X	3.6%	1.3%	1.4%		
FAU-900	2.5%	1.5%	1.4%		
Average	6.7%	3.3%	1.3%	–	–

Comparing the amount of leached metal of the different zeolites (as in Table 7) has to be done with care, since the mass of impregnated zeolite used in the catalytic tests was not identical (but the substance amount was, cf. Table 3). To facilitate such comparisons, Table 8 shows the mass percentage of the loaded metal that has leached into the organic phase.

These mass percentages were calculated from the quantities determined experimentally by AAS (Table 7), and the known metal loading quantities presented in Table 3.

As Table 8 shows, leaching is overall moderate, and the average leaching for a metal over all zeolites tend to follow the metal oxide solubilities in water.

Although the very high leaching of Cs from **BEA** corresponds to a high diglycerol concentration (cf. Table 10), this is not a general trend. In general, mass percentage leached is uncorrelated to diglycerol formation.

Next we move on to the glycerol oligomer distributions, as determined by gas chromatography. Table 9 presents the results for the ten monofunctional materials.

The gas chromatography method used for the analyses is less accurate for high glycerol concentrations. So samples with high reactant concentration might have a total percentage which deviates slightly from 100%.

Table 9. Glycerol composition after **G6**-treatment (6 h at 260 °C). Normalised values of glycerol composition in parenthesis. Data obtained by GC analyses.

Zeolite	Si/Al	Mass percentages			
	ratio	G	PG-2	PG-3	Rest
USY	1020	80.5 (88.9)	9.6 (5.5)	1.0 (0.6)	8.9 (5.1)
ZSM-5P	4200	89.7 (93.4)	3.4 (2.2)	0	6.9 (4.4)
BEA	180	86.8 (92.2)	4.9 (2.9)	0	8.3 (4.9)
MOR	45	79.0 (87.2)	9.1 (5.6)	0.9 (0.6)	11.0 (6.7)
FAU-780	40	15.2 (46.9)	10.2 (6.4)	5.4 (3.4)	69.2 (43.3)
FAU-760	30	36.2 (64.6)	16.3 (9.1)	5.8 (3.2)	41.7 (23.2)
FAU-720	15	91.0 (95.1)	5.1 (2.8)	0	3.9 (2.1)
FAU-600	2.6	80.9 (88.1)	11.4 (7.1)	1.1 (0.7)	6.6 (4.1)
FAU-13X	2.5	51.4 (73)	25.5 (14.2)	6.1 (3.4)	17.0 (9.4)
FAU-900	2.4	81.7 (88.9)	10.6 (6.5)	0	7.7 (4.7)

The so called “normalised values” (given in parenthesis) are a construct of my own, constructed to account for the fact that the amounts of zeolite and glycerol was not identical throughout all tests. To compensate for that effect, and make the glycerol percentages directly comparable, the normalised values were invented. The calculation of the normalised values rests on the assumption that the change in catalyst mass is linearly correlated to the change in glycerol/polyglycerol ratio.

For example, **FAU-900** holds a glycerol amount of 81.7%, diglycerol amount of 10.6% and 7.7% of higher polyglycerols. All values are original sample values. The “normalised” values are calculated as in the following. The mass of zeolite used in this catalytic test was 1.64 g, and the mass of glycerol at start was 74.8 g. Now we “normalise” the zeolite mass to exactly one gram. All product percentages are thus multiplied by a factor $\frac{1}{m_{zeol}}$, and the reactant percentage is calculated as

$$\text{norm. reactant m}\% = 1 - \left(\frac{1}{m_{zeol}} (1 - \mathbf{F}_{glyc}) \right)$$

where m_{zeol} is the original zeolite mass, and \mathbf{F}_{glyc} the glycerol mass fraction (0.817 for **FAU-900**). Essentially, I am just assuming a linear relationship between catalyst mass and mass of products formed, and adjusting the mass of the reactant in the other direction. I cannot prove the validity of this assumption; in fact, I know it is not the whole truth. Several other factors may affect the conversion of the catalyst, other than mass. But this “normalisation”, as I like to call it, is a simple way of correcting for the largest factor, which is the catalyst mass.

The overall trend in Table 9 with respect to PG-2 conversion is that the faujasites, except for **FAU-720**, hold the top six positions. Among those, **FAU-600** and **FAU-900** are the most selective with respect to diglycerol, and they also have low amounts of higher polyglycerols. On the other hand, **FAU-760** and **FAU-780** show very large amounts of higher polyglycerols formed (23.2% and 43.3%, respectively) and bad PG-2 selectivity. So, among the faujasites, the more acidic **FAU-600** and **FAU-900** performed significantly better than the less acidic **FAU-760** and **FAU-780**. **FAU-720**, which lies in between these extremes regarding acidity, showed good selectivity but low conversion.

Tables 10, 11 and 12 presents the glycerol/polyglycerol composition after **G6IM**-treatment for caesium, magnesium and manganese impregnated zeolite materials.

The results show that compared to the clean zeolite, addition of metal does not increase the oligomerisation of glycerol independently of the zeolite. Notably, **MOR**, **FAU-600** and **FAU-13X** performed worse with metal than without. **MOR** and **FAU-600** are actually almost equally bad for all metals, while **FAU-13X** shows high diglycerol concentration for Mg and Mn, and low concentration for Cs.

Two zeolites, **FAU-900** and **BEA**, showed improved performance with all metals, especially with Cs. **BEA** performed especially well with Cs, increasing the diglycerol mass percentage after six hours from 2.9% to 14.7% (normalised values). On the downside, leaching of Cs from **BEA** was extensive, suggesting that the catalysis could very well have been taking place on Cs_2O particles outside the zeolites.

It is really encouraging though, to see that higher oligomers and cyclic by-products form in very low concentrations overall.

Tables 10, 11 and 12, on the next page, show the glycerol/polyglycerol composition of the Cs, Mg and Mn impregnated zeolites. Iron and molybdenum values are presented in section 4.3.

Table 10. Glycerol composition by Cs-**G6IM** after 6 h. Zeolites sorted by descending Si/Al-ratio. Normalised values in parenthesis. Data obtained by GC analyses.

Material	G	PG-2	CPG-2	PG-3	CPG-3	PG-4	PG-5
Cs- USY	80.0 (88.9)	16.5 (9.2)	0.3 (0.2)	1.4 (0.8)	0	0.2 (0.1)	0.1 (0.1)
Cs- ZSM-5P	92.0 (95.6)	5.7 (3.2)	0	0.3 (0.2)	0	0	0.2 (0.1)
Cs- BEA	52.0 (74.7)	28.0 (14.7)	0.5 (0.2)	3.3 (1.7)	0.3 (0.2)	0.7 (0.4)	0.3 (0.2)
Cs- MOR	90.0 (94.7)	7.6 (4.0)	0	0.4 (0.2)	0	0	0.2 (0.1)
Cs- FAU-720	92.0 (95.6)	7.3 (4.1)	0	0.3 (0.2)	0	0	0.2 (0.1)
Cs- FAU-600	90.0 (94.1)	7.9 (4.6)	0	0.5 (0.3)	0	0	0.2 (0.1)
Cs- FAU-13X	0.4 (37.8)	3.7 (2.3)	7.4 (4.6)	4.2 (2.6)	2.1 (1.3)	6.0 (3.7)	7.1 (4.4)
Cs- FAU-900	73.0 (84.1)	20.0 (11.8)	0.4 (0.2)	2.1 (1.2)	0.2 (0.1)	0.2 (0.1)	0.2 (0.1)

Table 11. Glycerol composition by Mg-**G6IM** after 6 h. Zeolites sorted by descending Si/Al-ratio. Normalised values in parenthesis. Data obtained by GC analyses.

Material	G	PG-2	CPG-2	PG-3	CPG-3	PG-4	PG-5
Mg- USY	89.0 (94.2)	5.0 (2.6)	0	0.4 (0.2)	0	0.2 (0.1)	0.3 (0.1)
Mg- ZSM-5P	86.0 (92.2)	3.3 (1.8)	0	0.2 (0.1)	0.1 (0.1)	0	0.1 (0.1)
Mg- BEA	93.0 (96.1)	6.0 (3.3)	0	0.3 (0.2)	0	0	0.2 (0.1)
Mg- MOR	95.0 (97.4)	5.0 (2.6)	0	0.3 (0.2)	0	0	0.1 (0.1)
Mg- FAU-720	93.0 (95.9)	4.5 (2.6)	0	0.3 (0.2)	0	0	0.2 (0.1)
Mg- FAU-600	91.0 (94.7)	5.5 (3.2)	0	0.3 (0.2)	0.2 (0.1)	0	0.2 (0.1)
Mg- FAU-13X	65.0 (80.6)	24.0 (13.3)	0.5 (0.3)	3.7 (2.1)	0.2 (0.1)	0.7 (0.4)	0.2 (0.1)
Mg- FAU-900	82.0 (90.0)	14.0 (7.8)	0	0.9 (0.5)	0	0	0.2 (0.1)

Table 12. Glycerol composition by Mn-**G6IM** after 6 h. Zeolites sorted by descending Si/Al-ratio. Normalised values in parenthesis. Data obtained by GC analyses.

Material	G	PG-2	CPG-2	PG-3	CPG-3	PG-4	PG-5
Mn- USY	91.0 (94.7)	5.1 (3.0)	0	0.3 (0.2)	0	0.2 (0.1)	0.3 (0.2)
Mn- ZSM-5P	91.0 (95.0)	4.5 (2.5)	0	0.3 (0.2)	0	0	0.4 (0.2)
Mn- BEA	95.0 (97.2)	5.2 (2.9)	0	0.3 (0.2)	0	0	0.1 (0.1)
Mn- MOR	95.0 (97.2)	4.6 (2.6)	0	0.3 (0.2)	0	0.1 (0.1)	0.2 (0.1)
Mn- FAU-720	93.0 (95.6)	4.0 (2.5)	0	0.2 (0.1)	0.2 (0.1)	0	0.2 (0.1)
Mn- FAU-600	89.0 (93.1)	6.2 (3.9)	0	0.4 (0.3)	0.2 (0.1)	0	0.2 (0.1)
Mn- FAU-13X	69.0 (82.8)	23.0 (12.8)	0.4 (0.2)	2.9 (1.6)	0	0.3 (0.2)	0.2 (0.1)
Mn- FAU-900	80.0 (89.5)	17.0 (8.9)	0	1.4 (0.7)	0	0	0.2 (0.1)

4.1 Zeolite BEA

The trend in surface areas for **BEA** is a bit hard to understand in a logical way. The material clearly possesses a large surface area, independent of the treatment undergone by the material.

One would expect the surface area to decrease after a **G**-treatment, if for no other reason than at least because of coking. But we also calcine the material after the **G**-treatment to burn off the coke. This calcination may also lead to crystallite growth by sintering, which could affect the surface area. Although I find it really hard to envisage how sintering could lead to surface area increase.

The effect of larger surface area for the treated materials is most probably due to an experimental error in the determination of the clean material's value. This theory is supported by the fact that the other 12-member ring pore zeolites (FAU, MOR) all have larger surface areas.

The pore width distribution of the clean material, Fig. A.7a, shows that **BEA** has a very uniform pore size distribution, only surpassed by **FAU-13X** and **MOR**. The peak position in Fig. A.7a corresponds to a pore width of 6.5 Å.

Table 13. BEA BET data.

Zeolite	Measured surface area [m ² /g]			
	Clean	G1 -treated	G6 -treated	G6IM (Mg)
BEA	567 ± 3.5	859 ± 11	679 ± 7.6	795 ± 15

Table 14. Leaching of metal into organic phase after **G6IM**-treatment, given as part metal per million parts organic phase (determined by AAS), and as percentage of the metal mass loaded on the material.

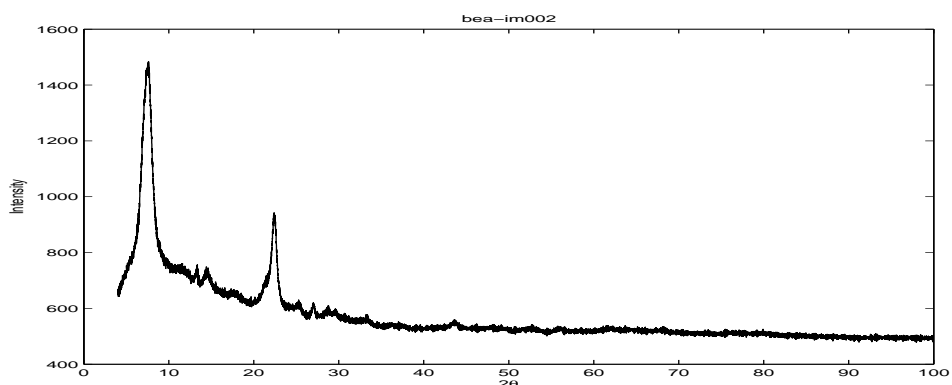
BEA	Cs	Mg	Mn
Mg metal/kg org. phase	19600	738	400
Mass percentage	28.2%	5.7%	1.3%

Table 14 shows that Cs leaches much more than Mg, which leaches more than Mn. **BEA** is the most siliceous zeolite among the ten candidates, and the atomic absorption spectroscopy results (Table 7) show that **BEA** is the most “leachy” zeolite. So, in this case, silicity corresponds to high leaching.

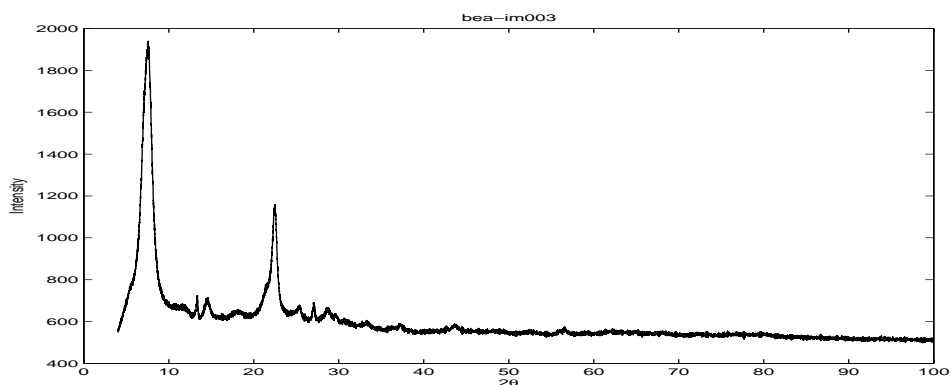
The detailed glycerol composition data (tables 15, 16, 17) collected for this zeolite shows that essentially no conversion takes place until after one hour of reaction. At six hours, the glycerol oligomer composition has changed insignificantly for all materials except the Cs-impregnated, which

cause extensive oligomerisation, creating diglycerol (14.7%), small amounts of identifiable oligomers (total 2.7%), as well as quite a lot of other organic compounds (7.8%).

Powder X-ray diffractograms for Mg-**BEA** and Mn-**BEA** are presented in Fig. 20. The Cs-impregnated zeolite caused lots of fluorescence with the Cu radiation source used; rendering the diffractogram useless. Additional powder X-ray diffractograms are shown in Fig. A.9.



(a) Mg-**BEA**



(b) Mn-**BEA**

Figure 20. Impregnated **BEA** PXRD diffractograms.

Table 15. Glycerol composition by **BEA** zeolites after 10 min. Normalised values in parenthesis.

Material	G	PG-2	CPG-2	PG-3	CPG-3	PG-4	PG-5	Rest
BEA	-	-	-	-	-	-	-	-
Cs-BEA	99.7 (99.8)	0.3 (0.2)	0	0	0	0	0	0
Mg-BEA	99.8 (99.9)	0.1 (0.1)	0	0	0	0	0	0.1 (0.1)
Mn-BEA	99.8 (99.9)	0.1 (0.1)	0	0	0	0	0	0.1 (0.1)

Table 16. Glycerol composition by **BEA** zeolites after 1 h. Normalised values in parenthesis.

Material	G	PG-2	CPG-2	PG-3	CPG-3	PG-4	PG-5	Rest
BEA	-	-	-	-	-	-	-	-
Cs-BEA	99.0 (99.5)	1.4 (0.7)	0	0	0	0	0	-0.4 (-0.2)
Mg-BEA	99.0 (99.4)	1.4 (0.8)	0	0	0	0	0.17 (0.1)	-0.6 (-0.3)
Mn-BEA	98.0 (98.9)	1.2 (0.7)	0	0	0	0.12 (0.1)	0	0.7 (0.4)

Table 17. Glycerol composition by **BEA** zeolites after 6 h. Normalised values in parenthesis.

Material	G	PG-2	CPG-2	PG-3	CPG-3	PG-4	PG-5	Rest
BEA	86.8 (92.2)	4.9 (2.9)	-	0	-	-	-	8.3 (4.9)
Cs-BEA	52 (74.7)	28 (14.7)	0.45 (0.2)	3.3 (1.7)	0.33 (0.2)	0.72 (0.4)	0.33 (0.2)	14.9 (7.8)
Mg-BEA	93 (96.1)	6 (3.3)	0	0.3 (0.2)	0	0	0.19 (0.1)	0.5 (0.3)
Mn-BEA	95 (97.2)	5.2 (2.9)	0	0.3 (0.2)	0	0	0.14 (0.1)	-0.6 (-0.4)

4.2 Zeolite FAU-13X

The measured surface area of the material (Table 18) shows a distinct decrease for all treated materials (compared to the clean). As with all other zeolites, the value for the impregnated zeolite surface area (422 m²/g) is measured *before* **G6IM**-treatment. The idea is to show how the metal oxide formation affects the surface area (compared to the clean zeolite). In this case, the impregnated material has roughly half the area of the clean zeolite. But even the impregnated material still has a large surface area. The **G1**- and **G6**-treated materials seem to have suffered a large reduction of surface area.

In the appendix Fig. A.7b, the pore width distribution of the clean **FAU-13X** zeolite is shown (peak at 6.5 Å). **FAU-13X** is clearly the zeolite with the best pore size uniformity among the ten tested. That indicates lack of crystallite aggregation, since that would lead to some meso- and macropore formation. This, subsequently, leads to a possible explanation for the large surface area reduction of the **G**-treated materials.

The lack of extensive crystallite aggregation means every zeolite crystallite is exposed to the glycerol phase, leading to an effective coking process in all pores or pore mouths. The clogged pores would reduce the surface area significantly.

Table 19 shows a curious dip in PG-2 value for the Cs-impregnated material. It seems this material converts the glycerol into higher oligomers and/or other organic substances to a large degree. Overall, the monofunctional material shows better results than the impregnated (bifunctional) material.

Regarding the leaching of metal after **G6IM**-treatment (Table 20), **FAU-13X** displays the same trend as most other zeolites. The relative leaching is largest for Cs, and slightly smaller for Mg and Mn, although the order between them is flipped.

Fig. 21 shows diffractograms collected with the Huber PXRD instrument. The diffractograms were analysed using GUPPI and PIRUM and the result compared with reference metal-oxide powder diffraction files. No distinct metal-oxide peaks were found in the diffractograms. Additional powder X-ray diffractograms are shown in Fig. A.10.

Table 18. FAU-13X BET data.

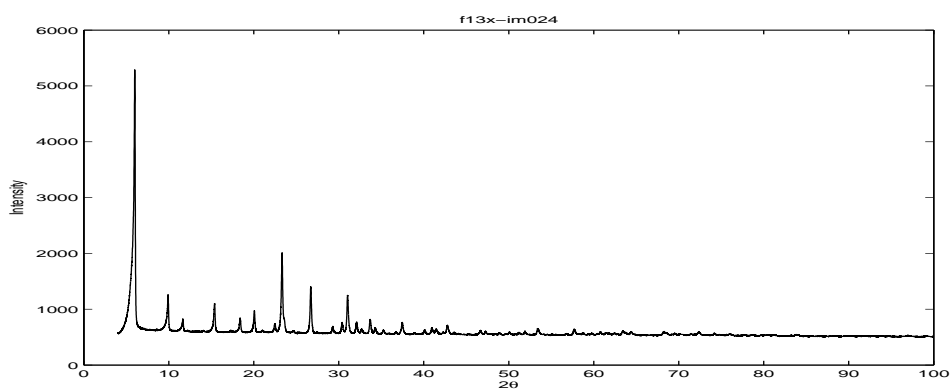
		Measured surface area [m ² /g]		
Zeolite	Clean	G1-treated	G6-treated	Mg-FAU-13X
FAU-13X	785 ± 9.4	57.9 ± 0.25	262 ± 2.5	422 ± 10

Table 19. Glycerol composition by FAU-13X zeolites after 6 h. Normalised values in parenthesis.

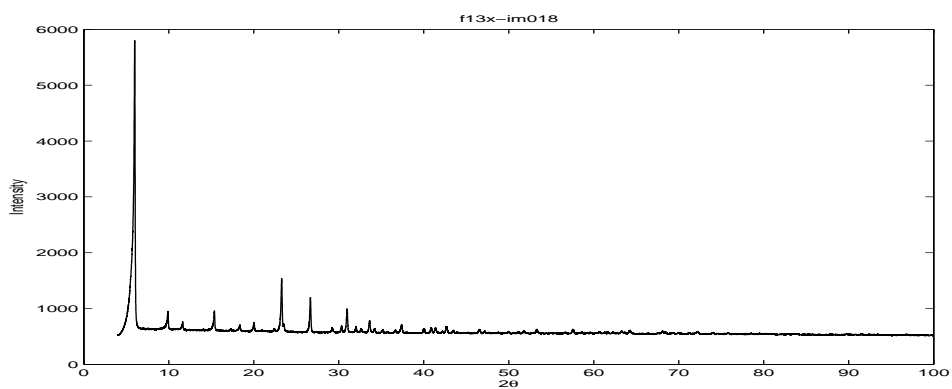
Material	G	PG-2	CPG-2	PG-3	CPG-3	PG-4	PG-5	Rest
FAU-13X	51.4 (73.0)	25.5 (14.2)	–	6.1 (3.4)	–	–	–	17.0 (9.4)
Cs-FAU-13X	0.4 (37.8)	3.7 (2.3)	7.4 (4.6)	4.2 (2.6)	2.1 (1.3)	6.0 (3.7)	7.1 (4.4)	69.2 (43.3)
Mg-FAU-13X	65.0 (80.6)	24.0 (13.3)	0.5 (0.3)	3.7 (2.1)	0.2 (0.1)	0.7 (0.4)	0.2 (0.1)	5.7 (3.2)
Mn-FAU-13X	69.0 (82.8)	23.0 (12.8)	0.4 (0.2)	2.9 (1.6)	0	0.3 (0.2)	0.2 (0.1)	4.2 (2.3)

Table 20. Leaching of metal into organic phase after G6IM-treatment, given as part metal per million parts organic phase (determined by AAS), and as percentage of the metal mass loaded on the material.

FAU-13X		Cs	Mg	Mn
Mg metal/kg org. phase	2700	165	387	
Mass percentage	3.6%	1.3%	1.4%	



(a) Mg-FAU-13X



(b) Mn-FAU-13X

Figure 21. Impregnated FAU-13X PXRD.

4.3 Zeolite FAU-600

This zeolite was impregnated with five different metals: caesium, magnesium, manganese, iron, and molybdenum. The surface area of the three first, as well as of the **G**-treated and the clean material is shown in Table 21. The impregnated Mg and Mn materials show similar areas, while the area of the Cs-impregnated material is significantly smaller. The simple explanation is that Cs is the larger metal atom among the selected metals. Since an equimolar amount of metal was impregnated in all zeolites, the largest atom should occupy the largest space. The highest peak in the pore width distribution (Fig. A.6d) corresponds to 7.5 Å.

In Table 22, the leaching of metal into the organic phase for different metals is shown. Fe and Mo leach extensively considering they were only subjected to one hour of treatment.

Tables 23 and 24 show the glycerol composition for **FAU-600** and its impregnated variants. The clean material performs slightly better than the Cs, Mg and Mn impregnated materials, which are almost equal with respect to final composition after six hours. Fe and Mo performed best, with Fe the better of the two thanks to its higher selectivity low oligomers (Mo gives about 20% of higher oligomers and other unidentified substances).

Fig. 22 displays the powder X-ray diffractograms for the impregnated materials. Although Fig. 22a and Fig. 22b are bad quality, it is evident that all materials are crystalline and have the same peak positions, but slightly different relative intensities. Which is expected since they all have the same structure. Again, no distinct metal peaks could be identified. Additional powder X-ray diffractograms are shown in Fig. A.11.

Table 21. FAU-600 BET surface areas (m²/g).

Clean	G1 -treated	G6 -treated	Impregnated zeolite		
			Mg	Mn	Cs
643 ± 6.6	443 ± 6.2	476 ± 5.0	545 ± 13	561 ± 13	245 ± 5.5

Table 22. Leaching of metal into organic phase after **G6IM**-treatment (except for Fe and Mo, which correspond to a **G1IM**-treatment), given as part metal per million parts organic phase (determined by AAS), and as percentage of the metal mass loaded on the material.

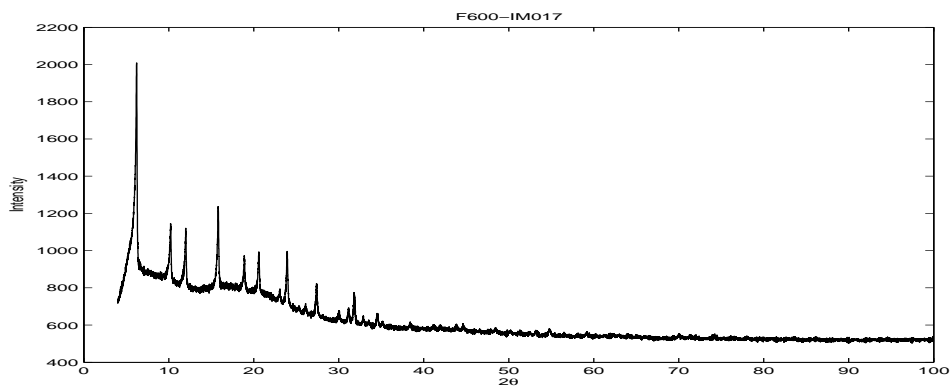
FAU-600	Cs	Mg	Mn	Fe	Mo
Mg metal/kg org. phase	1800	134	195	1700	2600
Mass percentage	2.6%	1.0%	0.7%	5.5%	5.5%

Table 23. Glycerol composition by **FAU-600** zeolites after 1 h. Normalised values in parenthesis.

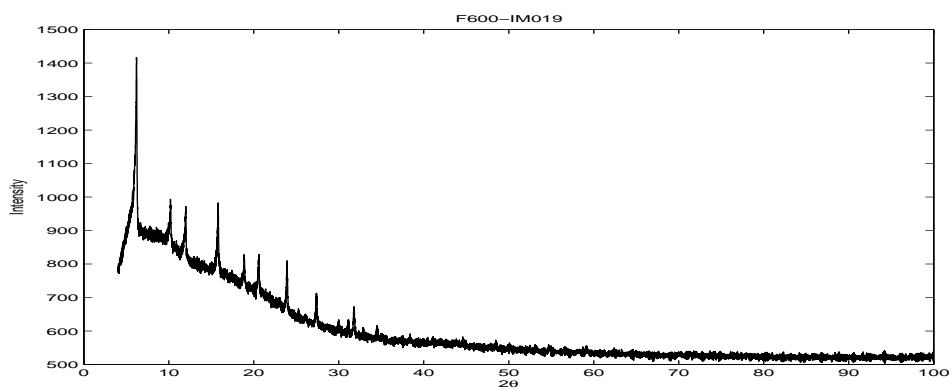
Material	G	PG-2	CPG-2	PG-3	CPG-3	PG-4	PG-5	Rest
FAU-600	-	-	-	-	-	-	-	-
Cs-FAU-600	-	-	-	-	-	-	-	-
Mg-FAU-600	-	-	-	-	-	-	-	-
Mn-FAU-600	-	-	-	-	-	-	-	-
Fe-FAU-600	75.0 (86.1)	17.9 (9.9)	0.4 (0.2)	2.1 (1.2)	0.3 (0.2)	0.3 (0.2)	0	4.0 (2.2)
Mo-FAU-600	38.8 (61.8)	19.4 (12.1)	1.3 (0.8)	4.0 (2.5)	1.1 (0.7)	1.1 (0.7)	0.3 (0.2)	34.1 (21.3)

Table 24. Glycerol composition by **FAU-600** zeolites after 6 h. Normalised values in parenthesis.

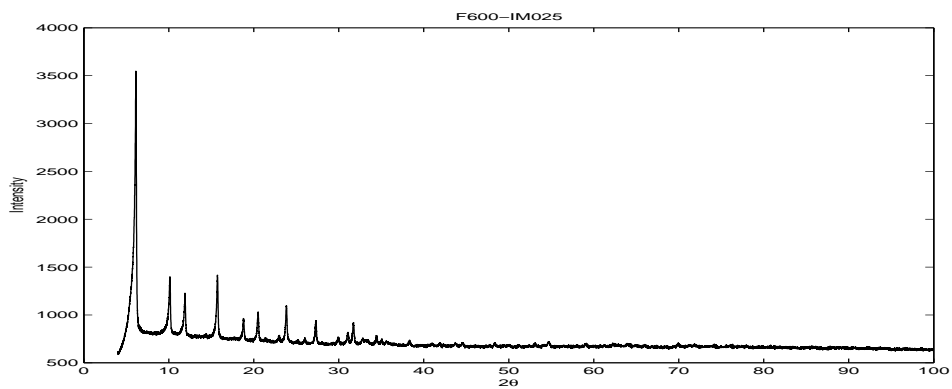
Material	G	PG-2	CPG-2	PG-3	CPG-3	PG-4	PG-5	Rest
FAU-600	80.9 (88.1)	11.4 (7.1)	-	1.1 (0.7)	-	-	-	6.6 (4.1)
Cs-FAU-600	90.0 (94.1)	7.9 (4.6)	0	0.5 (0.3)	0	0	0.2 (0.1)	1.4 (0.8)
Mg-FAU-600	91.0 (94.7)	5.5 (3.2)	0	0.3 (0.2)	0.2 (0.1)	0	0.2 (0.1)	2.8 (1.7)
Mn-FAU-600	89.0 (93.1)	6.2 (3.9)	0	0.4 (0.3)	0.2 (0.1)	0	0.2 (0.1)	4.0 (2.5)
Fe-FAU-600	-	-	-	-	-	-	-	-
Mo-FAU-600	-	-	-	-	-	-	-	-



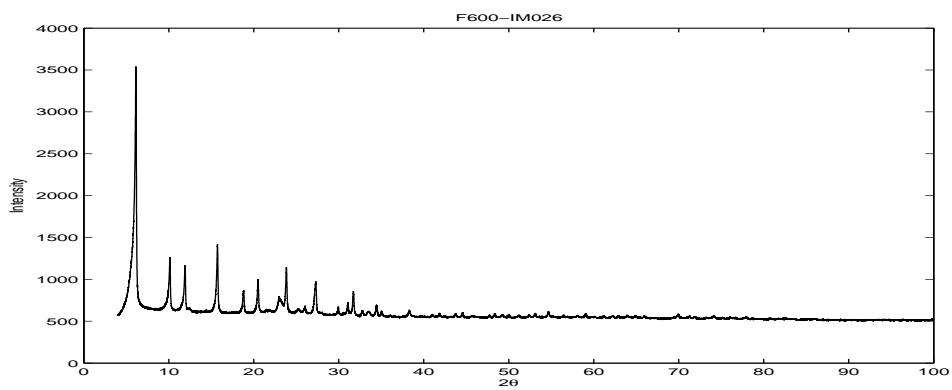
(a) Mg-FAU-600



(b) Mn-FAU-600



(c) Fe-FAU-600



(d) Mo-FAU-600

Figure 22. Impregnated FAU-600 PXRD.

4.4 Zeolite FAU-720

FAU-720 shows good BET area results, with very high surface area for the clean material (1380 m²/g), and less than 40% of that area for the **G**-treated material. The impregnated material (three materials were impregnated, but only one of them was analysed to reduce instrument time) had a surface area about 50% of the clean material's. The extremely high surface area of the clean material compared to other faujasite zeolites indicates that **FAU-720** has a smaller crystallite size. The pore size distribution of **FAU-720** is presented in Fig. A.6a (highest peak corresponding to a diameter of 8.5 Å).

The glycerol oligomer distribution (Table 26) after **G6**- and **G6IM**-treatment shows good selectivity towards diglycerol, but poor conversion. The best among the poor alternatives is the Cs-impregnated material. The good selectivity looks a little weird in light of the small crystallite size (remember, we chose to interpret the large surface area as an evidence of small crystallites), since small crystallites means a large relative extracrystalline surface (i.e., catalyst sites with essentially no shape selectivity) although the result does not indicate bad selectivity. Of course, this is not really a problem. The good selectivity is easily explained by the fact that the oligomerisation is a step-wise reaction (triglycerol cannot form until some diglycerol has formed first, by simple probability, and so on) and thus the good selectivity and very low concentration of the first oligomer is because the oligomerisation is very slow. After six hours, the reaction is apparently only starting.

The leaching of metal (Table 27) off **FAU-720** is higher than usual for Mg, but otherwise at par with the other zeolites.

Powder X-ray diffractograms for the Mg and Mn impregnated material is shown in Fig. 23. Additional powder X-ray diffractograms are shown in Fig. A.12.

Table 25. FAU-720 BET data.

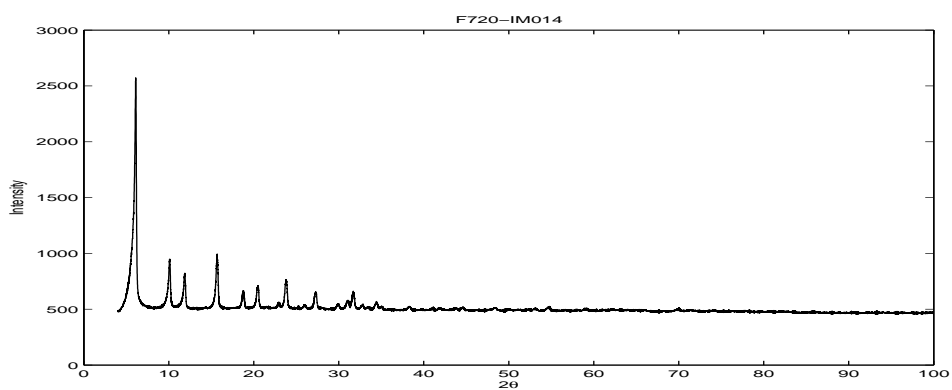
Measured surface area [m ² /g]			
Clean	G1-treated	G6-treated	Mg-FAU-720
1382 ± 10	532 ± 7.5	508 ± 7.4	643 ± 14

Table 26. Glycerol composition by FAU-720 zeolites after 6 h. Normalised values in parenthesis.

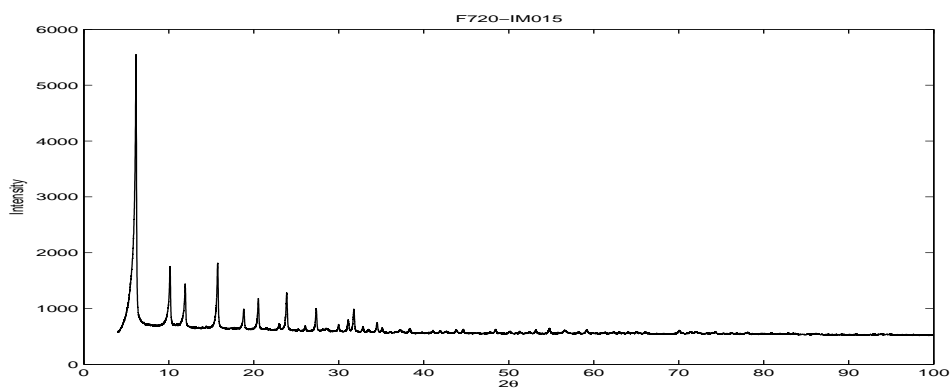
Material	G	PG-2	CPG-2	PG-3	CPG-3	PG-4	PG-5	Rest
FAU-720	91.0 (95.1)	5.1 (2.8)	–	0	–	–	–	3.9 (2.1)
Cs-FAU-720	92.0 (95.6)	7.3 (4.1)	0	0.3 (0.2)	0	0	0.2 (0.1)	0.2 (0.1)
Mg-FAU-720	93.0 (95.9)	4.5 (2.6)	0	0.3 (0.2)	0	0	0.2 (0.1)	2.0 (1.2)
Mn-FAU-720	93.0 (95.6)	4.0 (2.5)	0	0.2 (0.1)	0.2 (0.1)	0	0.2 (0.1)	2.4 (1.5)

Table 27. Leaching of metal into organic phase after G6IM-treatment, given as part metal per million parts organic phase (determined by AAS), and as percentage of the metal mass loaded on the material.

FAU-720	Cs	Mg	Mn
Mg metal/kg org. phase	1900	665	294
Mass percent	2.6%	5.0%	1.0%



(a) Mg-FAU-720



(b) Mn-FAU-720

Figure 23. Impregnated FAU-720 PXRD.

4.5 Zeolite FAU-760

Zeolite **FAU-760**, and also **FAU-780** in the next section, were excluded from most test steps quite early in the project. Since seven of the zeolites were faujasites, it would have been uneconomical to go through with all of them. Instead, the two least selective zeolites (**FAU-760** and **FAU-780**) were dropped and instead other framework type zeolites were studied.

Zeolite **FAU-760** has a large surface area (cf. Table 28), and the **G**-treated materials' surface area decreases as expected, although the **G1** area is lower than the **G6**. The pore width distribution (Fig. A.6b) shows a multitude of pore sizes, with the majority in the nanopore range. The highest peak in the distribution curve corresponds to 7.5 Å.

In Table 29, the oligomer composition after six hours is shown. The diglycerol percentage is not bad at all, but the large amount of higher oligomers and unidentified compounds formed places this zeolite among the worse.

Table 28. FAU-760 BET data.

Measured surface area [m ² /g]	
Clean	G1 -treated G6 -treated
920 ± 6.5	525 ± 5.7 732 ± 6.3

Table 29. Glycerol composition by FAU-760 after 6 h. Normalised values in parenthesis.

Material	G	PG-2	CPG-2	PG-3	CPG-3	PG-4	PG-5	Rest
FAU-760	36.2 (64.6)	16.3 (9.1)	-	5.8 (3.2)	-	-	-	41.7 (23.2)

4.6 Zeolite FAU-780

Zeolite **FAU-780**, like **FAU-780** in the previous section, was excluded from most test steps beyond monofunctional catalytic testing and surface area measurements.

Zeolite **FAU-780** displays a large surface area (cf. Table 30) in the clean state, and surprisingly an even larger area after **G1**-treatment. We will not linger at this oddity, since it could be simply caused by some random error outside of our control.

The pore width distribution of the clean **FAU-780** material is appended in Fig. A.6c. The distribution is more compact than for **FAU-760**, which is positive. The highest peak corresponds to a pore diameter of 6.5 Å.

In Table 31, the oligomer composition after six hours is shown. The diglycerol percentage is again moderate, but the very large amount of higher oligomers and unidentified compounds formed makes this zeolite the worst in that regard.

Table 30. FAU-780 BET data.

Measured surface area [m^2/g]	
Clean	G1 -treated G6 -treated
874 ± 4.6	1024 ± 11 761 ± 7.0

Table 31. Glycerol composition by FAU-780 zeolite after 6 h. Normalised values in parenthesis.

Material	G	PG-2	CPG-2	PG-3	CPG-3	PG-4	PG-5	Rest
FAU-780	15.2 (46.9)	10.2 (6.4)	-	5.4 (3.4)	-	-	-	69.2 (43.3)

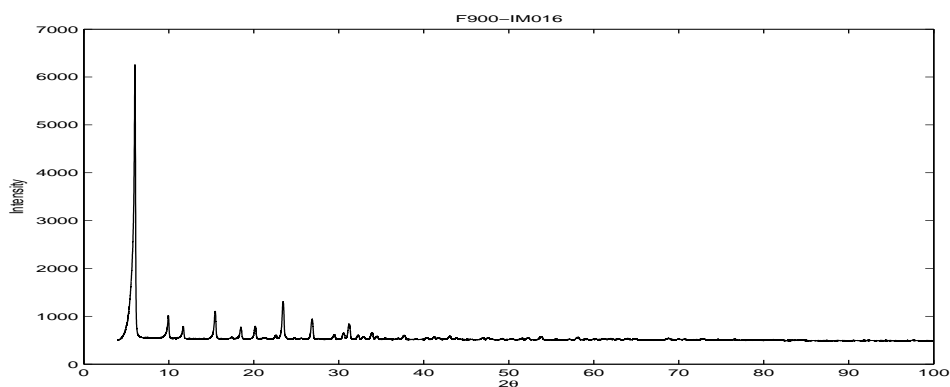
4.7 Zeolite FAU-900

Fig. 24 below displays two powder X-ray diffractograms for two impregnated **FAU-900** materials. The peak positions are identical in between them, since they have the same structure. Actually, all faujasites have identical peak positions. But it is almost impossible to positively identify any metal oxide phase peaks in the diffractogram. Perhaps the adsorbed metal oxide particles are too small to produce a detectable signal. Additional powder X-ray diffractograms are shown in Fig. A.15.

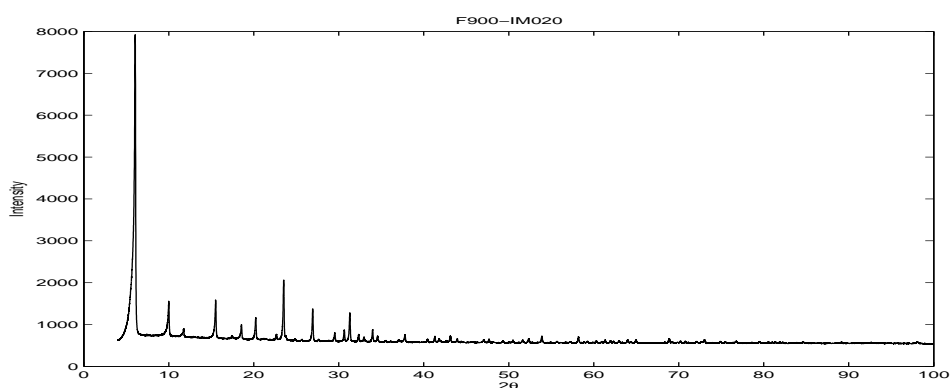
The oligomer distribution after six hours reaction, displayed in Table 33, shows that all metals contribute positively to the diglycerol ratio, with Cs as the best. Overall, **FAU-900** performs moderately good, with good selectivity towards diglycerol and only small amounts of higher oligomers.

Metal leaching off the bifunctional catalyst is moderate (see Table 34).

Pore width distribution (Fig. A.7c) shows a very good size uniformity with a peak at 6.5 Å.



(a) Mg-FAU-900



(b) Mn-FAU-900

Figure 24. Impregnated **FAU-900** PXR. D.

Table 32. FAU-900 BET data.

Measured surface area [m ² /g]	
Clean	G1 -treated G6 -treated
835 ± 9.9	101 ± 0.32 205 ± 0.35

Table 33. Glycerol composition by **FAU-900** zeolites after 6 h. Normalised values in parenthesis.

Material	G	PG-2	CPG-2	PG-3	CPG-3	PG-4	PG-5	Rest
FAU-900	81.7 (88.9)	10.6 (6.5)	–	0	–	–	–	7.7 (4.7)
Cs- FAU-900	73.0 (84.1)	20.0 (11.8)	0.4 (0.2)	2.1 (1.2)	0.2 (0.1)	0.2 (0.1)	0.2 (0.1)	3.9 (2.3)
Mg- FAU-900	82.0 (90.0)	14.0 (7.8)	0	0.9 (0.5)	0	0	0.2 (0.1)	2.9 (1.6)
Mn- FAU-900	80.0 (89.5)	17.0 (8.9)	0	1.4 (0.7)	0	0	0.2 (0.1)	1.4 (0.7)

Table 34. Leaching of metal into organic phase after **G6IM**-treatment, given as part metal per million parts organic phase (determined by AAS), and as percentage of the metal mass loaded on the material.

FAU-900	Cs	Mg	Mn
Mg metal/kg org. phase	1900	194	370
Mass percent	2.5%	1.5%	1.4%

4.8 Zeolite MOR

Now we leave the faujasites behind us, and take on the only mordenite among the zeolites. Mordenite has an essentially one-dimensional pore system, and contains no cages (as described earlier).

The clean material has a moderate surface area (Table 36), smaller than the faujasites but larger than **BEA** and **ZSM-5P**. The impregnated material has a smaller area than the clean material, which makes sense. The increase in surface area from **G1**- to **G6**-treated material, on the other hand, does not make sense at a quick glance. Actually, not even at a longer glance. Given the number of multipoint BET analyses I have performed during this project (almost 40), I would not be too surprised if some displays irregularities.

In Fig. 25, the Mg and Mn impregnated zeolite diffractograms are showed. **MOR**, of course, has a different peak distribution compared to the faujasites. Additional powder X-ray diffractograms of **MOR** are shown in Fig. A.16.

The metal leaching off **MOR**, as determined by atomic absorption spectroscopy, is shown in Table 35. The results show relatively high leaching overall, but no surprises.

The pore size distribution of **MOR** (Fig. A.7d) shows an excellent uniformity, with a pore size of 6.5 Å.

Tables 37, 38 and 39 show the progressive development of the oligomer distribution. Clearly, nothing much happens until after one hour of heating. At six hours, the monofunctional material is more active than the bifunctional, independently of metal. The addition of a metal appears to increase the selectivity and reduce the activity (conversion) of the catalyst.

Table 35. Leaching of metal into organic phase after **G6IM**-treatment, given as part metal per million parts organic phase (determined by AAS), and as percentage of the metal mass loaded on the material.

MOR	Cs	Mg	Mn
Mg metal/kg org. phase	4200	470	457
Mass percent	5.9%	3.7%	1.6%

Table 36. **MOR** BET data.

Measured surface area [m ² /g]			
Clean	G1 -treated	G6 -treated	G6IM -treated (Mg)
657 ± 6.5	496 ± 10	775 ± 5.3	442 ± 9.8

Table 37. Glycerol composition by **MOR** zeolites after 10 min. Normalised values in parenthesis.

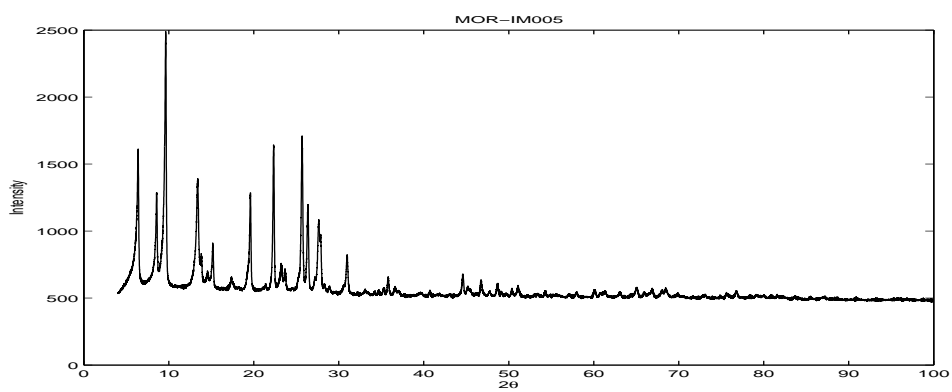
Material	G	PG-2	CPG-2	PG-3	CPG-3	PG-4	PG-5	Rest
MOR	–	–	–	–	–	–	–	–
Cs-MOR	99.7 (99.8)	0.2 (0.1)	0	0	0	0	0	0.1 (0.1)
Mg-MOR	99.8 (99.9)	0.1 (0)	0	0	0	0	0	0.1 (0.1)
Mn-MOR	99.8 (99.9)	0	0	0	0	0	0	0.1 (0.1)

Table 38. Glycerol composition by **MOR** zeolites after 1 h. Normalised values in parenthesis.

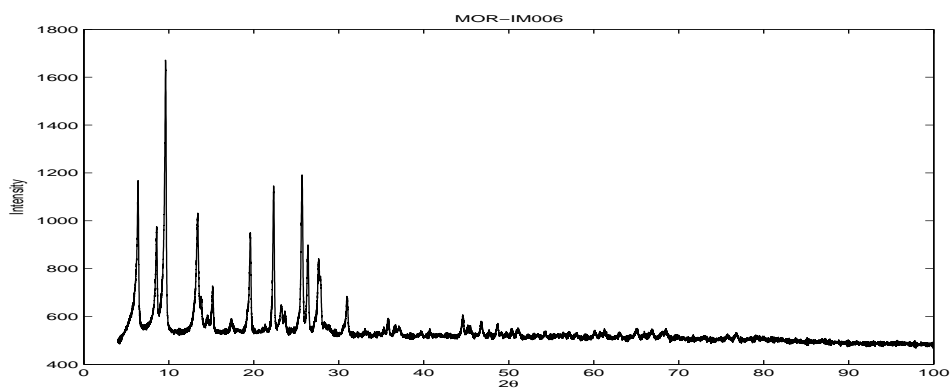
Material	G	PG-2	CPG-2	PG-3	CPG-3	PG-4	PG-5	Rest
MOR	–	–	–	–	–	–	–	–
Cs-MOR	98.0 (98.9)	1.4 (0.7)	0	0	0	0	0.2 (0.1)	0.4 (0.2)
Mg-MOR	99.3 (99.6)	0.5 (0.3)	0	0	0	0	0	0.2 (0.1)
Mn-MOR	99.3 (99.6)	0.6 (0.3)	0	0	0	0	0	0.1 (0.1)

Table 39. Glycerol composition by **MOR** zeolites after 6 h. Normalised values in parenthesis.

Material	G	PG-2	CPG-2	PG-3	CPG-3	PG-4	PG-5	Rest
MOR	79.0 (87.2)	9.1 (5.6)	–	0.9 (0.6)	–	–	–	11.0 (6.7)
Cs-MOR	90.0 (94.7)	7.6 (4.0)	0	0.4 (0.2)	0	0	0.2 (0.1)	1.8 (1.0)
Mg-MOR	95.0 (97.4)	5.0 (2.6)	0	0.3 (0.2)	0	0	0.1 (0.1)	-0.4 (-0.2)
Mn-MOR	95.0 (97.2)	4.6 (2.6)	0	0.3 (0.2)	0	0.1 (0.1)	0.2 (0.1)	-0.2 (-0.1)



(a) Mg-MOR



(b) Mn-MOR

Figure 25. Impregnated MOR PXRD.

4.9 Zeolite USY

USY is special among the faujasites since it has a very low aluminium content, which makes the material very siliceous (non-acidic) and a bad ion-exchanger. This seems to be reflected in the relatively high overall leaching of metals from this zeolite (in percent, see Table 42).

The surface area (Table 40) is similar to the other faujasites. The impregnated material has a reduced surface area (compared to the clean material), probably due to pore blockage by the metal deposits. The **G1**-treated material's surface area is larger than that of the **G6**-treated material, which is a little counter-intuitive, and lacking a good explanation, I have to resort to the all-encompassing "experimental error." Peak size distribution (Fig. A.8b) shows several peaks, with the highest at 7.5 Å.

The powder X-ray diffractograms (Fig. 26) have the same peak positions as the other faujasites in this project, which confirms that they have the same structure. No distinct metal or metal oxide peaks were identifiable. Additional powder X-ray diffractograms are shown in the appendix, Fig. A.17.

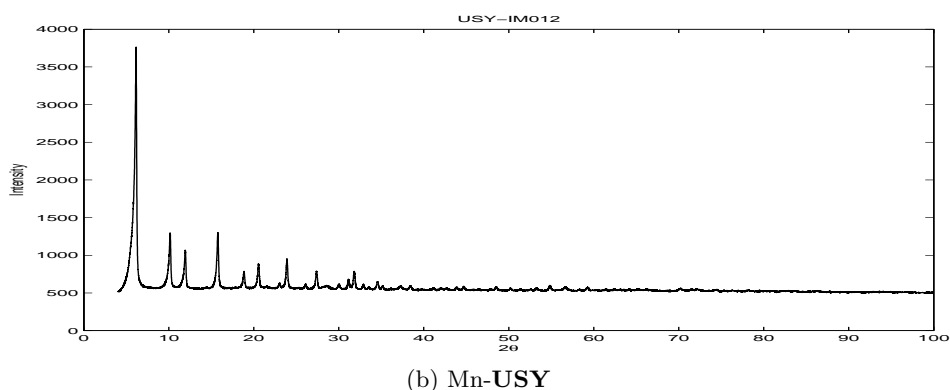
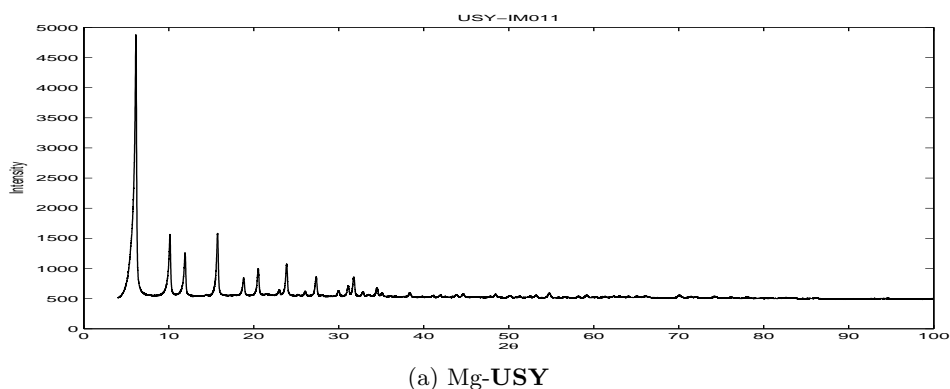


Figure 26. Impregnated USY PXR.

Table 40. **USY** BET data.

Measured surface area [m ² /g]			
Clean	G1 -treated	G6 -treated	Mg-USY
729 ± 6.5	650 ± 8.8	761 ± 7.3	608 ± 13

Table 41. Glycerol composition by **USY** zeolites after 6 h. Normalised values in parenthesis.

Material	G	PG-2	CPG-2	PG-3	CPG-3	PG-4	PG-5	Rest
USY	80.5 (88.9)	9.6 (5.5)	–	1.0 (0.6)	–	–	–	7.7 (4.7)
Cs-USY	80.0 (88.9)	16.5 (9.2)	0.3 (0.2)	1.4 (0.8)	0	0.2 (0.1)	0.1 (0.1)	1.5 (0.8)
Mg-USY	89.0 (94.2)	5.0 (2.6)	0	0.4 (0.2)	0	0.2 (0.1)	0.3 (0.1)	5.1 (2.7)
Mn-USY	91.0 (94.7)	5.1 (3.0)	0	0.3 (0.2)	0	0.2 (0.1)	0.3 (0.2)	3.1 (1.8)

Table 42. Leaching of metal into organic phase after **G6IM**-treatment, given as part metal per million parts organic phase (determined by AAS), and as percentage of the metal mass loaded on the material.

USY	Cs	Mg	Mn
Mg metal/kg org. phase	3500	783	694
Mass percent	5.2%	6.1%	2.3%

4.10 Zeolite ZSM-5P

The powder X-ray diffractograms displayed in Fig. 27, especially Fig. 27a, is rather noisy. This is because the amount of sample used was in excess. But it is still clear that **ZSM-5P** is structurally different from the other zeolites. Additional powder X-ray diffractograms for **ZSM-5P** are shown in Fig. A.18.

Tables 43, 44 and 45 show that conversion takes place sometime after one hour of heating, and that Mg-impregnation reduces selectivity and activity while Cs and Mn increased selectivity and activity, compared to the monofunctional material.

As for the surface area (see Table 46), **ZSM-5P** has the lowest surface area of all tested zeolites. This is mainly because of the pellet form of this zeolite. The **G1**- and **G6**-treated materials showed almost no change of surface area compared to the clean material. The impregnated material showed only a small decrease in surface area. The pore size distribution (Fig. A.8a) of the clean material showed a large peak at 6.5 Å, and several smaller peaks in the macropore range. These peaks correspond well to the larger intraparticle voids we would expect to find in this extruded material.

The leaching off this material (Table 47) is slightly below average compared to the other zeolites, suggesting that the material has a low Si/Al ratio (high acidity). The real value is a balance between the clay and the zeolite itself.

Another feature of this material was the extensive attrition it suffered after the catalytic test, especially the impregnated **ZSM-5P**. I believe the continuous shaking applied during the impregnation step, destabilised the pellets which caused them to crumble during the six-hour long catalytic test.

Table 43. Glycerol composition by **ZSM-5P** zeolites after 10 min. Normalised values in parenthesis.

Material	G	PG-2	CPG-2	PG-3	CPG-3	PG-4	PG-5	Rest
ZSM-5P	–	–	–	–	–	–	–	–
Cs- ZSM-5P	99.8 (99.9)	0.1 (0.1)	0	0	0	0	0	0.1 (0)
Mg- ZSM-5P	99.9 (99.9)	0	0	0	0	0	0	0.1 (0.1)
Mn- ZSM-5P	99.7 (99.8)	0.2 (0.1)	0	0	0	0	0	0.1 (0.1)

Table 44. Glycerol composition by **ZSM-5P** zeolites after 1 h. Normalised values in parenthesis.

Material	G	PG-2	CPG-2	PG-3	CPG-3	PG-4	PG-5	Rest
ZSM-5P	–	–	–	–	–	–	–	–
Cs- ZSM-5P	99.3 (99.6)	0.7 (0.4)	0	0	0	0	0	0
Mg- ZSM-5P	99.6 (99.8)	0.3 (0.2)	0	0	0	0	0	0.1 (0.1)
Mn- ZSM-5P	99.2 (99.6)	0.6 (0.3)	0	0	0	0	0	0.2 (0.1)

Table 45. Glycerol composition by **ZSM-5P** zeolites after 6 h. Normalised values in parenthesis.

Material	G	PG-2	CPG-2	PG-3	CPG-3	PG-4	PG-5	Rest
ZSM-5P	89.7 (93.4)	3.4 (2.2)	–	0	–	–	–	6.9 (4.4)
Cs- ZSM-5P	92.0 (95.6)	5.7 (3.2)	0	0.3 (0.2)	0	0	0.2 (0.1)	1.8 (1.0)
Mg- ZSM-5P	86.0 (92.2)	3.3 (1.8)	0	0.2 (0.1)	0.1 (0.1)	0	0.1 (0.1)	10.3 (5.7)
Mn- ZSM-5P	91.0 (95.0)	4.5 (2.5)	0	0.3 (0.2)	0	0	0.4 (0.2)	3.8 (2.1)

Table 46. ZSM-5P BET data.

Measured surface area [m ² /g]			
Clean	G1-treated	G6-treated	G6IM-treated (Mg)
311 ± 3.0	282 ± 2.2	322 ± 3.7	260 ± 3.8

Table 47. Leaching of metal into organic phase after G6IM-treatment, given as part metal per million parts organic phase (determined by AAS), and as percentage of the metal mass loaded on the material.

ZSM-5P	Cs	Mg	Mn
Mg metal/kg org. phase	2000	225	333
Mass percent	2.9%	1.8%	1.1%

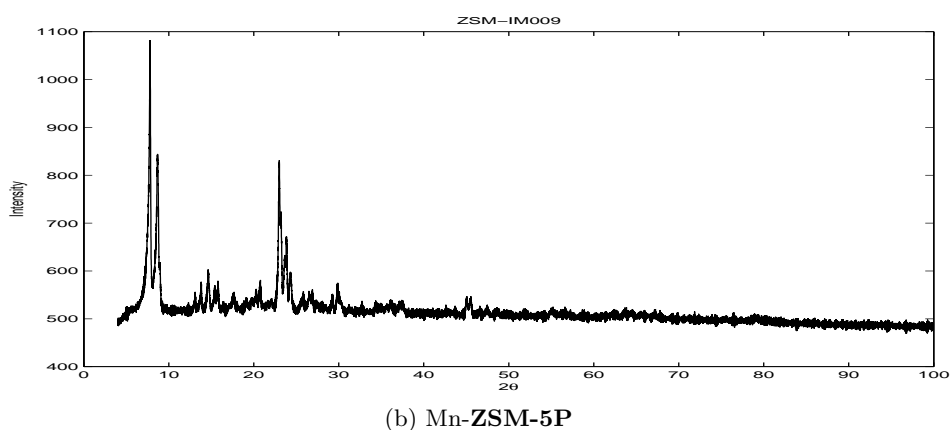
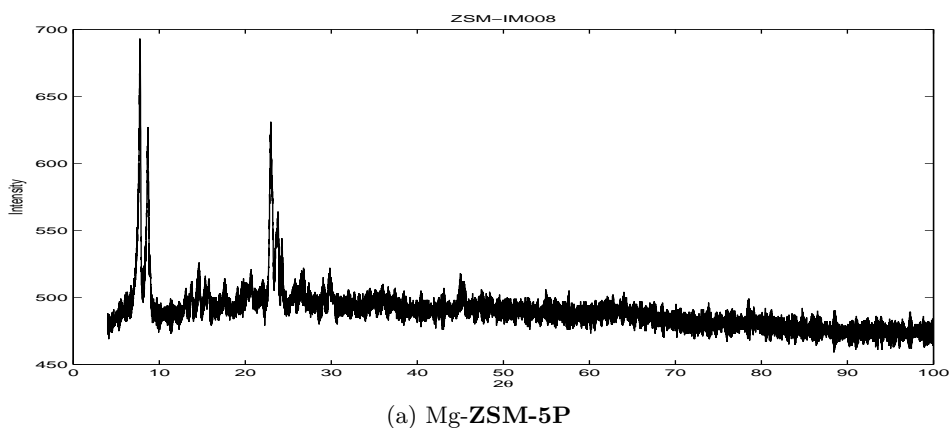


Figure 27. Impregnated ZSM-5P PXRD.

5 Discussion & conclusions

For the monofunctional catalytic materials, there are a few variables that may or may not be related to each other. Most importantly, we should investigate the relation, if any, between pore size, acidity, leaching, surface area and the diglycerol ratio (which is essentially a measure of conversion).

For the bifunctional catalysts, the impregnated metal is an additional factor.

Table 48. Comparing change in surface area among the monofunctional catalysts, by setting the area measured for the clean material as 100%, and relating all other values to the clean area of each material.

Zeolite	Surface area relative to clean area			
	Clean state	After G1 -treatment	After G6 -treatment	After impregnation
FAU-720	100%	38.5%	36.8%	46.5%
FAU-760	100%	57.1%	79.6%	–
FAU-780	100%	117%	87.1%	–
FAU-900	100%	12.1%	24.6%	–
FAU-13X	100%	7.4%	33.4%	53.8%
USY	100%	89.2%	104%	83.4%
MOR	100%	75.5%	118%	67.3%
FAU-600	100%	68.9%	74.0%	84.8%
BEA	100%	152%	120%	140%
ZSM-5P	100%	90.7%	104%	83.6%

Among the monofunctional catalysts, four different kinds of behavior of the surface area can be observed (cf. Table 48), in my opinion. **FAU-760**, **FAU-900**, **FAU-600** and **FAU-13X** decrease markedly after the **G1**-treatment, and then rise a little after the **G6**-treatment. Their treated surface area is always lower than the clean area.

USY, **MOR** and **ZSM-5P** drop a little after **G1**-treatment, and then bounce back above 100% after the **G6**-treatment. They show only small changes in surface area for all treatments. **FAU-780** shows a similar behavior, only in the other direction (it is higher than 100% after **G1** and lower after **G6**).

BEA increases its surface area after all treatments, which is a little odd.

The only zeolite that behaves as I would have expected is **FAU-720**, which decreases after **G1**-treatment, and decreases more after **G6**-treatment.

The reader should keep in mind that these perceived “trends” are derived from only one measurement per sample, and may contain random errors.

In terms of surface area, the ideal catalytic material should preserve its

area as far as possible during all treatments. The catalysts that best preserve their area, among the tested, are **MOR**, **USY**, **ZSM-5P**, **FAU-780** and, with some good will, **FAU-600**.

The relative surface area after treatment (**G1** and **G6**) depends on the Si/Al ratio (cf. Fig. 28), to some degree; the less acidic zeolites preserve more of their area, in general.

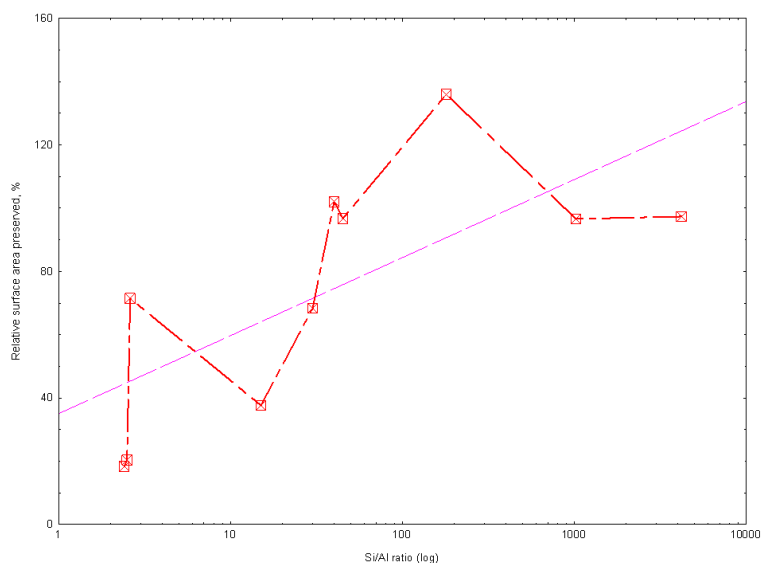


Figure 28. The average preserved relative area after **G1**- and **G6**-treatment (cf. Table 48) plotted against acidity. The less acidic zeolites preserve their surface area to a larger extent than more acidic zeolites.

There is no simple relationship between pore size (as given in Fig. A.6–Fig. A.8) and diglycerol ratio. There probably would be if all other variables, especially the acidity, were kept constant.

Acidity (Si/Al ratio) seems to be correlated to the diglycerol ratio after six hours of monofunctional catalytic testing (see Fig. 29). The correlation is not perfect, but as evidenced by the graph, high acidity bears a higher average conversion. Incorporating the surface areas of the clean materials shows that there is no relationship between area and conversion.

Again, this would probably not be the case if other variables, like acidity, were possible to hold constant. This must be an effect of the fact that the chemical interaction between the catalytic material and the feed is much more important than the physical properties of the catalyst, such as surface area or pore size.

All things considered, **FAU-600** is the best performing monofunctional catalyst. It shows good activity (high conversion), good selectivity (low amounts of higher oligomers and other products) and a good ability to maintain its surface area throughout a catalytic test.

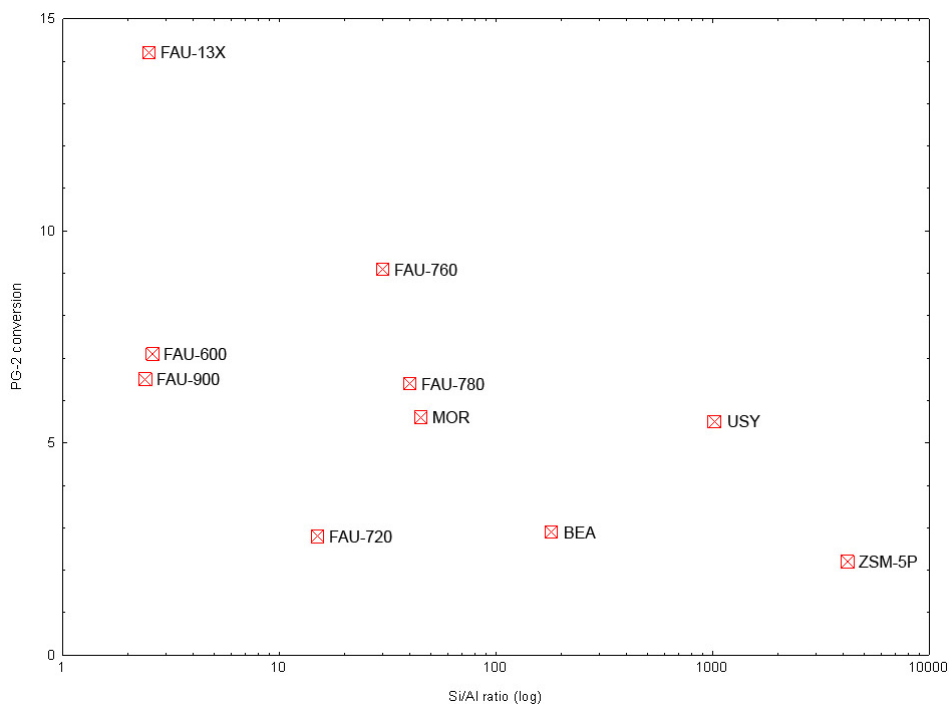


Figure 29. Si/Al ratio (acidity) plotted against concentration of diglycerol after six hours for the monofunctional catalyst materials. High acidity (low Si/Al ratio) seems to be favoured.

A correlation between acidity and diglycerol ratio can be discerned (Fig. 30) for the impregnated zeolites (bifunctional catalysts). The effect of the impregnated metal is very pronounced for some zeolites, such as **FAU-13X** or **BEA**, for example. For other zeolites, the difference is only moderate. Still, Cs clearly renders the bifunctional material the highest activity, almost regardless of zeolite (only exception is **FAU-13X**).

The large positive effect of Cs on **BEA** and **USY** is interesting. In the **BEA** case, the increase is likely caused by extensive leaching off the zeolite (cf. Table 8). In the **USY** case, leaching is comparable to that of **MOR**, so something else has to be happening. The explanation that almost jumps at us is the high basicity of Cs-**USY**. Cs₂O is a basic oxide, and **USY** is the least acidic zeolite tested. Combined, this must make the most basic bifunctional zeolite in this test.

In any way, it is evidently the combination of zeolite and metal that determines the properties of the bifunctional catalytic material, and not the zeolite or metal by itself.

Some zeolites increase their activity when combined with any metal (compared to its performance without metal), e.g., **FAU-900** and **BEA**, but most zeolites either increase or decrease their activity depending on the

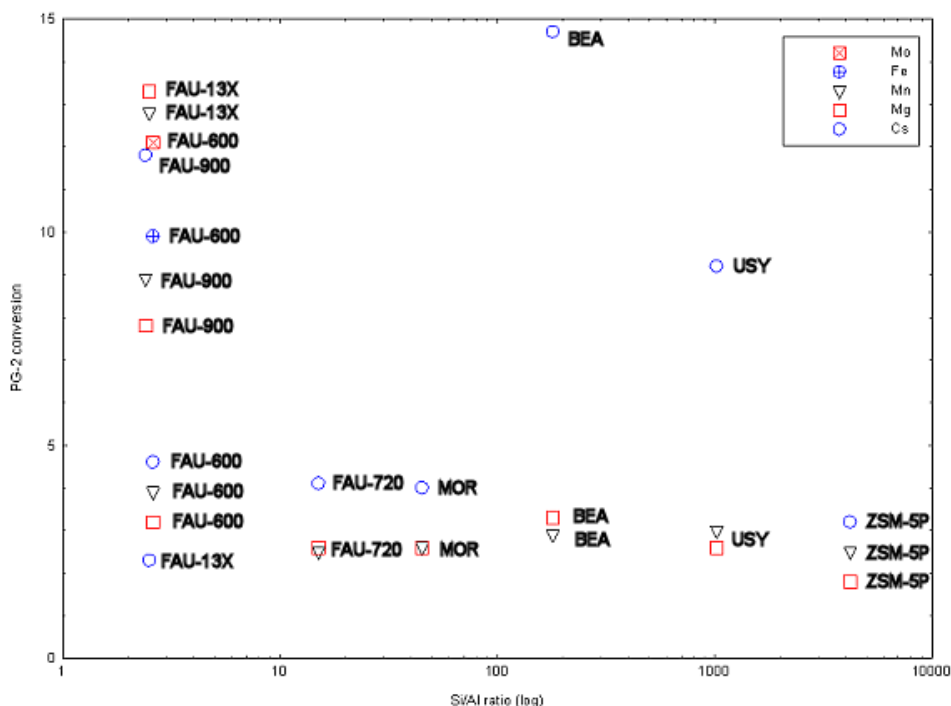


Figure 30. Si/Al ratio (acidity) of the clean material plotted against concentration of diglycerol after six hours (one hour for Fe and Mo) for the bifunctional catalyst materials.

metal, e.g., **FAU-600**, **USY** and **ZSM-5P**. And yet other zeolites, namely **FAU-13X** and **MOR**, decrease their activity regardless of metal.

So there is no clear-cut winner among the bifunctional materials, but a few good candidates can be discerned. Cs-**USY** shows good activity (significantly higher than **USY**), good selectivity and low metal leaching. Fe-**FAU-600** has a higher activity than Cs-**USY**, and comparable selectivity and leaching. And finally, I must mention Cs-**FAU-900**, which shows good selectivity and conversion and low leaching.

Unfortunately, we have no surface area measurements of the impregnated materials *after* catalytic testing, so we cannot see if the trend discovered for the monofunctional materials (zeolites preserve area better with higher acidity) also holds for the bifunctional. But the powder X-ray diffractograms show that the crystallinity is preserved, anyway.

5.1 Concluding remarks

Over the duration of this project, it has become evident that, (i) zeolites do have a positive effect on the oligomerisation of glycerol, (ii) different zeolites impact the oligomerisation to different degrees, and (iii) the addition of an

impregnated metal to the zeolite often increases the activity of the catalyst.

There is however, opportunity to improve both experimental methods and analysis techniques. Most importantly, the catalytic testing could be improved by using a setup that allows for continuous flow of the glycerol feed over the catalyst. As for the analytical methods, in addition to the current ones, I think electron microscopy and element analysis could prove very useful, especially in determining the amount of metal on the zeolite and the way it is dispersed on the crystallites.

All things considered, this project has been a lot of fun, involving both some organic chemistry and traditional inorganic and structural chemistry. The commercial interest of the glycerol issue has made this project all the more interesting.

Acknowledgements

I would like to thank my supervisors, Mats Johnsson and Neil Cruise, for all their support, encouragement and patience.

I would like to give my special thanks to the technical staff at the department, for their help in constructing the catalytic test setup among many other things.

Thanks to all the other wonderful people at the department—you are always helpful and full of advice to a poor undergrad. Thanks, all!

Last, but not the least, my very sincere thanks to all the staff at Perstorp's analytical lab. Your work made this project possible!

6 References

- J. Barrault, Jean-Marc Clacens, and Y. Pouilloux. Selective oligomerization of glycerol over mesoporous catalysts. *Topics in Catalysis*, 27(1–4):137–142, 2004. DOI: 10.1023/B:TOCA.0000013548.16699.1c.
- Mark Bowden. ConvX—PXR file converter, 2007. <http://www.ccp14.ac.uk/ccp/web-mirrors/convx> [071030].
- Stephen Brunauer, P. H. Emmett, and Edward Teller. Adsorption of gases in multimolecular layers. *Journal of the American Chemical Society*, 60: 309–319, 1938. <http://pubs.acs.org/cgi-bin/archive.cgi/jacsat/1938/60/i02/pdf/ja01269a023.pdf> [071027].
- N. Y. Chen, Jr. Thomas F. Degnan, and C. Morris Smith. *Molecular transport and reaction in zeolites: design and application of shape selective catalysis*. VCH Publishers, New York, 1994. ISBN 0-89573-765-5.
- Jean-Marc Clacens, Y. Pouilloux, J. Barrault, C. Linares, and M. Goldwasser. Mesoporous basic catalysts: comparison with alkaline exchange zeolites (basicity and porosity). application to the selective etherification of glycerol to polyglycerols. *Studies in Surface Science and Catalysis*, 118:895–902, 1998.
- Jean-Marc Clacens, Y. Pouilloux, and J. Barrault. Selective etherification of glycerol to polyglycerols over impregnated basic MCM-41 type mesoporous catalysts. *Applied Catalysis, A: General*, 227(1–2):181–190, 2002. DOI: 10.1016/S0926-860X(01)00920-6.
- Jennifer L. Dashnau, Nathaniel V. Nucci, Kim A. Sharp, and Jane M. Vanderkooi. Hydrogen Bonding and the Cryoprotective Properties of Glycerol/Water Mixtures. *Journal of Physical Chemistry B*, 110(27): 13670–13677, 2006. DOI: 10.1021/jp0618680.
- Mary Ann David. Glycerol: A Jack of All Trades, 1996. http://www.chem.yorku.ca/hall_of_fame/essays96/glycerol.htm [071103].
- Dow Epoxy. Dow Epoxy Advances Glycerine-To-Epichlorohydrin and Liquid Epoxy Resins Projects by Choosing Shanghai Site, 2007. <http://epoxy.dow.com/epoxy/news/2007/20070326b.htm> [071103].
- Marina Enguádanos, Antonio Soria, Boyan Kavalov, and Peder Jensen. Techno-economic analysis of Bio-diesel production in the EU: a short summary for decision-makers, May 2002. <ftp://ftp.jrc.es/pub/EURdoc/eur20279en.pdf> [071102].

- EU Commission. Directive 98/86/ec (E475 and E476), 1998.
<http://eur-lex.europa.eu/LexUriServ/LexUriServ.do?uri=OJ:L:1998:334:0001:0063:EN:PDF> [080209].
- European Oleochemicals and Allied Products Group. Glycerine from petrochemical feedstock, 2007. <http://www.apag.org/oleo/glycerine.htm> [071109].
- Thomas Foglia, Richard Ashby, Victor Wyatt, and Daniel Solaiman. Industrial Products from Biodiesel Glycerol. *International Symposium on Biocatalysis and Bioenergy*, 2006. http://www.ars.usda.gov/research/publications/publications.htm?SEQ_NO_115=200285 [071102].
- Marie-Cecile Henard. Impacts on oilseed industry following biofuel boom, 2007. <http://www.fas.usda.gov/gainfiles/200702/146280213.pdf> [071028].
- Huber. Huber Imaging Plate Guinier Camera 670. Technical report, HUBER Diffraktionstechnik GmbH & Co. KG, 2007. <http://www.xhuber.com/en/diffractometer/guinier/670/670.htm> [071030].
- Gerald Jakobson and Werner Siemanowski. Process for preparing polyglycerols, 1990. <http://www.freepatentsonline.com/4960953.html> [071028].
- Jens Weitkamp and Lothar Puppe (eds.). *Catalysis and Zeolites: Fundamentals and Applications*. Springer-Verlag, Berlin, 1999. ISBN 3540636501.
- Thomas Z. Li. Process for improving stability of glycerin. Technical report, Cognis Corporation, 1998. <http://patft.uspto.gov/netacgi/nph-Parser?Sect1=PT01&Sect2=HITOFF&d=PALL&p=1&u=6784326&RS=PN/6784326> [070509].
- Elaine M. McCash. *Surface Chemistry*. Oxford University Press, 2002. ISBN 0198503288.
- mentoronline.se. Perstorp köper bioenergijätte.
<http://www.mentoronline.se/iuware.aspx?pageid=3172&ssoid=69582> [071029].
- Micromeritics. The Dynamics of Adsorption, 2008.
<http://www.micromeritics.com/pdf/Articles/Theorption.pdf> [080114].
- Carlos Márquez-Alvarez, Enrique Sastre, and Joaquín Pérez-Pariente. Solid catalysts for the synthesis of fatty esters of glycerol, polyglycerols and sorbitol from renewable resources. *Topics in Catalysis*, 27(1–4): 105–117, 2004. DOI: 10.1023/B:T0CA.0000013545.81809.bd.
- James T. Richardson. *Principles of Catalyst Development*. Fundamental and applied catalysis. Plenum Press, 1989. ISBN 0-306-43162-9.

- Rolando M.A. Roque-Malherbe. *Adsorption and Diffusion in Nanoporous Materials*. CRC Press, 2007. ISBN 1-4200-4675-6.
- Paul Seiden and James Bruce Martin. Process for preparing polyglycerol, 1976. <http://patft.uspto.gov/netacgi/nph-Parser?Sect1=PT01&Sect2=HITOFF&d=PALL&p=1&u=3968169&RS=PN/3968169> [071028].
- Solvay Chemicals, Inc. EPICEROL™: An innovative environmental breakthrough in epichlorohydrin production, 2007. http://www.solvaychemicals.com/info/0,0,1000574-_EN,00.html [071113].
- Solvay Chemicals, Inc. Polyglycerols in personal care, 2004. <http://www.solvaychemicals.us/static/wma/pdf/6/6/9/2/PGL-03-001.pdf> [071025].
- Solvay Chemicals, Inc. Polyglycerols in industrial applications, 2005. http://www.solvaychemicals.us/static/wma/pdf/6/6/9/0/PGL_Industrial_Application.pdf [071025].
- Solvay Chemicals, Inc. Material safety data sheet—triglycerol, 2003. <http://www.solvaychemicals.us/static/wma/pdf/6/6/8/8/PG3.pdf> [071028].
- Solvay S. A. Solvay to build world-class Epicerol™ plant in Thailand, 2007. <http://www.solvaypress.com/static/wma/pdf/1/1/3/4/0/20070906EpicerolMapTaPhutEN.pdf> [071113].
- Solvay S. A. Polyglycerols—General Overview, 2005. http://www.solvaypolyglycerol.com/docroot/glycerol/static_files/attachments/polyglycerols_general_overview.pdf [071025].
- Spiral Software. EasyPlot—scientific graphing, 2006. <http://www.amion.com/ep/eplot.html> [071030].
- Structure Commission of the International Zeolite Association. *Atlas of zeolite framework types*. Elsevier, 2001.
- The Glycerol Challenge Consortium. The Glycerol Challenge, 2007. <http://theglycerolchallenge.org> [071103].
- The Royal Swedish Academy of Sciences. The Nobel Prize in Chemistry 2007, 2007. http://nobelprize.org/nobel_prizes/chemistry/laureates/2007/info.pdf [071214].
- John Meurig Thomas and Robert J. P. Williams. Catalysis: principles, progress, prospects. *Philosophical Transactions of the Royal Society A*, (363):765–791, 2005. DOI: 10.1098/rsta.2004.1534.

Paul A. Webb and Clyde Orr. *Analytical Methods in Fine Particle Technology*. Micromeritics Instrument Corporation, 1997. ISBN 0-9656783-0-X.

Wikipedia. Hydrophilic-lipophilic balance — wikipedia, the free encyclopedia, 2007a. http://en.wikipedia.org/w/index.php?title=Hydrophilic-lipophilic_balance&oldid=110052862 [080210].

Wikipedia. Biodiesel—wikipedia, the free encyclopedia, 2007b. <http://en.wikipedia.org/w/index.php?title=Biodiesel&oldid=167517596> [071028].

Wikipedia. Biodiesel production—wikipedia, the free encyclopedia, 2007c. http://en.wikipedia.org/w/index.php?title=Biodiesel_production&oldid=165093853 [071102].

A Appendix

Table A.1. **G1** heating cycles (zeolite and glycerol at 260 °C for 1 h) with experimental masses of each component.

Zeolite	Batch no.	Mass percent of catalyst	Mass of catalyst [g]	Mass of glycerol [g]	Minutes above 250 °C [min]
FAU-760	GL2	2.99%	1.8114	60.58	N/A
ZSM-5P	GL3	2.86%	1.9396	67.74	58.2
FAU-13X	GL4	2.73%	1.845	67.47	64.3
MOR	GL5	2.41%	1.745	72.4	60.5
FAU-600	GL6	2.39%	1.2138	50.7	53.3
FAU-900	GL8	1.34%	0.8704	64.9	63.0
FAU-780	GL9	1.56%	1.0111	64.9	66.5
FAU-720	GL10	2.44%	1.4786	60.7	74.5
USY	GL11	2.02%	1.2779	63.4	56.5
BEA	GL12	2.18%	1.6	73.3	65.0

Table A.2. Overview of **G6** heat cycles.

Zeolite	Batch no.	Mass percent of catalyst	Mass of catalyst [g]	Mass of glycerol [g]	Minutes above 250 °C [min]
USY	GX1	2.13%	1.7564	82.5	359.5
BEA	GX2	2.05%	1.6831	82.1	363
FAU-780	GX3	2.12%	1.5964	75.3	360
ZSM-5P	GX4	2.06%	1.5557	75.4	359
FAU-900	GX5	2.20%	1.643	74.8	362
FAU-13X	GX6	2.29%	1.7991	78.6	364
FAU-720	GX7	2.27%	1.8356	80.7	362
MOR	GX8	2.17%	1.6348	75.5	363
FAU-600	GX9	2.12%	1.6	75.4	362
FAU-760	GX10	2.27%	1.8	79.4	361

Table A.3. Overview of **G6IM** heat cycles.

Material	Batch no.	Mass percent of catalyst	Mass of catalyst [g]	Mass of glycerol [g]	Minutes above 250°C [min]
Cs-BEA	GT1	2.34%	1.9	81.2	369.8
Mg-BEA	GT2	2.27%	1.8	79.4	361.8
Mn-BEA	GT3	2.30%	1.8	78.3	362.8
Cs-MOR	GT4	2.41%	1.9	78.7	362
Mg-MOR	GT5	2.36%	1.9	80.6	362
Mn-MOR	GT6	2.27%	1.8	79.2	361.3
Cs-ZSM-5P	GT7	2.24%	1.8	80.4	361
Mg-ZSM-5P	GT8	2.24%	1.8	80.3	360
Mn-ZSM-5P	GT9	2.36%	1.8	76.3	361
Cs-USY	GT10	2.13%	1.8	84.4	361
Mg-USY	GT11	2.36%	1.9	80.5	361.3
Mn-USY	GT12	2.23%	1.7	76.1	360
Cs-FAU-720	GT13	2.36%	1.8	76.4	360
Mg-FAU-720	GT14	2.19%	1.7	77.6	361
Mn-FAU-720	GT15	2.06%	1.6	77.7	361.5
Mg-FAU-900	GT16	2.24%	1.8	80.2	360
Mg-FAU-600	GT17	2.24%	1.7	75.9	361
Mn-FAU-13X	GT18	2.22%	1.8	81.0	361
Mn-FAU-600	GT19	1.99%	1.6	80.6	363
Mn-FAU-900	GT20	2.12%	1.9	89.7	360
Cs-FAU-900	GT21	2.30%	1.7	73.9	360 ^a
Cs-FAU-600	GT22	2.07%	1.7	82.3	360 ^a
Cs-FAU-13X	GT23	2.11%	1.6	75.9	361
Mg-FAU-13X	GT24	2.23%	1.8	80.7	360
Fe-FAU-600	GT25	2.34%	1.8	76.9	208
Mo-FAU-600	GT26	1.86%	1.6	86.0	64.7

^aExperiment (heating, mixing) suspended for 30 minutes at ~300 mins due to major power outage (see <http://www.dn.se/DNet/jsp/polopoly.jsp?d=1298&a=699250>).

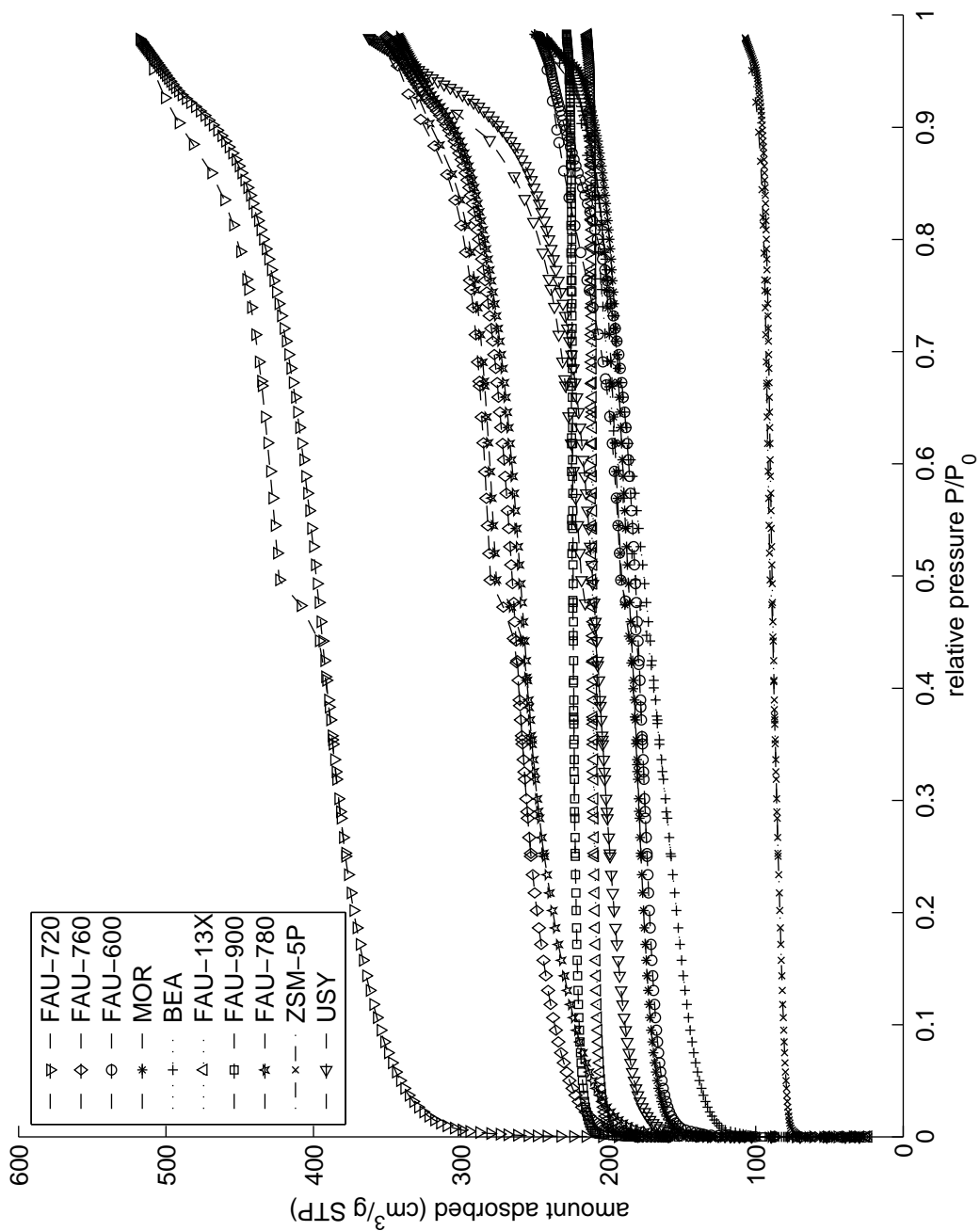


Figure A.1. Isotherms of clean untreated zeolite materials.



Figure A.2. Overview of catalytic test setup in fume hood. This setup was used for G1, G6, and G6IM heating programs.

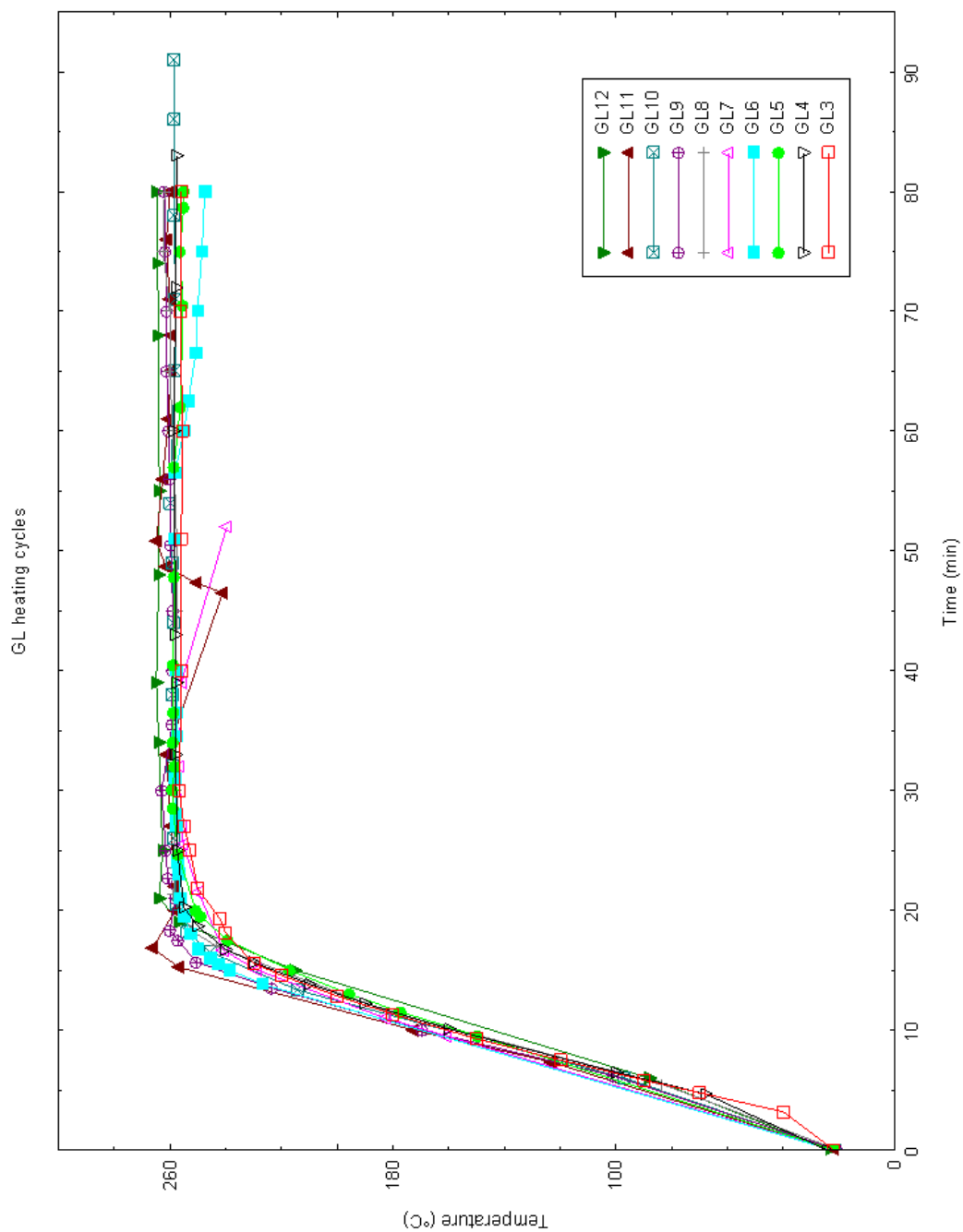


Figure A.3. G1 heating programs.

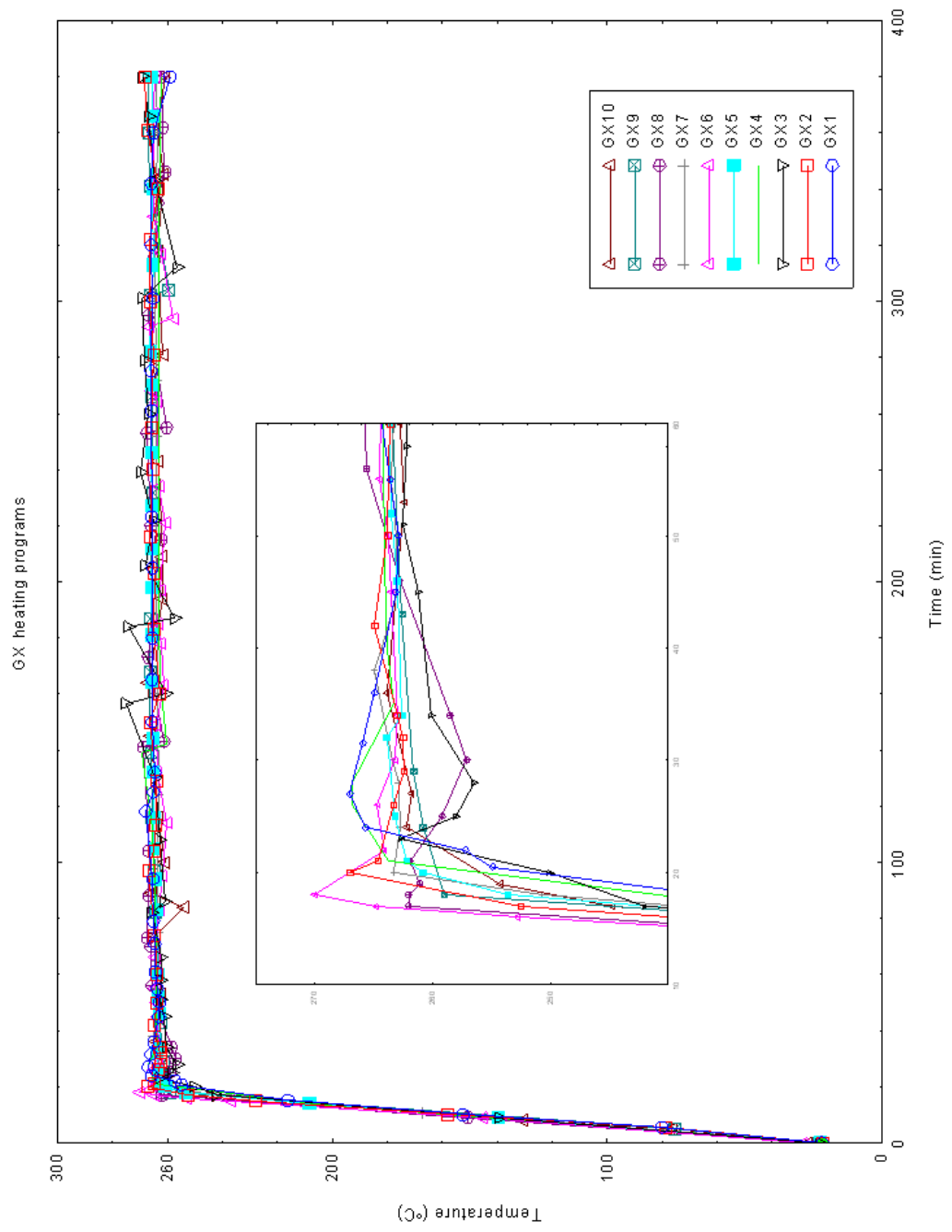


Figure A.4. G6 heating programs. Inset shows detail on the startup phase.

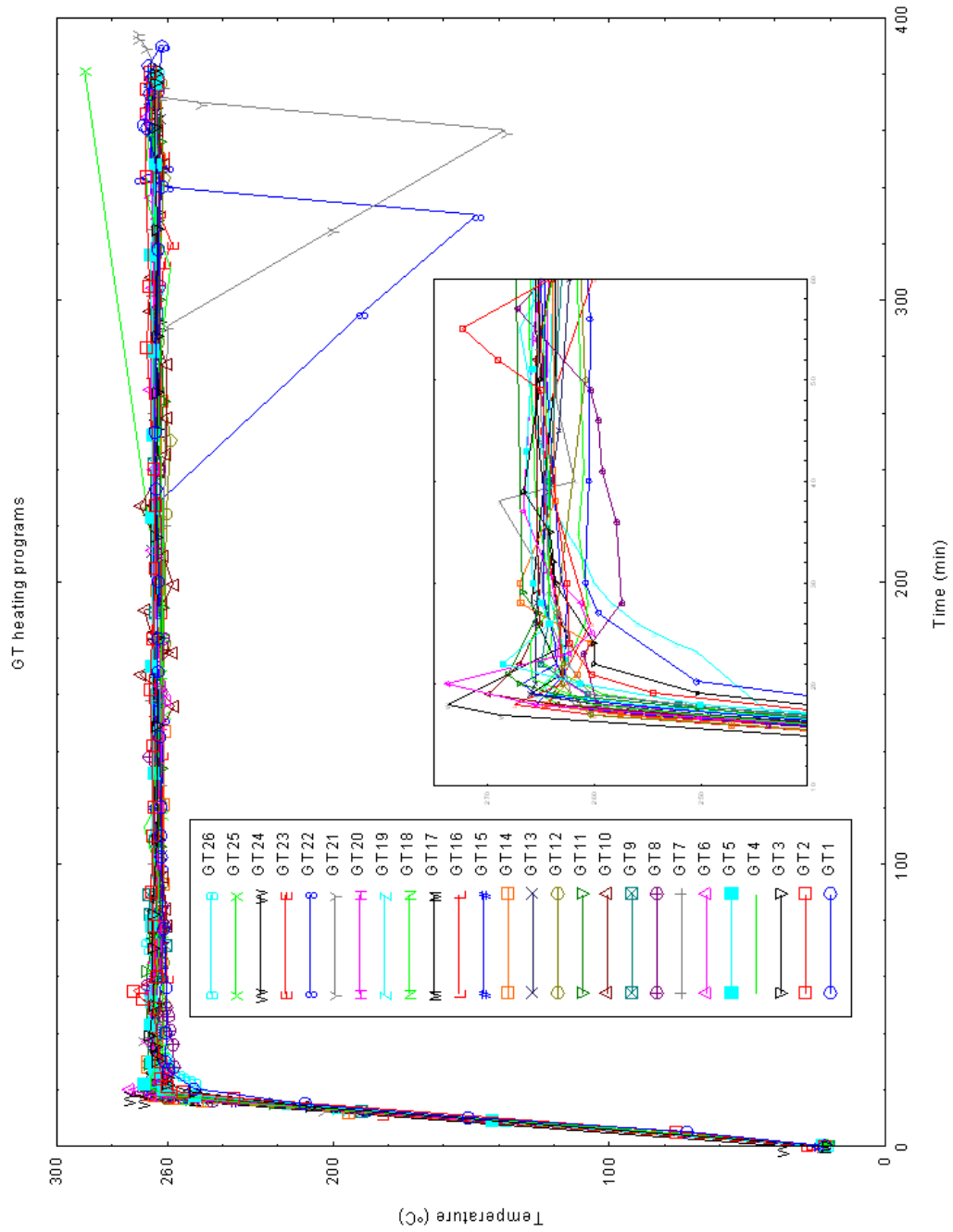
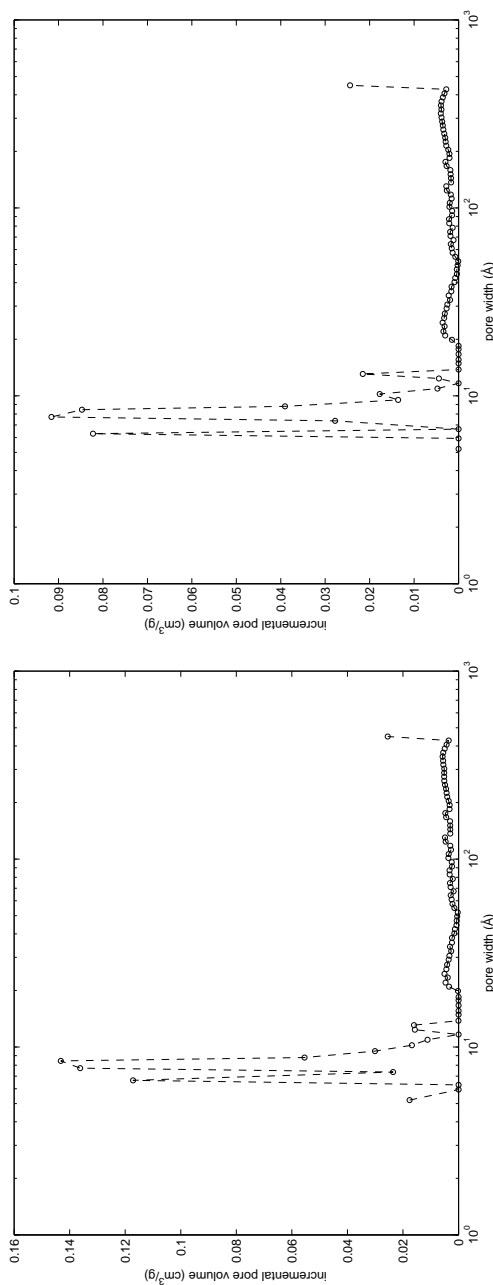
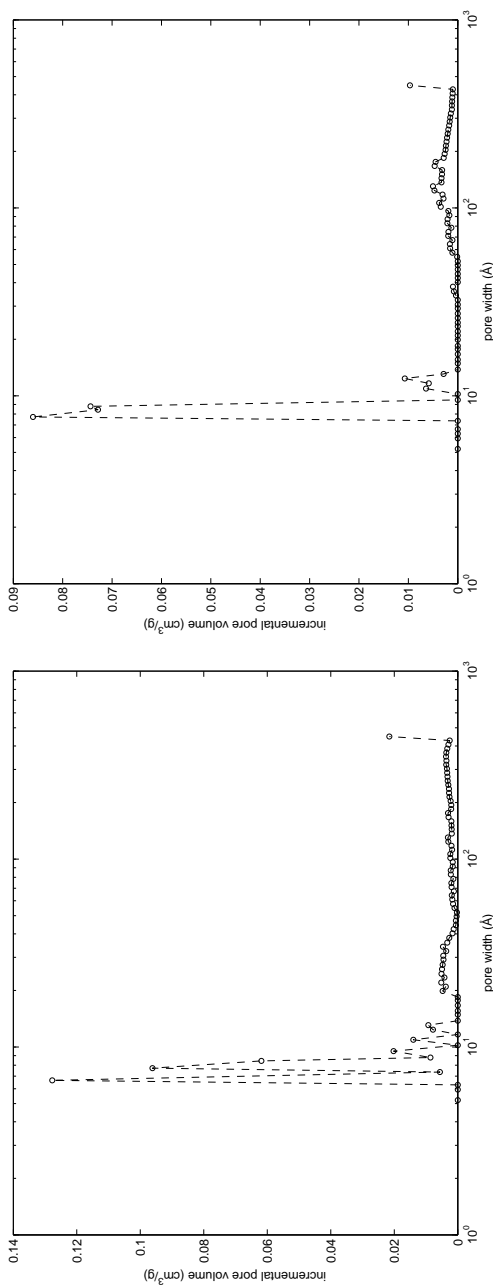


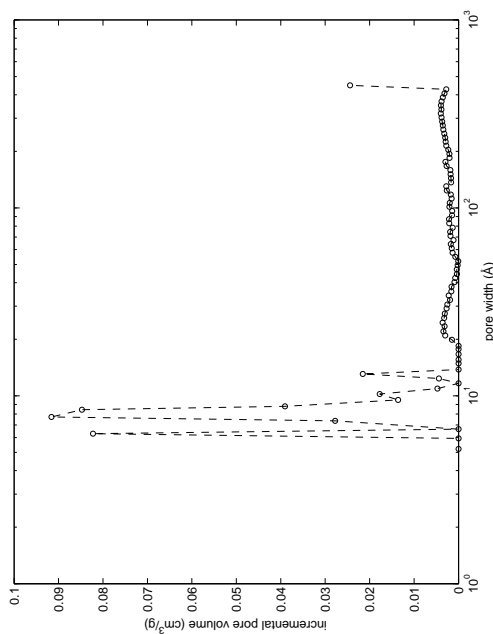
Figure A.5. G6IM heating programs. Inset shows detail on the startup phase.



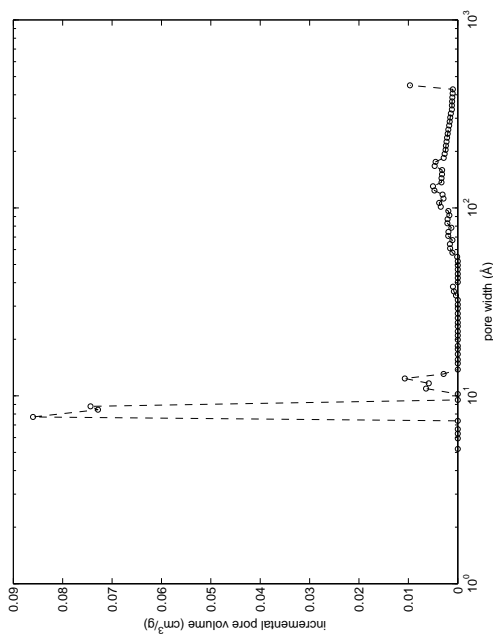
(a) FAU-720



(c) FAU-780



(b) FAU-760



(d) FAU-600

Figure A.6. Pore width in Ångström plotted versus incremental pore volume. The peaks shows the distribution of pore sizes in the zeolite. Plot calculated using Micromeritics DFT Plus software following collection of full isotherm data at liquid N₂ temperature. The rise at the far end of the curve is probably an artefact due to the calculation method.

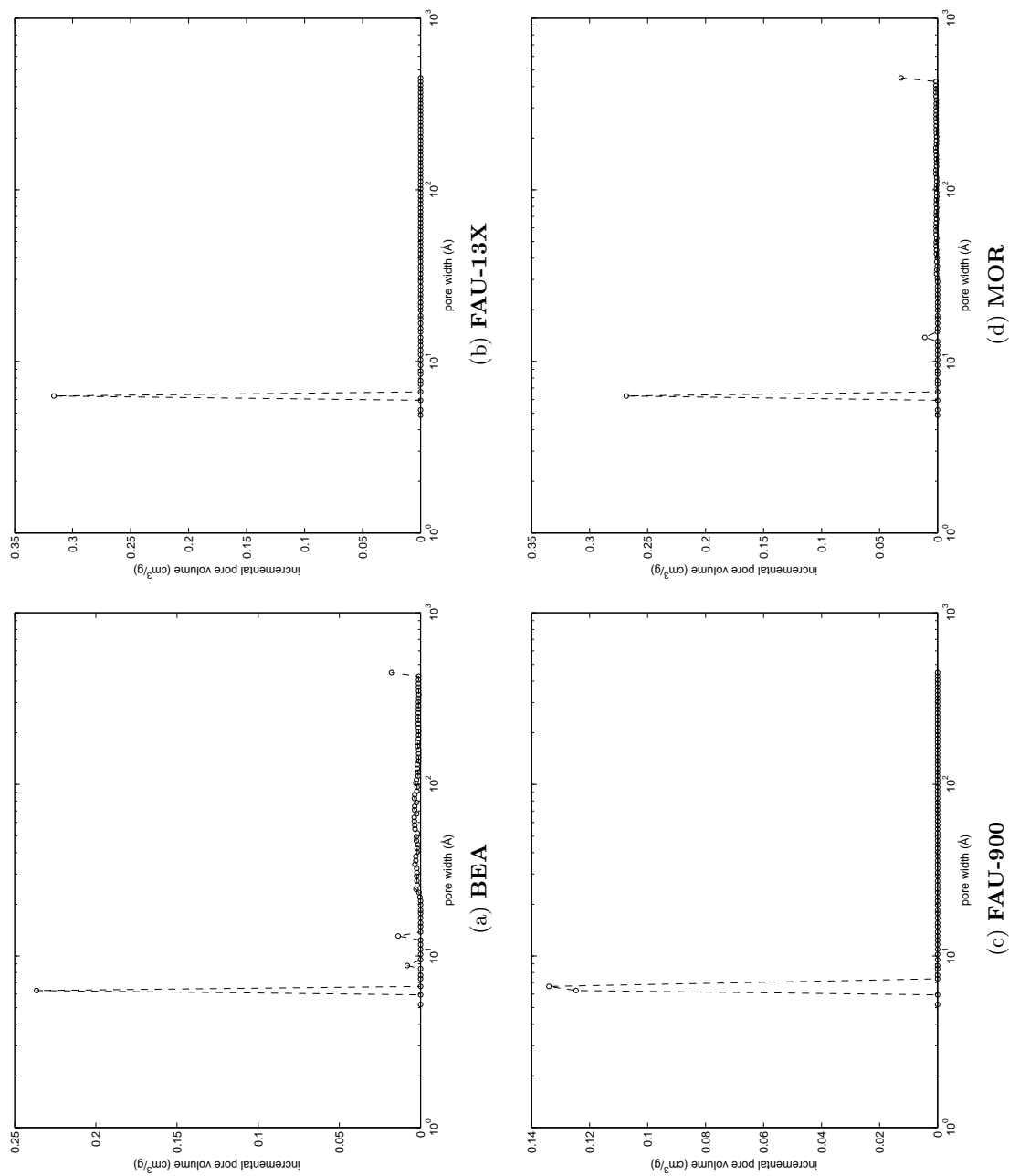
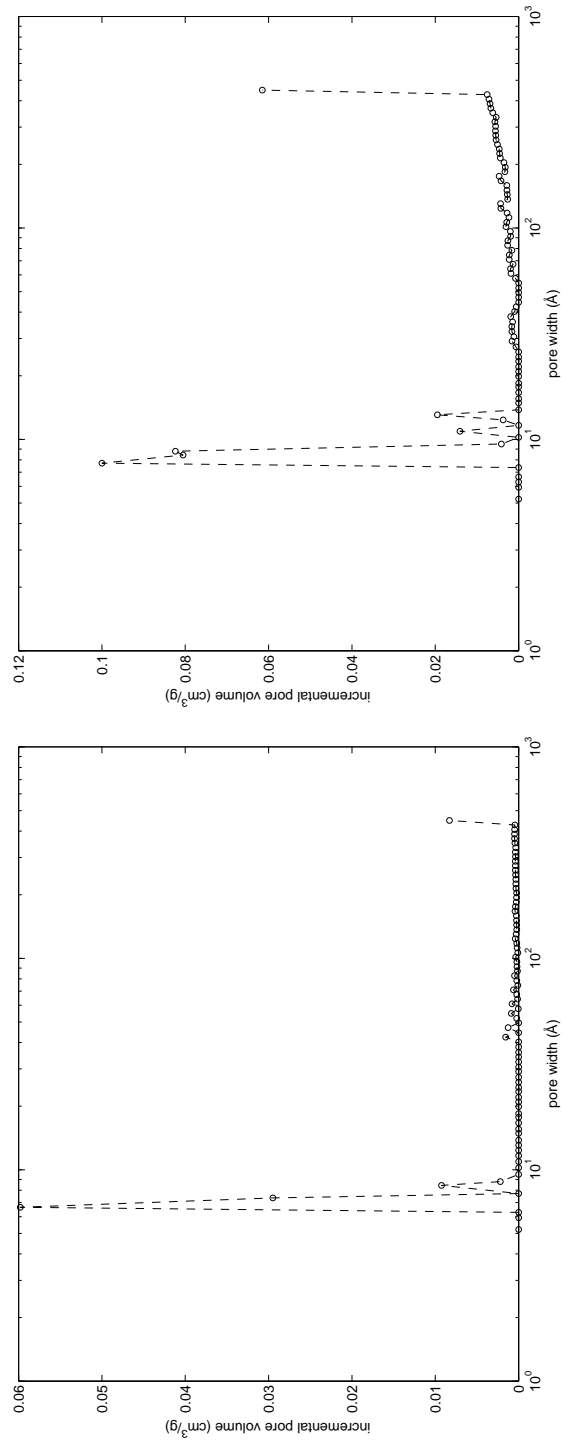


Figure A.7. Pore width in Ångström plotted versus pore volume. The peaks shows the distribution of pore sizes in the material. Plot calculated using Micromeritics DFT Plus software following collection of full isotherm data at liquid N₂ temperature. The rise at the far end of the curve is probably an artefact due to the calculation method.



(b) USY

(a) ZSM-5P

Figure A.8. Pore width in Ångström plotted versus pore volume. The peaks shows the distribution of pore sizes in the material. Plot calculated using Micromeritics DFT Plus software following collection of full isotherm data at liquid N₂ temperature. The rise at the far end of the curve is probably an artefact due to the calculation method.

Table A.4. MATLAB M-file function that reads a *.dat or *.xy file and stores the plot data as two MATLAB variables `x_column` (x) and `intensity` (y). The function then returns these variables to the calling script, where the data can be used to plot the graph.

```
function [intensity,x_column] = xyreader(sample_filename)
format long;

t = sample_filename;
fid = fopen(t,'rt');%t for text-mode

rn=0;
while 1
    rn=rn+1;
    string_file{rn} = fgetl(fid);
    if ~ischar(string_file{rn})
        break;
    end
end

filtyp = sample_filename(end-1:end);
if filtyp == 'at'
    for k = 1:rn-2
        num_file(k,1:2) = str2num(string_file{k+1});
    end
else
    for k = 1:rn-1
        num_file(k,1:2) = str2num(string_file{k});
    end
end

intensity = num_file(:,2);
x_column = num_file(:,1);
status = fclose(fid);
```

Table A.5. MATLAB M-file that plots the Guinier-Hägg PXRD data. It calls the function given in Table A.4 to fetch the data, then draws it using MATLAB's `plot` command. The graph is saved as an `*.eps` and `*.pdf` file.

```
function ghplot(sample_filename)
format long;

xy_file_exist = exist(sample_filename);
if xy_file_exist == 2
    disp('Reading XY data...');
    [intensity,xvalues] = xyreader(sample_filename);
else
    disp('Cannot find the file');
end

disp('Plotting...');
hubergraph = plot(xvalues,intensity,'-');
xlabel('2\theta');
ylabel('Intensity');
p = sample_filename(1:end-4);
title(p);

disp('Saving...');
t = sample_filename(1:end-4);
t = [t,'.eps'];
saveas(hubergraph,t);

callstr = 'pdffromeps';
status = dos(callstr);
close all
```

Table A.6. MATLAB M-file that plots the Huber PXRD data. It calls the function given in Table A.4 to fetch the data, then draws it using MATLAB's plot command. The graph is saved as an *.eps and *.pdf file.

```
function huberplot(sample_filename)
format long;

xy_file_exist = exist(sample_filename);
if xy_file_exist == 2
    disp('Reading XY data...');
    [intensity,xvalues] = xyreader(sample_filename);
else
    disp('Converting *.GDF to *.XY');
    samplename = sample_filename(1:end-3);
    dosstring = ['gdf2xy < ',samplename,'.gdf > ',sample_filename];
    status = dos(dosstring);
    disp('Reading XY data...');
    [intensity,xvalues] = xyreader(sample_filename);
end

disp('Plotting...');
hubergraph = plot(xvalues,intensity,'-');
xlabel('2\theta');
ylabel('Intensity');
p = sample_filename(1:end-4);
title(p);

disp('Saving...');
t = sample_filename(1:end-3);
t = [t,'.eps'];
saveas(hubergraph,t);

callstr = 'pdffromeps';
status = dos(callstr);
close all
```

Table A.7. MATLAB M-file that checks which datatype is present and calls the appropriate script from the ones given above. Created for convenience rather than necessity.

```
function plotpxrd(sample_name)
format long;

sample_name_gdf = [sample_name, '.gdf'];
xy_exist = exist(sample_name_gdf);

sample_name_dat = [sample_name, '.dat'];
dat_exist = exist(sample_name_dat);

if (xy_exist == 2 && dat_exist == 2)
    disp('Getting DAT data...');
    ghplot(sample_name_dat);
else if xy_exist == 2
    disp('Getting GDF data...');
    sample_name = [sample_name, '.xy'];
    huberplot(sample_name);
else if dat_exist == 2
    disp('Getting DAT data...');
    ghplot(sample_name_dat);
else
    disp('Cannot find the file');
end
end
end
```

BEA

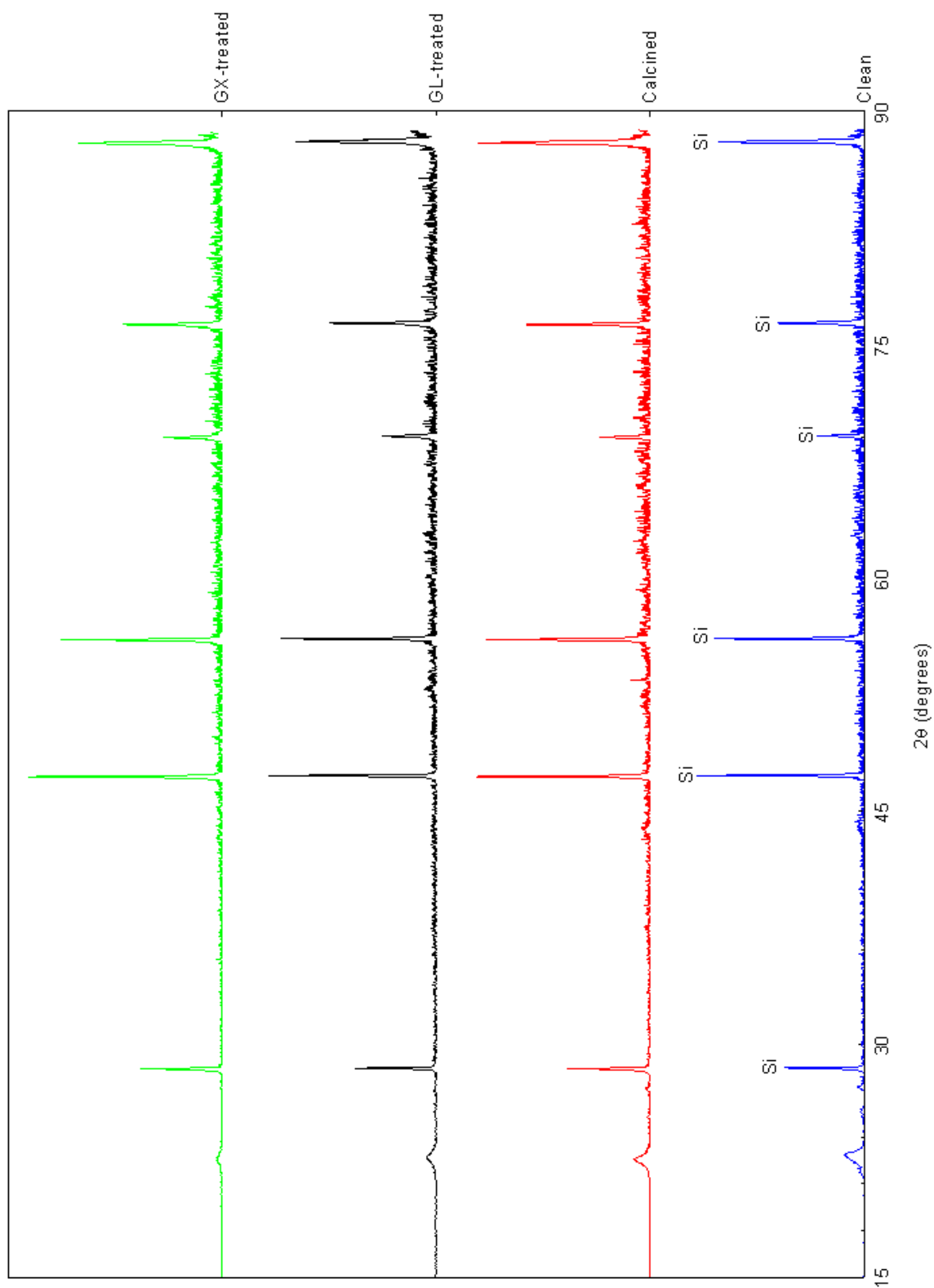


Figure A.9. BEA powder X-ray diffractograms, full set. From bottom to top curve: clean untreated **BEA** (blue), clean calcined **BEA** (red), GL-treated **BEA** (black), and GX-treated **BEA** (green).

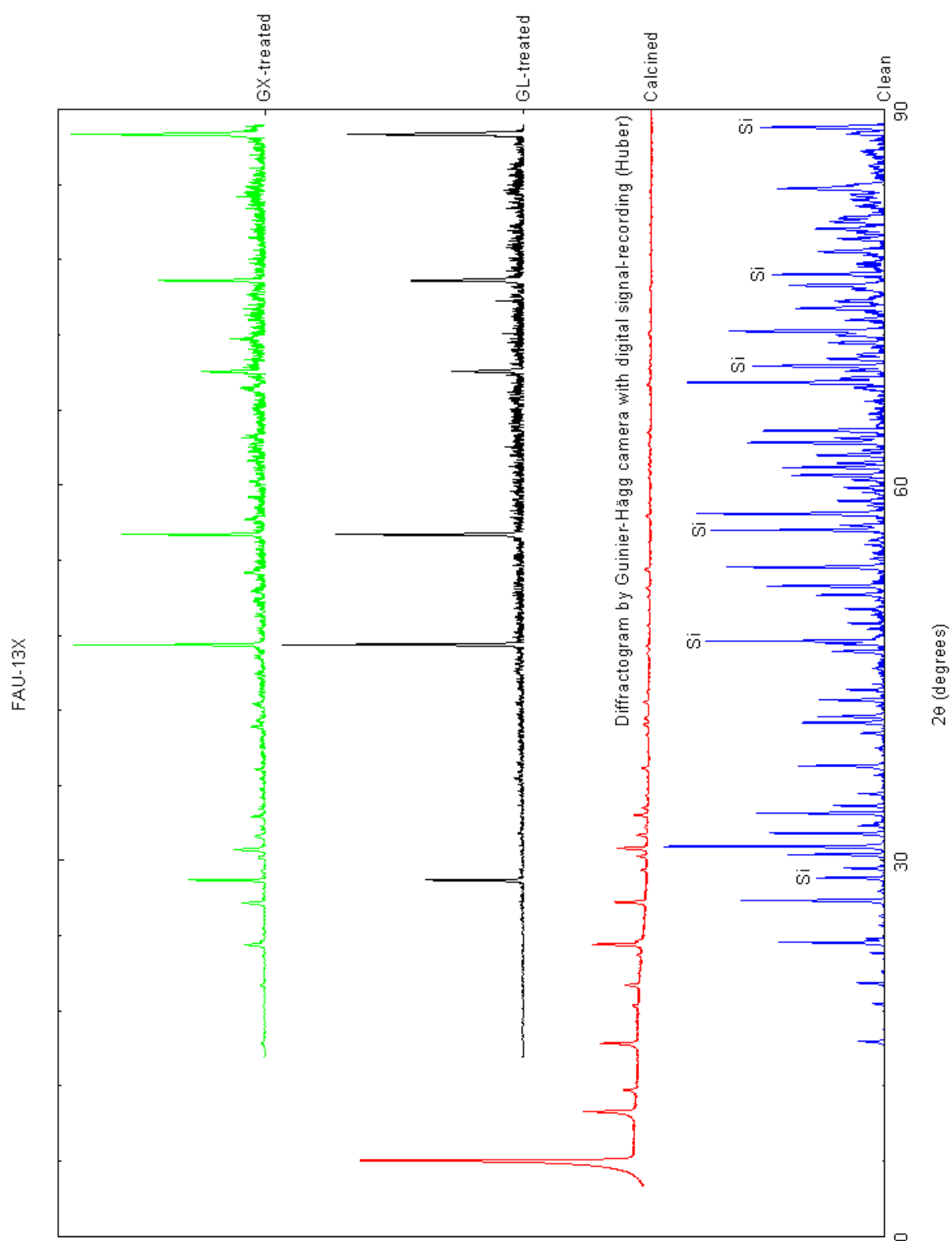


Figure A.10. FAU-13X powder X-ray diffractograms, full set.

FAU-600

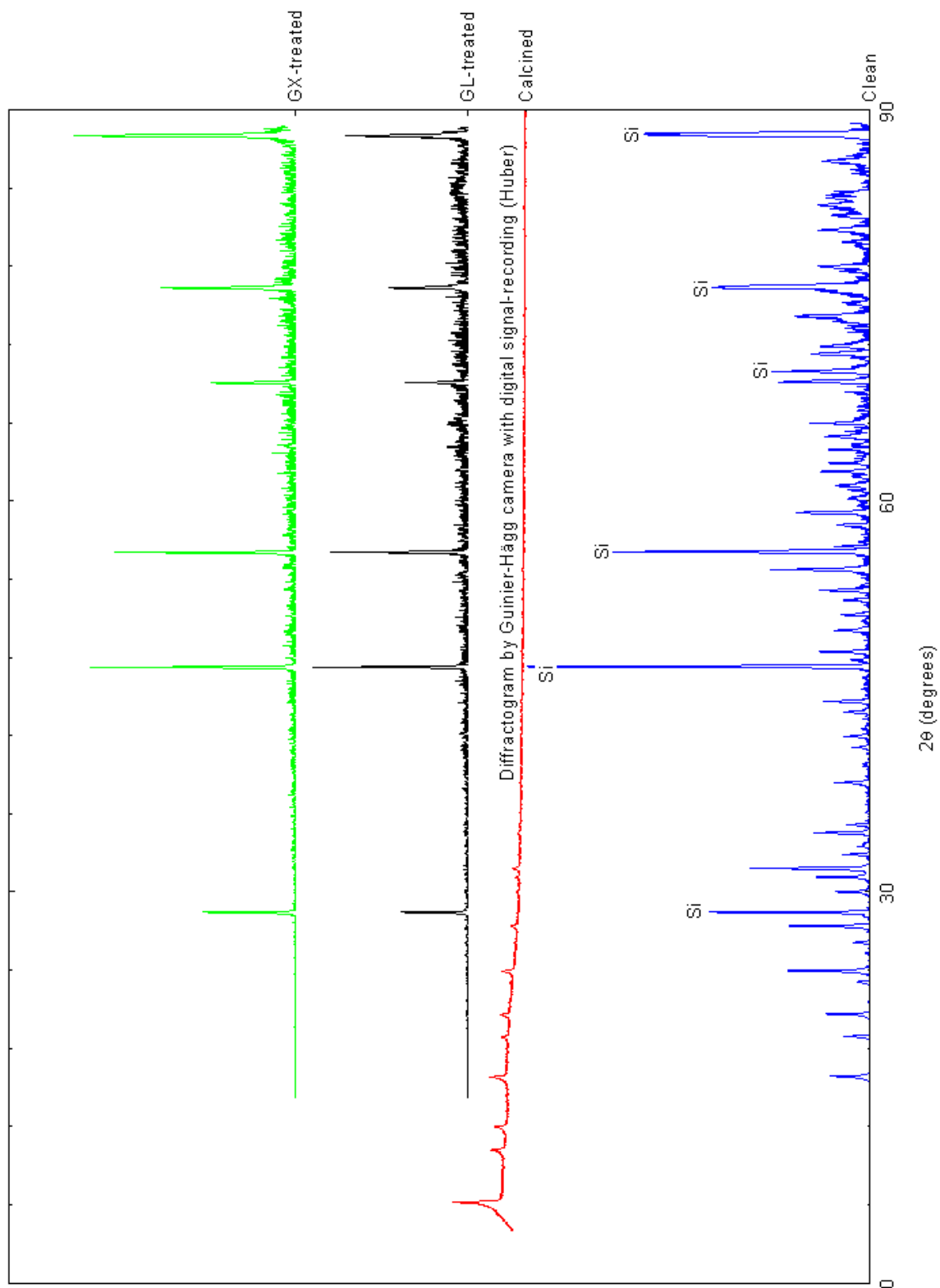


Figure A.11. FAU-600 powder X-ray diffractograms, full set.

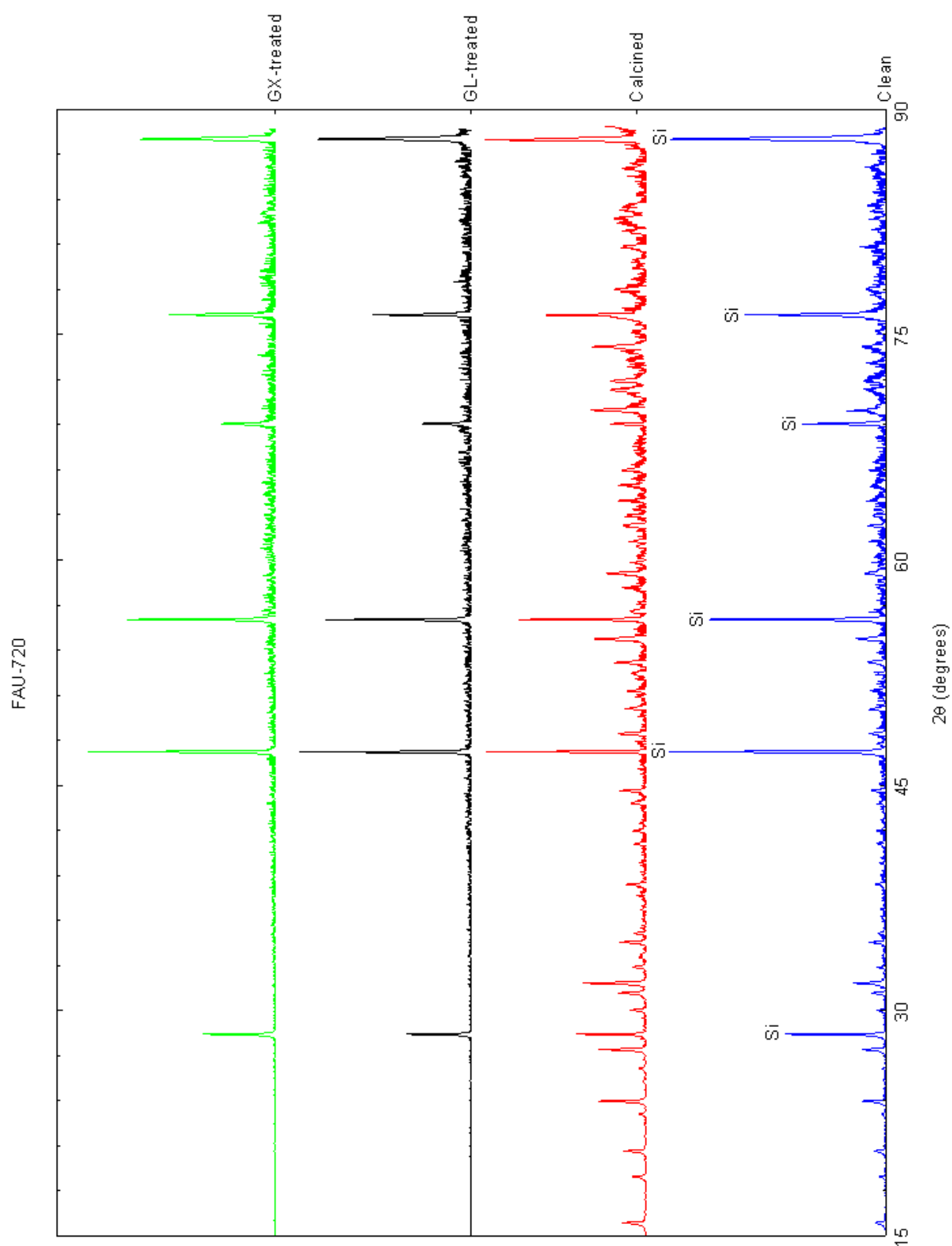


Figure A.12. FAU-720 powder X-ray diffractograms, full set.

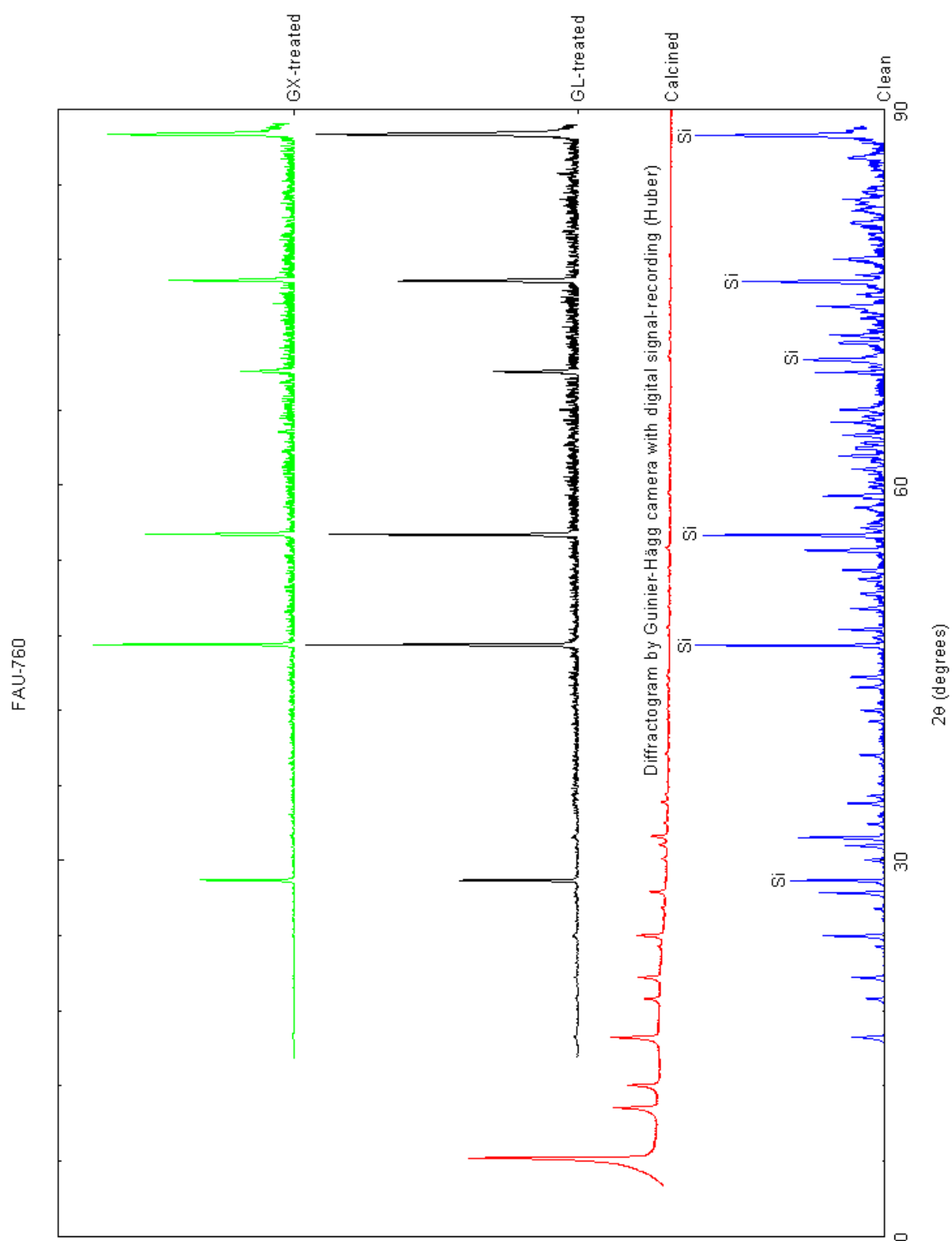


Figure A.13. FAU-760 powder X-ray diffractograms, full set.

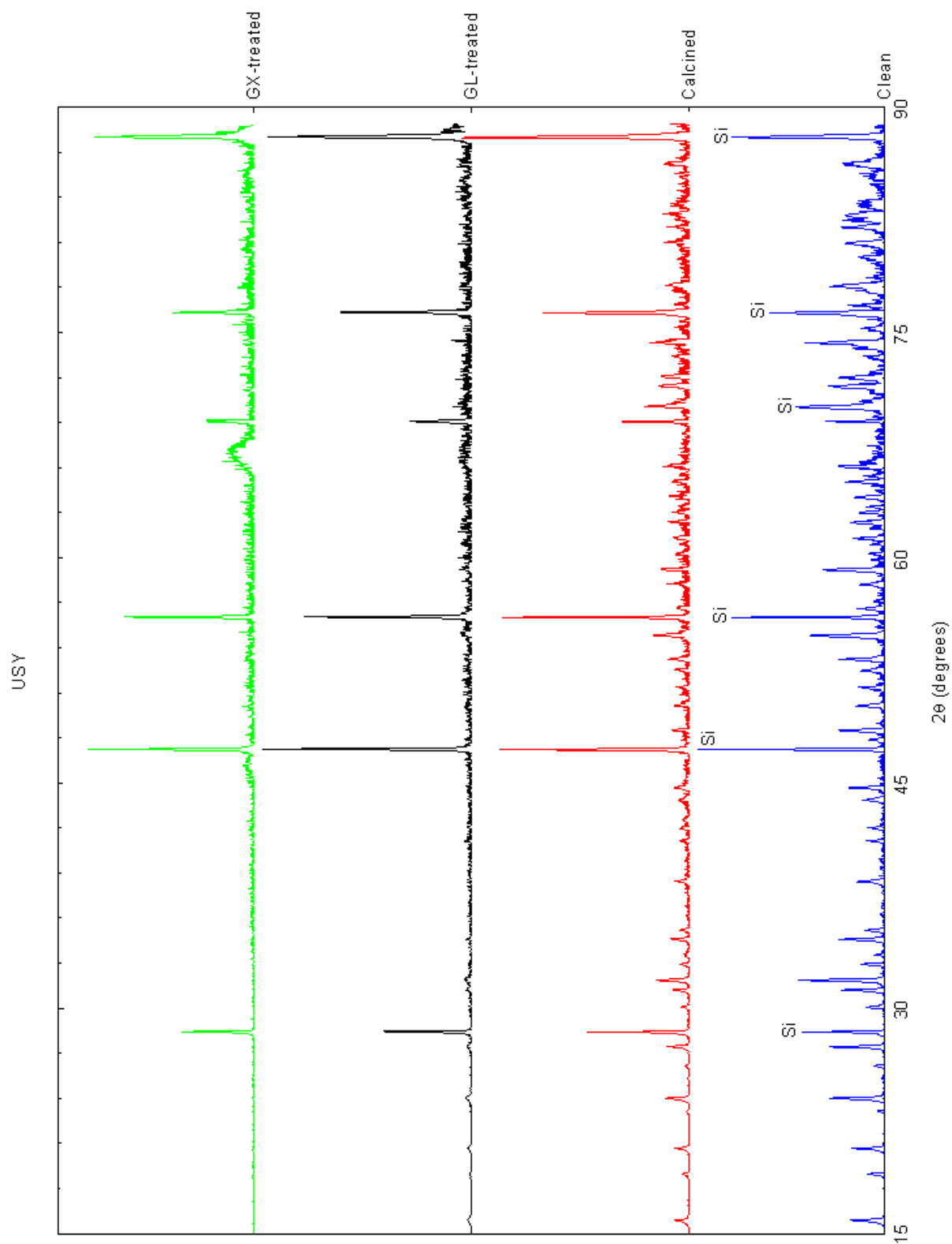


Figure A.17. USY powder X-ray diffractograms, full set.

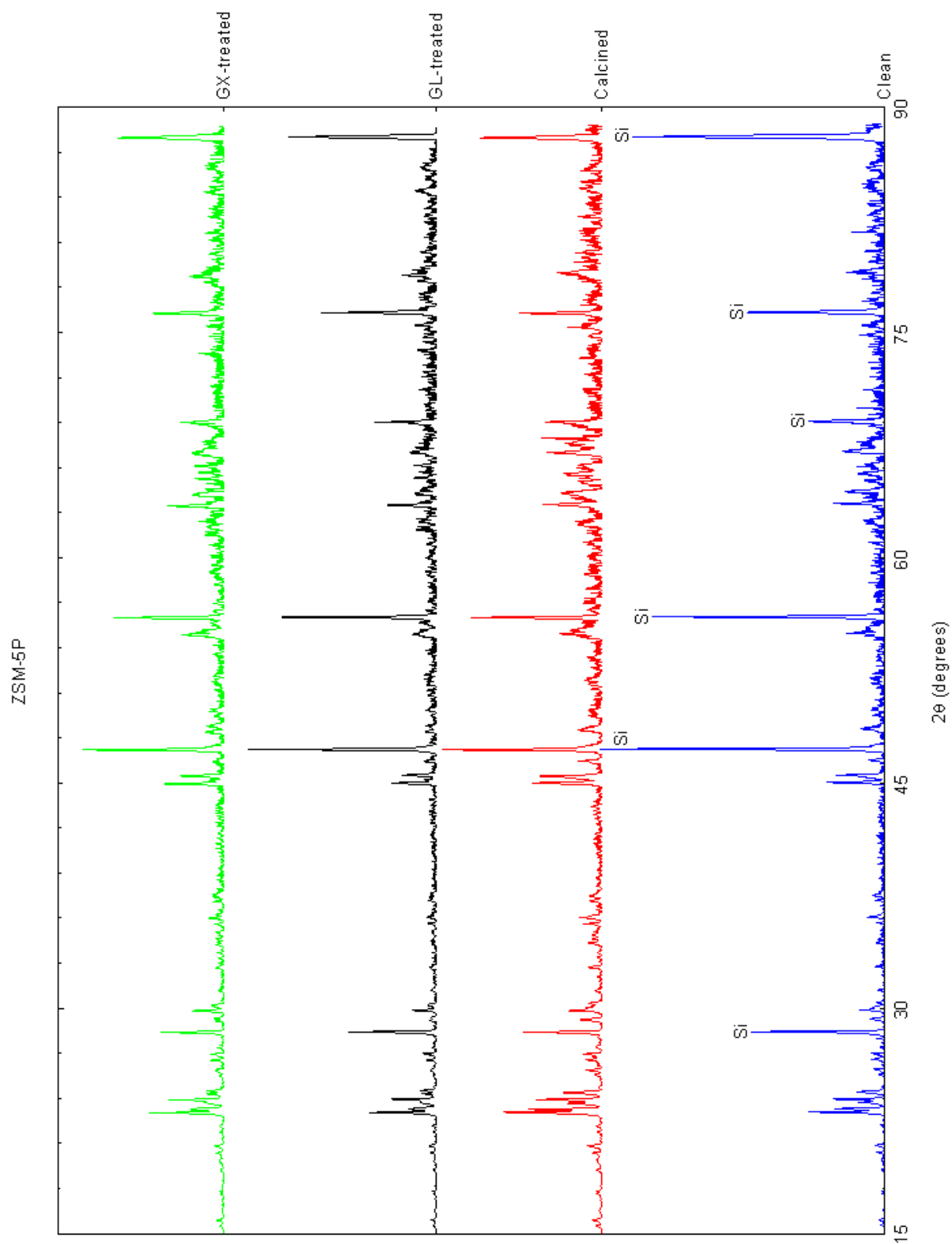


Figure A.18. ZSM-5P powder X-ray diffractograms, full set.